PASSIVE INTERMODULATION GENERATION BY NONLINEAR CONDUCTION PHENOMENA AT METAL/METAL-OXIDE/METAL INTERFACES IN UHF COMMUNICATIONS SYSTEMS

by
R.J.C. Bultitude

Prepared for The Canadian Government Department of Communications Under Department of Supplies and Services Contract No. OST78-00022
April 1980.

P
91
C655
B851
1980

P
91
C655
B851
1980

PASSIVE INTERMODULATION GENERATION BY NONLINEAR CONDUCTION PHENOMENA AT METAL/METAL-OXIDE/METAL INTERFACES IN UHF COMMUNICATIONS SYSTEMS

Industry Canada
Library Queen
JUL 20 1998
Industrie Canada
Bibliothèque Queen

COMMUNICATIONS CANADA
JUL 1984
LIBRARY – BIBLIOTHÈQUE

by
R.J.C. Bultitude

Prepared for The Canadian Government Department of Communications Under Department of Supplies and Services Contract No. OST78-00022
April 1980.

ABSTRACT

This report details theoritical investigations into the generation of passive intermodulation signals by nonlinearities at intermetallic interfaces as a result of conduction through thin metal oxide films formed on passive RF hardware components in UHF communication systems. A study of the relationships between nonlinear I-V characteristics and the intermodulation power/drive power response signatures of generated passive intermodulation signals is also investigated.

This report follows from an earlier report, submitted in August 1979, as part of the same contract with the communications research centre.

TABLE OF CONTENTS

	PAGE
ABSTRACT	i
TABLE OF CONTENTS	ii
LIST OF TABLES	v
LIST OF FIGURES	vii
GLOSSARY OF SYMBOLS	xii
CHAPTER I INTRODUCTION	
1.1 Introduction	1
1.2 Background	2
1.3 Report Organization	5
CHAPTER II CONDUCTION PROCESSES IN METAL/INSULATOR/METAL STRUCTURES	
2.1 Introduction	7
2.2 Metal/Insulator/Metal Structures with Ohmic Contacts	9
2.2.1 Ohmic Contacts	9
2.2.2 The Tunneling of Electrons Through the Potential Barrier Represented by an Insulator Between Two Ohmic Contacts.	11
2.2.3 Space Charge Limited Current Flow in Structures where Spacially Separated Ohmic Contacts are Made to an Insulator	20
2.3 Metal/Insulator/Metal Structures with Neutral Contacts	26
2.3.1 Neutral Contacts	26
2.3.2 Electron Conduction Through a Metal/Insulator/Metal Structure with Neutral Contacts	26
2.4 Metal/Insulator/Metal Structures with Blocking Contacts	29
2.4.1 Blocking Contacts	29
2.4.2 Electron Tunneling Through the Potential Barrier Presented by an Insulator Between Blocking Contacts	31
2.4.3 Thermionic Emission of Electrons at Blocking Contacts	31
2.5 Metal/Semiconductor Contacts	34
2.6 Summary	35

PAGE

CHAPTER III THE GENERATION OF PIM BY NONLINEAR CONDUCTION PROCESS IN NATURALLY OCCURRING OXIDES AT INTER-METALLIC CONTACTS

3.1 Introduction 39
3.2 Development of a Unit Equivalent Circuit for Use In Metal-Metal Contact Models 41
3.3 Calculations Concerning the Power of PIM Signals That Could be Generated as a Result of Tunneling Phenomena in Coaxial Connectors 49
3.3.1 Connector Geometries and Contact Models 51
3.3.2 The Power of PIM Signals Generated by Tunneling in a Long Contact Copper Connector 56
(a) PIM Generated at a Long Copper Connector Centre Conductor Contact 56
(b) PIM Generated at the Outer Conductor Contact in a Long Contact Copper Connector Outer Conductor Contact. 62
3.3.3 The Power of PIM Signals Generated by Tunneling in a Short Contact Copper Connector 67
(a) PIM Generated at the Short Contact Copper Connector Centre Conductor Contact 67
(b) PIM Generated at the Short Contact Copper Connector Outer Conductor Contact 76
3.3.4 The Power of PIM Signals Generated by Tunneling in Aluminum Connectors 83
3.4 Passive Intermodulation Signal Generation Due to Space Charge Limited Current Flow in Naturally Occurring Oxides at Metal/Oxide/Metal Interfaces 88
3.5 Summary and Discussion 91

CHAPTER IV INTERMODULATION POWER SIGNATURES

4.1 Introduction 95
4.2 The Characteristics of IM Signals Generated in a Symmetrical Nonlinear I-V Characteristic in which the Current Remains Constant after Reaching a Fixed Maximum (Symmetrical Current Limiter) 97
4.3 The Characteristics of IM Signals Generated by a Non-Symmetrical Nonlinearity in which Positive Currents Remain Constant after Reaching a Fixed Maximum and Negative Currents Vary Linearly as a Function of Voltage (Semilinearized Current Limiter) 105
4.4 The Characteristics of IM Signals Generated in a Symmetrical Nonlinearity in which Current Rises Rapidly as a Function of Voltage, (Symmetrical "current expander") 112

PAGE

4.5 The Characteristics of IM Signals Generated in a Non-Symmetrical Nonlinearity in which Current Rises Rapidly as a Function of Voltage in the Positive Voltage Region, and is an Almost Linear Function of Voltage in the Negative Voltage Region (semilinearized "Current Expander") 120
4.6 Discussion 127

CHAPTER V SUMMARY, CONCLUSIONS AND RECOMMENDATIONS

5.1 Summary 131
5.2 Conclusions 138
5.3 Recommendations for Further Investigation 144

REFERENCES 147

APPENDIX A Computer Programs "IMPWR" and "TUNEL"

A.1 Program IMPWR 150
A.1.1 Program Inputs 150
A.1.2 Program Outputs 153
A.1.3 Program Explanation (IMPWR) 155
A.1.4 Program Flow Chart (IMPWR) 157
A.1.5 Program Statement Listing (IMPWR) 161

A.2 Program TUNEL 165
A.2.1 Program Inputs 165
A.2.2 Program Outputs 166
A.2.3 Program Explanation 166
A.2.4 Program Statement Listing (TUNEL) 167

APPENDIX B Physical Constants 169

LIST OF TABLES

TABLE	CAPTION	PAGE
2-1	Tunnel Current Density (A/cm^2) as a Function of Oxide Thickness ($Al-Al_2O_3-Al$)	18
2-2	Tunnel Current Density (A/cm^2) as A Function of Oxide Thickness ($Cu-Cu_2O-Cu$)	19
3-1	I-V Characteristic Showing Nonlinear Resistance Values For Tunneling At A Long Contact Copper Connector Centre Conductor Contact (cuprous oxide thickness = 20 Å, contact area = 5×10^{14} $Å^2$).	58
3-2	Coefficients of the Best Fit Least Squares Polynomial Representation to the I-V Characteristic For Tunneling Through Cuprous Oxide 20 Å Thick ($T = 300^o$ K, $V \leq 900\mu V$)	59
3-3	Comparison Of Computed Tunnel Currents For A Long Contact Copper Connector Centre Conductor Contact With Currents Calculated Using A 9th Degree Least Squares Polynomial Approximation To The Computed I-V Characteristic.	60
3-4	I-V Characteristic Showing Nonlinear Resistance Values For Tunneling At A Short Contact Copper Connector Centre Conductor Contact (cuprous oxide thickness = 20 Å, contact area = 5×10^{12} $Å^2$).	69
3-5	Coefficients of the Best Fit Least Squares Polynomial Representation For the Tunneling I-V characteristic of the Short Contact Copper Connector Centre Conductor Contact ($T = 300^o$ K, D = 20 Å, $V_T \leq 82$ mV).	70
3-6	Comparison of Computed Tunnel Currents For A Short Contact Copper Connector Centre Conductor Contact With Currents Calculated Using a 9th Degree Least Squares Polynomial Approximation To The Computed I-V Characteristic	71
3-7	I-V Characteristic Showing Nonlinear Resistance Values For Tunneling At A Short Contact Copper Connector Outer Conductor Contact (cuprous oxide thickness = 20 Å, contact area = 6×10^{13} $Å^2$).	77
3-8	Coefficients of The Best Fit Least Squares Polynomial Approximation for the Tunneling Characteristic of the Short Conduct Copper Connector Outer Conductor Contact ($T = 300^o$ K, D = 20Å, $V \leq 8$mV).	78

LIST OF TABLES (cont'd)

TABLE	CAPTION	PAGE
3-9	Comparison of Computed Tunnel Currents For A Short Contact Copper Connector Outer Conductor Contact With Currents Calculated Using a 9th Degree Least Squares Polynomial Approximation To The Computed I-V Characteristic.	79
3-10	I-V Characteristic and Resistance Values For Tunneling At The Centre Conductor Contact Of A Short Contact Aluminum Connector (0V < V < 1 mV, oxide thickness = 20 Å).	84
3-11	I-V Characteristic and Resistance Values For Tunneling At The Centre Conductor Contact Of A Short Contact Aluminum Connector. (100 mV V 2V, oxide thickness = 20 Å).	85
4-1	Coefficients of The Power Series Polynomial Used To Generate The Arbitrary I-V Characteristic of Figure 4.1.	98
4-2	Coefficients of The Power Series Polynomial Used To Generate The Arbitrary I-V Characteristic of Figure 4.4.	106
4-3	Coefficients of The Power Series Polynomial Used To Generate The Arbitrary I-V Characteristic of Figure 4.11.	113
4-4	Coefficients of The Power Series Polynomial Used To Generate The Arbitrary I-V Characteristic of Figure 4-16.	121
4-5	Comparison of Results For "Limiter" and "Expander" Type I-V Characteristics.	128
4-6	Summary of Polynomial Characteristics for The Arbitrary Nonlinear I-V Characteristics Chosen For Investigation.	130
5-1	Summary of The Possibility of Passive Intermodulation Generation by Nonlinear Conduction Phenomena Studied In This Investigation.	134

LIST OF FIGURES

FIGURE	CAPTION	PAGE
2.1	Energy band relationships at an ohmic contact. ((a), (b), (c) - see text).	10
2.2	Pictorial diagram of a conducting structure in which an insulator is sandwiched between two metals.	12
2.3	Schematic representation of the energy relationships at a zero biased $Al-Al_2O_3-Al$ junction, including short range forces, (From Dubey [8]).	13
2.4	Normalized I-V characteristic for space-charge-limited current flow in a symmetrical metal/insulator/metal structure. (1.3 mV $\leq$ V $\leq$ 9.1 mV, at 20°C). (From Lindmayer, Reynolds, and Wrigley [11]).	22
2.5	Normalized I-V characteristic for space-charge-limited current flow in a symmetrical metal/insulator/metal structure, (2.6 mV $\leq$ V $\leq$ 2.6V, at 20°C). (From Lindmayer, Reynolds and Wrigley [11]).	23
2.6	I-V characteristic for space-charge-limited current flow in a copper/cuprous-oxide/copper structure. (Area = 10,000 Å, Oxide thickness = 10 Å).	25
2.7	Energy relationships at a zero biased neutral metal/insulator contact.	27
2.8	Energy band relationships at a blocking contact. ((a), (b), (c) - see text).	30
2.9	Energy relationships at a structure formed by two blocking contacts separated by an insulator. (a) zero bias, (b) bias voltage,(V_b) applied.	32
3.1	Pictorial diagram of a contact between two oxidized metal surfaces.	42
3.2	Model of a single "A" spot.	43
3.3	Equivalent circuit for a single "A" spot, (From Chapman and Darlington [3]).	44
3.4	Fixed geometry for the position of "A" spots at the metal/metal contact.	45
3.5	Reduced equivalent circuit for an "A" spot at UHF.	48

LIST OF FIGURES (cont'd)

FIGURE	CAPTION	PAGE
3.6	Passive intermodulation test circuit block diagram.	50
3.7 (a)	MIL Spec. drawing for a male type N RF connector (from MIL, C39012/1D)	52
3.7 (b)	MIL Spec. drawing for a female type N RF connector (from MIL -C-39012/2D)	53
3.8.	Schematic representation of the centre contact in a mated RF connector pair. The figure shows that physical contact is made only over a very small fraction of the contact pin length as a result of the bevel on the centre conductor pin.	54
3.9	Model for the assumed test circuit.	61
3.10	Test circuit model with the IM generator (connector centre pin) replaced by its Thevenin equivalent circuit.	61
3.11	Computed third order IM signal power dependence on total transmit power for IM signals generated by tunneling through 20 Å of cuprous oxide at a RF connector centre conductor contact. (contact area = 5×10^{14} Å^2).	63
3.12	Computed fifth order IM signal power dependence on total transmit power for IM signals generated by tunneling through 20 Å of cuprous oxide at a RF connector centre conductor contact, (contact area = 5×10^{14} Å^2).	64
3.13	Computed seventh order IM signal power dependence on total transmit power for IM signals generated by tunneling through 20 Å of cuprous oxide at a RF connector centre conductor contact, (contact area = 5×10^{14} Å^2).	65
3.14	Computed I-V characteristic for tunneling through 20 Å of cuprous oxide at a short contact copper connector centre conductor contact, (contact area = 5×10^{12} Å^2).	68
3.15	Computed third order IM signal power dependence on total transmit power for IM signals generated by tunneling through 20 Å of cuprous oxide at a RF connector centre conductor contact, (contact area = 5×10^{12} Å^2).	72

LIST OF FIGURES (cont'd)

FIGURE	CAPTION	PAGE
3.16.	Computed fifth order IM signal power dependence on total transmit power for IM signals generated by tunneling through 20 Å of cuprous oxide at a RF connector centre conductor contact, (contact area = 5×10^{12} Å^2).	73
3.17.	Computed seventh order IM signal power dependence on total transmit power for IM signals generated by tunneling through 20 Å of cuprous oxide at a RF connector centre conductor contact, (contact area = 5×10^{12} Å^2).	74
3.18.	Computed third order IM signal power dependence on total transmit power for IM signals generated by tunneling through 20 Å of cuprous oxide at a RF connector centre conductor contact, (contact area = 6.28×10^{13} Å^2).	80
3.19.	Computed fifth order IM signal power dependence on total transmit power for IM signals generated by tunneling through 20 Å of cuprous oxide at a RF connector centre conductor contact, (contact area = 6.28×10^{13} Å^2).	81
3.20	Computed seventh order IM signal power dependence on total transmit power for IM signals generated by tunneling through 20 Å of cuprous oxide at a RF connector centre conductor contact, (contact area = 6.28×10^{13} Å^2).	82
3.21	Computed I-V characteristic for tunneling at a short contact aluminum connector centre conductor contact. (aluminum oxide thickness = 20 Å, contact area = 5×10^{12} Å^2).	86
4.1	Symmetrical "limiter-type" I-V characteristic computed using the polynomial coefficients of Table 4-1 in Equation 1-4.	99
4.2	Computed third order IM signal power dependence on total transmit power for IM signals generated by application of a two frequency signal to the symmetrical "current limiter-type" I-V characteristic of Fig. 4.1.	100
4.3	Computed fifth order IM signal power dependence on total transmit power for IM signals generated by application of a two frequency signal to the symmetrical "current limiter-type" I-V characteristic of Fig. 4.1.	101

LIST OF FIGURES (cont'd)

FIGURE	CAPTION	PAGE
4.4	Computed seventh order IM signal power dependence on total transmit power for IM signals generated by application of a two frequency signal to the symmetrical "current limiter-type" I-V characteristic of Fig. 4.1.	102
4.5	The computed relative power of IM signals of consecutive order generated by the application of two frequency signals of different total power to the symmetrical "current limiter-type" I-V characteristic of Fig. 4.1.	103
4.6	Semilinearized "limiter-type" I-V characteristic computed using the coefficients of Table 4-2 in Equation 1-4.	107
4.7	Computed third order IM signal power dependence on total transmit power for IM signals generated by application of a two frequency signal to the semilinearized "current limiter-type" I-V characteristic of Fig. 4.6.	108
4.8	Computed fifth order IM signal power dependence on total transmit power for IM signals generated by application of a two frequency signal to the semi-linearized "current limiter-type" I-V characteristic of Fig. 4.6.	109
4.9	Computed seventh order IM signal power dependence on total transmit power for IM signals generated by application of a two frequency signal to the semi-linearized "current limiter-type" I-V characteristic of Fig. 4.6.	110
4.10.	The computed relative power of IM signals of consecutive order generated by the application of two frequency signals of different total power to the semi-linearized "current limiter-type" I-V characteristic of Fig. 4.6.	111
4.11.	Symmetrical "expander-type" I-V characteristic computed using the coefficients of Table 4-3 in Equation 1-4.	114
4.12.	Computed third order IM signal power dependence on total transmit power for IM signals generated by application of a two frequency signal to the symmetrical "current expander-type" I-V characteristic of Fig. 4.1.	115
4.13.	Computed fifth order IM signal power dependence on total transmit power IM signals generated by application of a two frequency signal to the symmetrical "current expander-type" I-V characteristic of Fig. 4.11.	116

LIST OF FIGURES (cont'd)

FIGURE	CAPTION	PAGE
4.14.	Computed seventh order IM signal power dependence on total transmit power for IM signals generated by application of a two frequency signal to the symmetrical "current expander-type" I-V characteristic of Fig. 4.11.	117
4.15.	The computed relative power of IM signals of consecutive order generated by the application of two frequency signals of different total power to the symmetrical "current expander-type" I-V characteristic of Fig. 4.11.	118
4.16	Semi-linearized "expander-type" I-V characteristic computed using the coefficients of Table 4-4 in Equation 1-4.	122
4.17	Computed third order IM signal power dependence on total transmit power for IM signals generated by application of a two frequency signal to the semi-linearized "current expander-type" I-V characteristic of Fig. 4.16.	123
4.18	Computed fifth order IM signal power dependence on total transmit power for IM signals generated by application of a two frequency signal to the semi-linearized "current expander-type" I-V characteristic of Fig. 4.16.	124
4.19	Computed seventh order IM signal power dependence on total transmit power for IM signals generated by application of a two frequency signal to the semi-linearized "current expander-type" I-V characteristic of Fig. 4.16.	125
4.20	The computed relative power of IM signals of consecutive order generated by the application of two frequency signals of different power to the semi-linearized "current expander-type" I-V characteristic of Fig. 3.16.	126

GLOSSARY OF SYMBOLS

Å	Angstroms
a_i, i=1, 2, 3...,n	Polynomial Coefficients
d	Oxide thickness (Å)
D	Void width
e	Electronic charge
E_1,E_2	Sinusoidal voltage amplitudes at frequencies f_1 & f_2
E	Energy
Eg	Insulator/oxide band gap energy
f_1,f_2	Transmit frequencies
h	Planck's constant
IM	Intermodulation
I_{IM}	Intermodulation product current
I_{IML}	Intermodulation current carried by a RF system load
IMPWR	Computer program name
J	Current density
k	Optical permittivity
k_o	Boltzman's constant
ℓ	length
L	Inductance
m	Mass of an electron
n	Arbitrary integer
N	Intermodulation product order
PIM	Passive intermodulation

q	Electronic charge
r	Radius
T	Temperature
W	Constant
$X(t)$	Independent variable
X_1, X_2	Constants
$Y(t)$	Dependent variable
Δ	Incremental value
ϵ	Static permittivity
Φ_o	Contact potential
Ψ_m, Ψ_i	Metal and insulator work functions respectively
ξ_m	Anode Fermi level
χ	Electron affinity
μ	Electron mobility
∂	Normalized current
γ	Normalized voltage

CHAPTER I
Introduction

1.1 Introduction

The Department of Electronics Engineering at Carleton University, Ottawa was commissioned by the Canadian Department of Communications, Communications Research Centre (CRC) to investigate the problem of Passive intermodulation (PIM) in high power UHF satellite communication systems. An earlier report, [1] "A Study of Passive Intermodulation in Multifrequency UHF Radio Communication Systems", issued in August 1979, covers a major portion of the work carried out under the contract. This report details additional theoretical investigations that were conducted to further develop findings of the initial study. Two topics within the study of PIM are dealt with in detail. These include an investigation into the generation of PIM by nonlinearities at inter-metallic interfaces as a result of conduction through thin metal oxide films, and a study of the relationship between nonlinear I-V characteristics and the IM power/drive power response signatures of PIM signals generated by the nonlinearities under multifrequency excitation. The later topic further explores the possibility of the identification of IM generators in functioning RF systems by the analysis of response signatures, first suggested as a tool for IM source identification in the previous report. Information contained herein is written in a "stand alone" manner such that a knowledge of the work presented in the first report is not necessary for comprehension.

1.2 Background

The spurious generation of intermodulation signals by passive components in multifrequency RF communication systems poses a serious threat of interference to desired communications signals. The problem is most acute in systems such as those used for communications with geosynchronous satellites, where highly sensitive receivers must function in close proximity with high power transmitters operating in the same frequency zone ($f_{receive} < 2f_{transmit}$). For instance, in the proposed Canadian Government Multi-Use-UHF Satellite (MUSAT) communication system, which will operate with a total transmit power of +49 dBm at UHF, passive intermodulation (PIM) signals with orders as high as the 19th [1] can have sufficient power to impair communications.

Intermodulation products are generated when multiple frequency signals are applied to a circuit element the output from which is nonlinearly dependent upon the input. Consider a circuit element which exhibits a third degree nonlinearity. If the input and output signal parameters of interest are designated as X(t) and Y(t) respectively, the transfer characteristic for the circuit element can be written as:

$$Y(t) = a_o + a_1\, x(t) + a_2\, x^2(t) + a_3\, x^3(t) \qquad (1\text{-}1)$$

Now, assume the input signal to be a two frequency sinusoid of the form:

$$X(t) = E_1 \cos(\omega_1 t) + E_2 \cos(\omega_2\, t) \qquad (1\text{-}2)$$

Then, a mathematical representation for the output signal Y(t) can be obtained by substitution of (1-2) in (1-1).

This yields,

$$Y(t) = \frac{a_2}{2}[E_1^2 + E_2^2] + [a_1E_1 + \frac{3}{2}a_3E_1E_2^2 + \frac{3}{4}a_3E_1^3]\cos\omega_1 t$$

$$+ [a_1E_2 + \frac{3}{2}a_3E_1^2E_2 + \frac{3}{4}a_3E_2^3]\cos\omega_2 t$$

$$+ a_2E_1E_2\cos(\omega_1 + \omega_2)t \qquad (1\text{-}3)$$

$$+ a_2E_1E_2\cos(\omega_1 - \omega_2)t$$

$$+ a_2\frac{E_1^2}{2}\cos 2\omega_1 t + a_2\frac{E_2^2}{2}\cos 2\omega_2 t + a_3\frac{E_1^3}{4}\cos 3\omega_1 t$$

$$+ a_3\frac{E_2^3}{4}\cos 3\omega_2 t + \frac{3a_3}{4}E_1^2E_2\cos(2\omega_1 - \omega_2)t$$

$$+ \frac{3a_3}{4}E_1^2E_2\cos(2\omega_1 + \omega_2)t$$

$$+ \frac{3a_3}{4}E_1E_2^2\cos(2\omega_2 - \omega_1)t + \frac{3a_3}{4}E_1E_2^2\cos(2\omega_2 - \omega_1)t$$

The components at the frequencies $(2\omega_1 \pm \omega_2)$ and $(2\omega_2 \pm \omega_1)$ are the 3rd order intermodulation products. For circuit elements which exhibit higher degrees of nonlinearity, higher order IM products would be generated.

Numerous naturally occurring nonlinear mechanisms which can exist in RF components (ex. RF connectors, transmission lines and antennas) which are normally considered to be passive and linear have been identified in the literature [1]. This report has singled out nonlinearities at metal/metal interfaces as a topic for study. The first portion of the

report details an investigation of the IM generating potential of I-V nonlinearities in naturally occurring metal oxides. Phenomenon which could produce such nonlinearities include tunneling, space charge limited current flow, and thermionic emission. PIM generation by tunneling has previously been studied by Higa [2] and Chapman and Darlington [3] for operation at microwave frequencies and by Bond, Guenzer, and Carosella [4] for conduction between planar metal electrodes at UHF. Space charge limited current flow was suggested by Chapman and Darlington [3] as a possible PIM generator in high power microwave systems. The investigation presented herein is concerned with PIM generation by tunneling and space charge limited conduction phenomena in RF connectors at UHF. The second portion of the report details a study of the relationship between IM signal power signatures and the form of the IM generating nonlinearity.

The procedure adopted for IM signal power calculations is to utilize equations found in the literature to compute I-V data for the conduction phenomena being studied, under the assumed operating conditions. A least squares polynomial approximation routine is then applied to the computed I-V data to obtain a polynomial representation of the form

$$I = a_o + a_1 V + a_2 V^2 + \ldots\ldots + a_n V^n \qquad (1\text{-}4)$$

for the nonlinearity. IM product currents are obtained by substitution of the polynomial coefficients in an algebraic equation derived by Sea [5]. Finally IM signal powers are calculated from the IM product currents using equations for the circuit model of the CRC PIM measurement circuit [1]. This permits comparison of results with previously computed and measured data [1].

1.3 Report Organization

Chapter II is an overview of the theory pertaining to the formation and electrical characteristics of ohmic, blocking and neutral contacts at metal/metal-oxide interfaces. Equations representing the I-V characteristic of each contact type are presented with limited mathematical analysis. References for more detailed information are included.

PIM generation by conduction nonlinearities in thin metal oxide films is the subject of Chapter III. First, a unit equivalent electrical circuit similar to that used by Chapman and Darlington [3] for their investigation of tunneling is developed. Based upon the dimensions of a type N RF coaxial connector, multiple unit equivalent circuits in parallel are used to model the contact surfaces in a "minimum area contact" coaxial connector and a "maximum area contact" coaxial connector. The theory and equations of Chapter II, combined with computer programs developed previously [1], are then applied in the computation of the power of IM signals generated by tunneling at copper and aluminum connector contacts. An investigation into the possibility of IM generation by space-charge-limited conduction phenomena is also reported. The final section of the chapter is a summary and discussion of results.

In Chapter IV, the relationship between non-linear I-V characteristics and the computed power signatures of IM product signals generated as a result of two frequency RF excitation is studied. Four different computer generated, arbitrary nonlinearities are used as a basis for IM power calculations. The nonlinearities represent symmetrical

and non-symmetrical versions of I-V characteristics in which current rises rapidly with increasing voltage increments and those in which current rises in slowly decreasing increments to a limiting value as voltage increases. The computed signatures of PIM signals generated by the arbitrary non-linearities are compared with each other, with the results presented in Chapter III and with experimental and theoretical results presented in the report of August, 1979 [1].

Chapter V includes a summary, conclusions, and recommendations for further investigation.

CHAPTER II

Conduction Processes in Metal/Insulator/Metal Structures

2.1 Introduction

Many metal/metal interfaces are present in electrical and non-electrical portions of RF communications systems. Due to the natural formation of insulating or semiconducting metal oxides between metals, electrical conduction across such interfaces can become nonlinear and result in the generation of PIM under multi-frequency excitation. It is therefore of importance to understand metal/oxide/metal interface conditions that can lead to nonlinear conduction phenomena.

This chapter presents an overview of the theory pertaining to electrical conduction in symmetrical metal/insulator/metal and metal/semiconductor/metal structures with different contact types. Only limited mathematical analysis is included, but references to more detailed work are given.

Section 2.1 deals with conduction in structures in which two spacially separated ohmic contacts are made to an insulator. The conduction processes of tunneling and space charge limited current flow are discussed. The subject of Section 2.3 is conduction between

two neutral contacts separated by an insulator. Section 2.4 outlines processes which take place when contacts to an insulator are of the blocking type. Section 2.5 is a summary of the chapter.

2.2 Metal/Insulator/Metal Structures with Ohmic Contacts

2.2.1 Ohmic Contacts

An ohmic contact is formed [6] at a metal/insulator interface when the work function of the metal is lower than that of the insulator. The energy band diagrams of Fig. 2.1 illustrate conditions that exist at the interface before and after contact.

Prior to physical contact between the metal and the insulator, the band diagram is as in Fig. 2.1(a). The Fermi levels (E_F) in the two materials have different separations from the vacuum energy level, and the energy bands are flat. If contact is made [7] by means of a conduction path between the metal and the insulator at some point other than at the interface shown in the figure, the Fermi levels are forced into alignment, as in Fig. 2.1(b). In order to satisfy energy requirements at the interface, electrons from the metal are injected into the conduction band of the insulator. This results in the formation of a negative charge on the surface of the insulator near the interface, and a corresponding opposite positive charge on the metal surface. An electric field ($\vec{E}$) is thus created in the metal/insulator gap, (Fig. 2.1.(b)). As the width of the gap is decreased, the surface charges grow, increasing the magnitude of the electric field which results in a distortion of the energy bands in the insulator as shown in the figure. When contact is made the energy barrier presented by the air gap disappears, leaving a reservoir of electrons in the insulator near the interface to supply current as demanded by the bias conditions. As shown in Fig. 2.1(c), the contact potential (Φ_o) is equal to the difference in magnitude between the

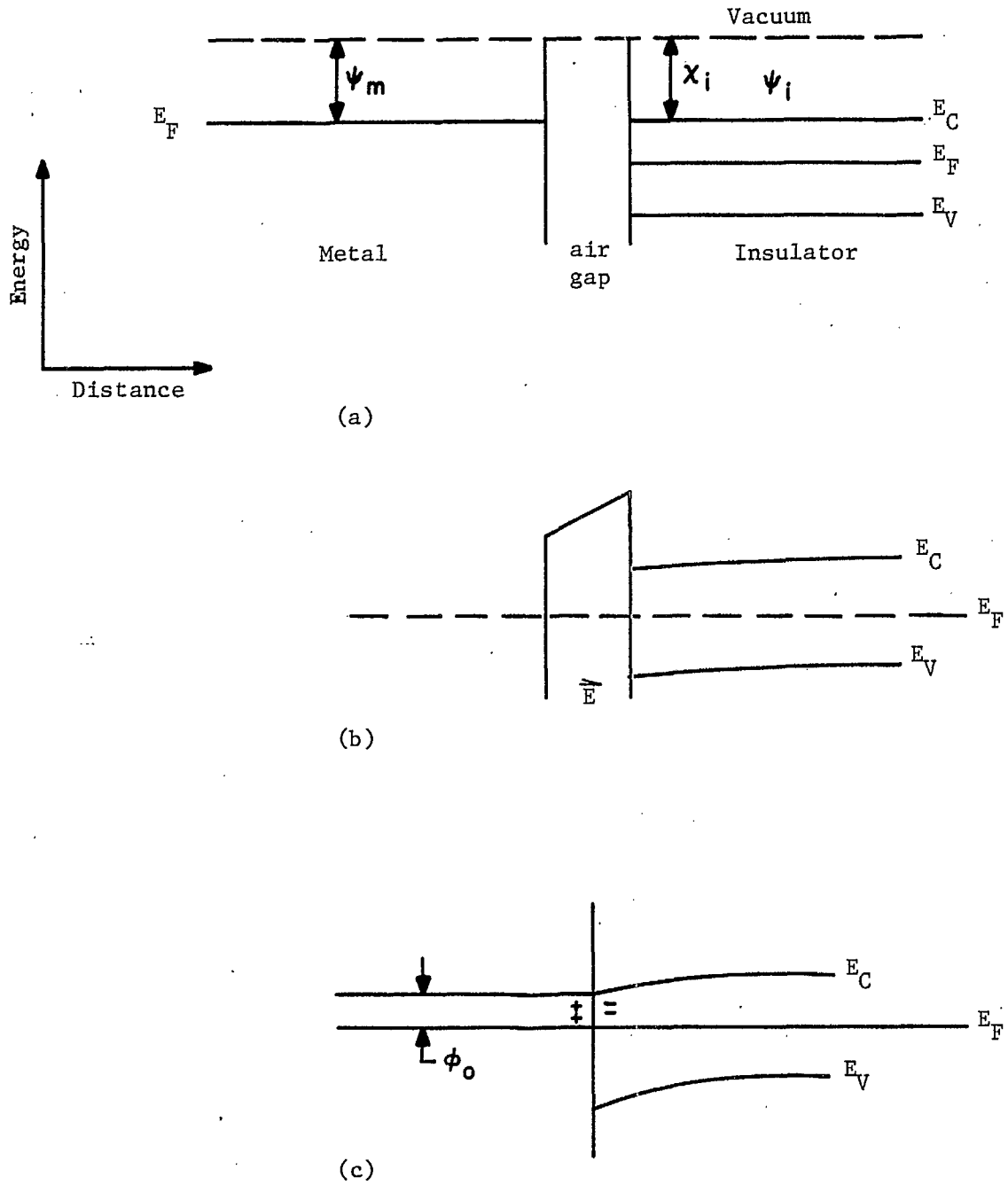

Fig. 2.1 Energy band relationships at an ohmic contact. ((a), (b), (c) - see text).

work function (ψ_m) of the metal and the electron affinity (χ_i) of the insulator, or

$$\Phi_o = \psi_m - \chi_i \qquad (2\text{-}1)$$

2.2.2 The Tunneling of Electrons Through the Potential Barrier Represented by an Insulator Between two Ohmic Contacts.

Consider a metal/insulator/metal structure (Fig. 2.2) in which spacially separated ohmic contacts are made to the insulator. When image forces [7, 8] are accounted for, the energy band diagram for the structure might appear as that in Fig. 2.3 which represents energy relations in an aluminum/aluminum-oxide/aluminum junction.

From classical physics [3, 9], it would be anticipated that an electron on either side of the potential barrier would have to acquire an energy, $E = mc^2$, greater than the barrier height in order to flow through the insulator between contacts. From quantum mechanical considerations, however, there exists a finite probability [$P(E_x)$], arrived at through solution of Schrodinger's Equation, that an electron can "tunnel" through the barrier at a constant energy level. The probability of tunneling increases with increasing electron energy (bias voltage), and as an inverse function of the height and width (effectively the insulator thickness [3]), of the potential barrier.

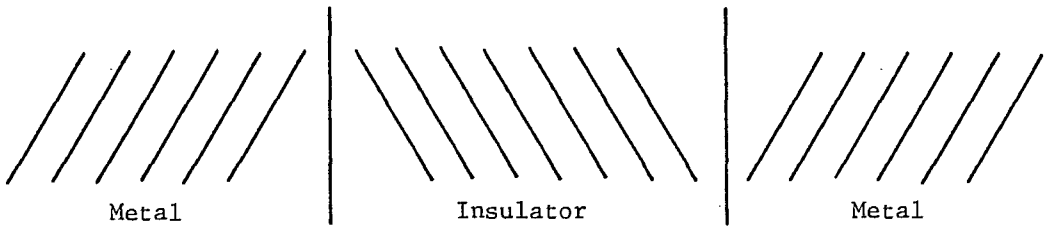

Fig. 2.2 Pictorial diagram of a conducting structure in which an insulator is sandwiched between two metals.

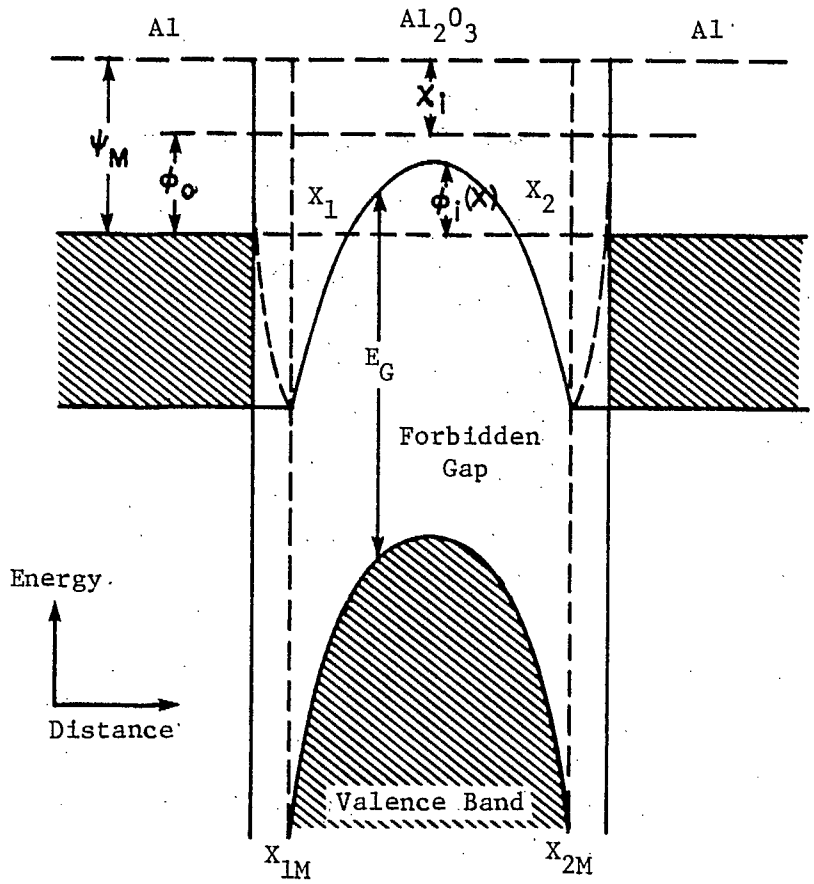

Fig. 2.3. Schematic representation of the energy relationships at a zero biased $Al-Al_2O_3-Al$ junction, including short range forces, (From Dubey [8]).

The density of electron current flowing between two metals separated by an insulator [6, 8] is given by:

$$J = \frac{4\pi em}{h^3} \int_0^{\infty} dE[f_c(E) - f_a(E)] \int_0^{E} P(E_x)dE_x, \qquad (2\text{-}2)$$

where,

$$f_c = [1 + e^{(E-E_F)/K_oT}]^{-1}$$

and

$$f_a = [1 + e^{(E+eV-E_F)/K_oT}]^{-1}$$

are the electron distributions in the cathode and the anode respectively.

E_x is the x-directed electron energy

K_o is Boltzmans' constant

E is the energy of the electron

and E_F is the energy of the system Fermi level.

Dubey [8] has shown that for a potential barrier which has a parabolic shape, equation 2-2 can be rewritten as:

$$J = \frac{4\pi meK_oT}{h^3} \int_0^{\infty} P(E_x) \times \mathrm{Ln}\left[\frac{1+\exp[(\S_m-E_x)/K_oT]}{1+\exp[\S_m-E_x-eV)/K_oT]}\right]dE_x \qquad (2\text{-}3)$$

where $\S_m$ denotes the Fermi level of the anode

and V is the applied voltage.

After deriving an expression for $P(E_x)$ Dubey was able to further reduce equation 2-3 to the more tractable form;

$$J = \frac{4\pi me}{h^3 B^2} \exp(-A\Phi_i^{1/2}) \left[\frac{\pi B K_o T}{\sin(\pi B K_o T)}\right] \times \left[1-\exp(-BeV)\right] \ (A/m^2), \quad (2\text{-}4)$$

where

$$m = \text{electron mass} = \frac{\text{electron energy}}{c^2}$$

$$= \frac{0.511 \times 10^6 \text{ eV}}{(3 \times 10^8 \text{ m/s})^2}$$

$$= 5.6857 \times 10^{-12} \frac{\text{eV s}^2}{\text{m}^2}$$

h = Plancks' constant = 4.1356×10^{-15} eV.s

$\hbar = h/2\pi$

e = electron charge = 1.602×10^{-19} coulombs

K = optical (high frequency) permittivity of the oxide

K_o = Boltzman's Constant = 8.6171×10^{-3} eV/K

$B = A/(2\Phi_i^{1/2})$

---

* B as defined in Dubey's article [8] is a misprint and must be as above to make the units correct.

$$A = 2(2m)^{1/2}\left[(X_2-X_1)/\hbar\right]$$

$$X_1 = \frac{3.00}{K\Phi_o}$$

$$X_2 = d\left\{1-\frac{(23.04/Kd)}{[3\Phi_o + (10.02/Kd) - 2eV]}\right\} + X_1 \text{ , for } eV<\Phi_o$$

$$X_2 = \left[\Phi_o - (14.02/Kd)\right] \times (d/eV), \quad \text{for } eV>\Phi_o$$

eV = bias in electron volts

d = oxide thickness in Angstroms

$$\Phi_o = \Psi_m - \chi_i \quad \text{where} \quad \chi_i \simeq (\Psi_i - E_g/2)$$

$$\overline{\Phi}_i = \Phi_o - \frac{eV}{2d}(X_1 + X_2) - \frac{2.88}{K(X_2-X_1)} \quad \text{Ln}\left[\frac{X_2(d-X_1)}{X_1(d-X_2)}\right]$$

$$+ \frac{2.88\,\eta}{K(X_2-X_1)}\left[\left[\frac{1}{X_1} - \frac{1}{X_2} + \frac{1}{(d-X_2)} - \frac{1}{(d-X_1)}\right]\right.$$

$$\left. + \frac{2}{d}\,\text{Ln}\left[\frac{X_2(d-X_1)}{X_1(d-X_2)}\right]\right]$$

$$\eta = \frac{2.88}{4KW_a}$$

and $W_a = \Psi_m + E_F \simeq 5.0$ for Aluminum

A computer program similar to that presented by Chapman and Darlington* [3] was written to compute tunneling current densities in accordance with equation 2-4. This program was later modified for use in passive intermodulation calculations and can be seen in modified form as Program TUNEL in Appendix A. Tables 2.1 and 2.2 show tunnel current densities computed by TUNEL for various oxide thicknesses and voltages applied to aluminum/aluminum-oxide/aluminum and copper/cuprous-oxide**/copper structures respectively. The tables show that current density has a very sensitive inverse dependence on oxide thickness and a direct dependence on applied voltage.

It is clear from eqn. 2-4 that the current voltage relationship for this type of tunneling is very nonlinear. Under the proper conditions of RF excitation, it is believed [1, 2, 3, 4] that this phenomenon could generate passive intermodulation signals at interfering power levels.

---

* A plus sign in line 210 of the Philco Ford report [3],was found to be in error and replaced by a minus sign.

** Note that pure cuprous oxide is a p-type semiconductor, and would not form an ohmic contact with copper. It has been shown [3, 10], however, that impurities near the copper/cuprous-oxide interface are sufficient to make the oxide an n-type semiconductor, and permit the establishment of an ohmic contact.

Table 2.1

Tunnel Current Density (A/cm^2) as a Function of Oxide Thickness ($Al-Al_2O_3-Al$)

Voltage(V)	.001	.01	.1	1
Thickness (Å)				
10	1.78×10^{3}	1.78×10^{4}	1.85×10^{5}	6.5×10^{6}
20	1.27×10^{-2}	1.28×10^{-1}	1.37	3.2×10^{2}
30	9.63×10^{-8}	9.68×10^{-7}	1.09×10^{-5}	2.19×10^{-2}
40	7.8×10^{-13}	7.85×10^{-12}	9.46×10^{-11}	—
50	6.85×10^{-18}	6.9×10^{-17}	9.0×10^{-16}	2.0×10^{-10}

Table 2.2

Tunnel Current Density (A/cm^2) as A Function of Oxide Thickenss ($Cu-Cu_2O-Cu$)

Voltage(V)	.001	.01	0.1
Thickness (Å)			
10	4.09×10^{5}	4.015×10^{6}	3.17×10^{7}
20	1.16×10^{3}	1.18×10^{4}	1.54×10^{5}
30	2.96	3.05×10^{1}	5.14×10^{2}
40	1.19×10^{-2}	1.26×10^{-1}	3.58
50	4.3×10^{-5}	4.1×10^{-4}	5.7×10^{-3}

2.2.3 Space Charge Limited Current Flow in Structures Where Spacially Separated Ohmic Contacts are made to an Insulator

If ohmic contacts are made to an insulator, [6,11-19] current flow can result from the injection of electrons into the conduction band of the insulator. The conduction process, however, is limited by the establishment of a space charge in the insulator, which results in a non-linear relationship between current and applied voltage.

Consider again the metal/insulator/metal structure of Fig. 2.2. If a bias voltage is applied, electrons are injected from the cathode, and form a space charge in the insulator [6,11]. The density of space charge is highest near the cathode, and gradually decreases, becoming very small at the anode.

If it is assumed [11] that the insulator (metal-oxide) is trap-free, and that the current is primarily due to the established electric field, limited mathematical manipulation of Poisson's Equation leads to the current density-voltage relationship.

$$J = \frac{9}{8} \frac{\mu\varepsilon}{d^3} V^2 , \qquad (2\text{-}5)$$

where μ = electron mobility in the insulator

ε = the static value of permittivity for the insulator

d = insulator thickness

V = applied voltage.

More recent investigations [6, 16-19] have made use of digital computers to solve the complicated equations which result when the effects of energy traps and diffusion current are considered. The result is that the I-V characteristic has been found to be composed of three regions [6]. At very low applied voltages, the characteristic is linear, or ohmic. Then, if energy traps are present in the insulator, a lesser square law relationship is followed until all the traps are filled. Finally after the trap-filled limit is reached, the originally predicted square law relationship of eqn. 2-5 is followed. If the contacts to both sides of the insulator are of the same metal, the I-V characteristic is symmetrical about zero volts.

To facilitate space charge current calculations, Lindmayer, Reynolds, and Wrigley [11] have plotted a normalized I-V characteristic (figures 2.4 and 2.5) that can be applied to any symmetrical structure in which ohmic contacts are separated by an insulator if the appropriate parameters are used to compute the normalized variable (δ or γ) for use in the figures,

where $$\delta = \frac{d^3 J \, (q/KT)^2}{\varepsilon \mu} \qquad (2\text{-}6)$$

and $$\gamma = \frac{qV}{KT} \qquad (2\text{-}7)$$

Consider now a copper/cuprous-oxide/copper structure of 10,000 Angstroms in area, in which the oxide thickness is 10 Å. When the appropriate constants from Appendix B are substituted in

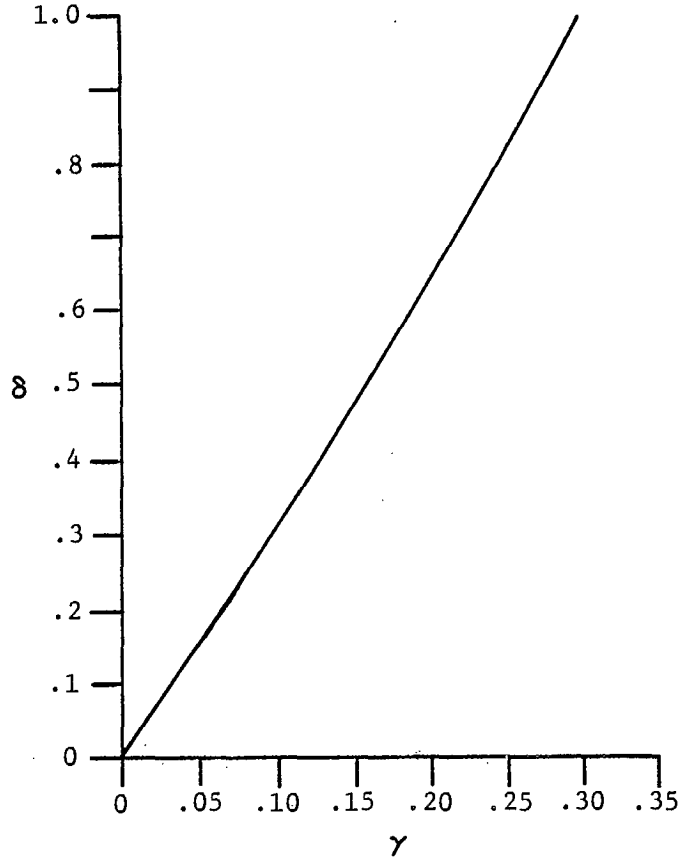

Fig. 2.4. Normalized I-V characteristic for space-charge-limited current flow in a symmetrical metal/insulator/metal structure. (1.3 mV $\leq$ V $\leq$ 9.1 mV, at 20°C). (From Lindmayer, Reynolds, and Wrigley [11]).

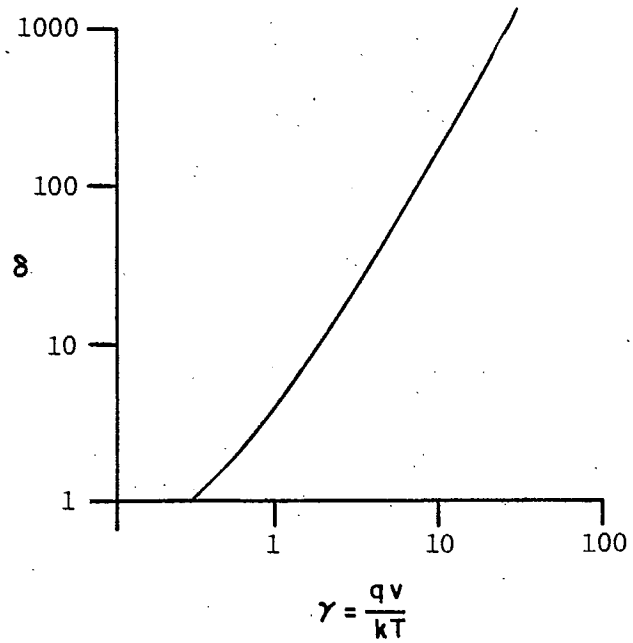

Fig. 2.5. Normalized I-V characteristic for space-charge-limited current flow in a symmetrical metal/insulator/metal structure, (2.6 mV $\leq$ V $\leq$ 2.6V, at 20°C). (From Lindmayer, Reynolds and Wrigley [11]).

eqn. 2-7, current density in the $Cu/cu_2O/Cu$ structure is given by

$$J = \frac{(1.0998 \times 10^{-13})\delta}{2} \quad A/cm^2$$

The I-V characteristic of Fig. 2.6 results when J and V are read from figures 2.4 and 2.5. This curve is clearly nonlinear and indicates that space charge limited current flow at oxidized metal-metal interfaces is a possible source for Passive Intermodulation.

It should be noted that although tunneling and space charge limited current flow require the same metal/insulator/metal energy relationships, calculations (Ch.III) show that the dependence of space charge limited current flow on electron mobility restricts this phenomenon to a much lower probability of occurrence in naturally occurring metal oxides.

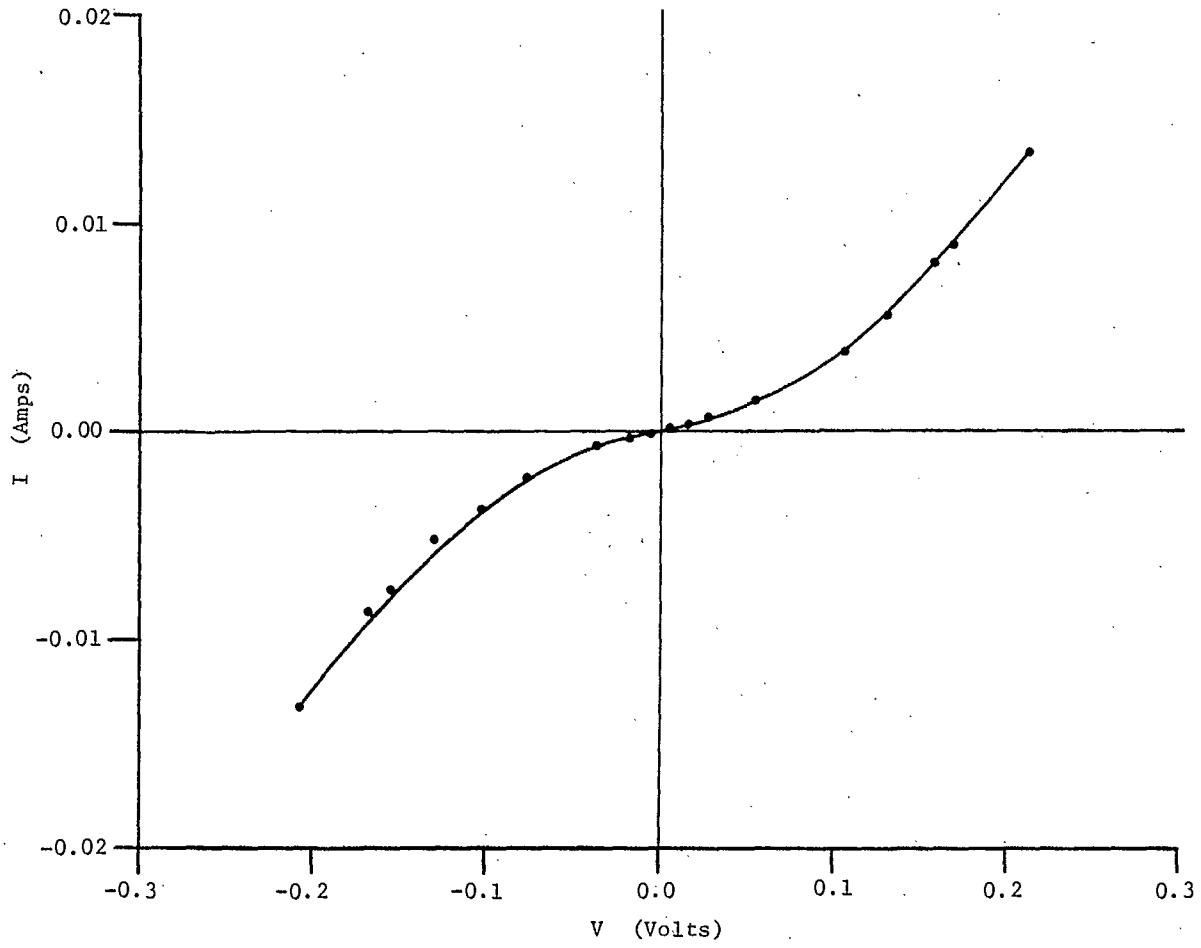

Fig. 2.6 I-V characteristic for space-charge-limited current flow in a copper/cuprous-oxide/copper structure. (Area = 10,000 Å, Oxide thickness = 10 Å).

2.3 Metal/Insulator/Metal Structures with Neutral Contacts

2.3.1 Neutral Contacts

When a metal with work function (Ψ_m) makes contact [6] with an insulator which has an equivalent work function ($\Psi_i = \Psi_m$) the vacuum and Fermi levels in the metal and the insulator line up naturally without the necessity of charge transfer. Since no space charge exists within the insulator, no energy band distortion occurs and, on contact, the energy bands in the insulator remain flat, all the way to the metal-insulator interface (Fig. 2.7). As for the ohmic contact, the height of the interfacial energy barrier is:

$$\Phi_o = \Psi_m - \chi_i . \qquad (2\text{-}8)$$

2.3.2 Electron Conduction Through a Metal/Insulator/Metal Structure with Neutral Contacts

When two spacially separated neutral contacts are made to an insulator, conduction through the structure is ohmic for low bias voltages [6]. There is a limit, however, to the current that can be supplied by the cathode, known as the thermionic saturation current. When this limit has been reached, conduction ceases to be ohmic and becomes electrode limited. At this point, current density is a nonlinear function of the bias-induced electric field within the insulator.

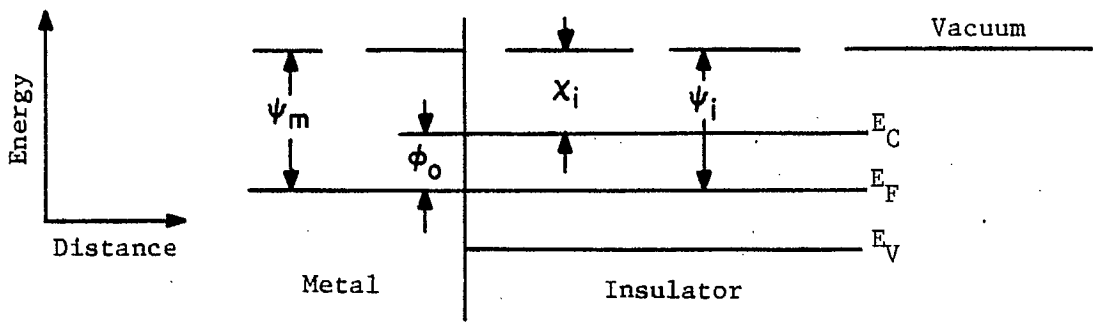

Fig. 2.7 Energy relationships at a zero biased neutral metal/insulator contact.

In RF systems, the bias voltage values at interfaces with typical dimensions for UHF operation would not be sufficient for nonlinear conduction. Naturally occurring neutral contacts are not, therefore, considered to be potential sources for IM generation.

2.4 Metal/Insulator/Metal Structures with Blocking Contacts

2.4.1 Blocking Contacts

A blocking contact is formed at a metal/insulator interface [6] when the work function of the metal is greater than the work function of the insulator. The energy band diagrams of Fig. 2.8 illustrate the processes that take place during the establishment of contact.

Before contact is made, the band diagram is as shown in Fig. 2.8(a). The energy bands in both materials are flat, and the Fermi levels within the materials are at different energies relative to the vacuum level. If contact is made other than at the interface shown in the figure, the Fermi levels are forced into alignment, and the band diagram is altered, becoming as shown in Fig. 2.8(b). To maintain thermodynamic equilibrium at the interface, electrons flow via the unshown conduction path from the insulator into the metal. A negative charge is thus formed on the metal surface and an equal positive charge is formed on the surface of the insulator. This leads to the establishment of an electric field in the metal-insulator gap, and is accompanied by a deformation of the energy bands, also shown in Fig. 2.8(b). As the gap is narrowed, the charges on the material surfaces increase in magnitude, and the field becomes greater, causing increased bending of the bands in an upwards direction toward the interface. When the metal-insulator gap is comparable with inter-atomic distances, the potential barrier presented by the air gap disappears, and the

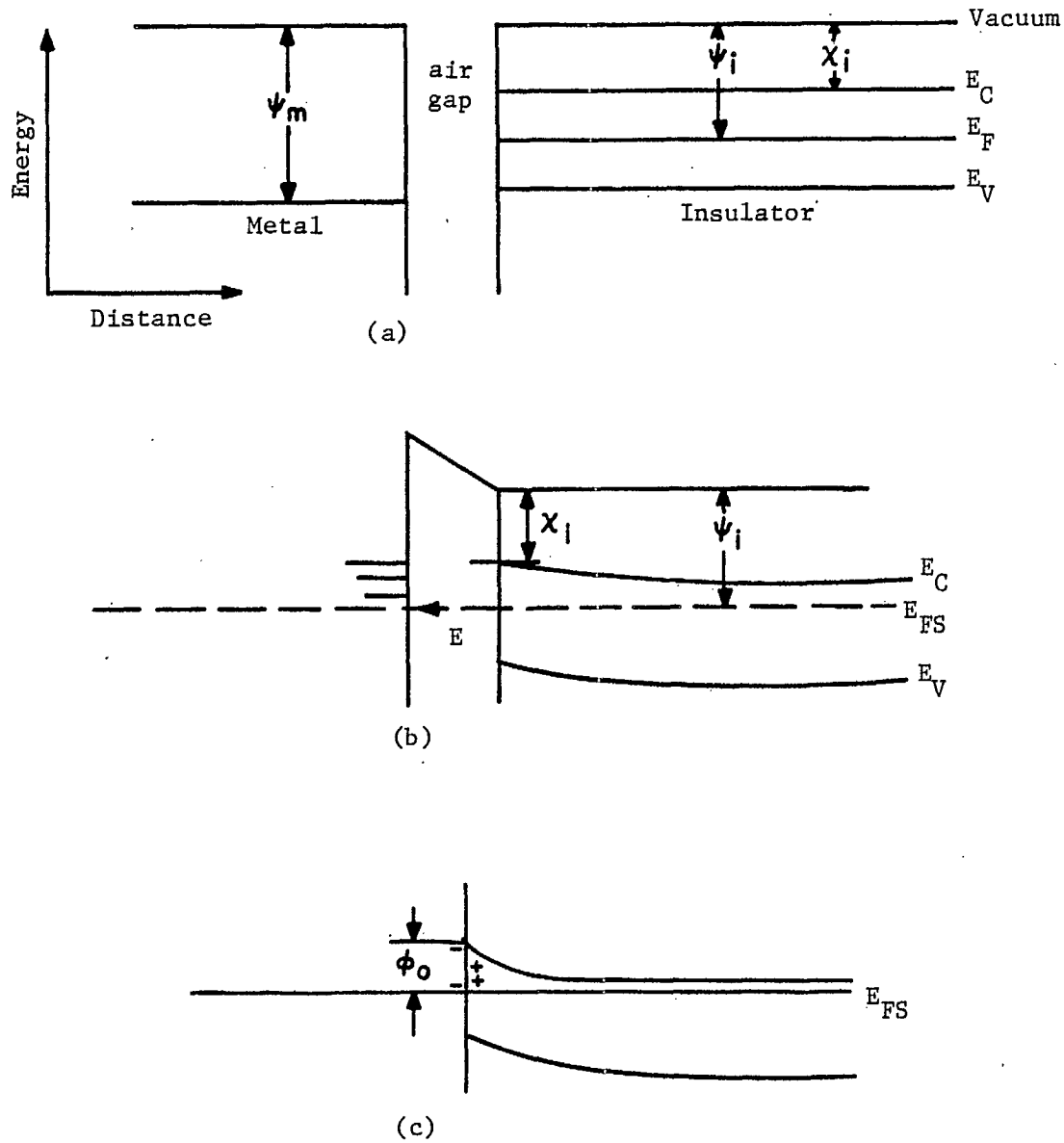

Fig. 2.8. Energy band relationships at a blocking contact. ((a), (b), (c) - see text).

barrier at the interface has a magnitude given by

$$\Phi_o = \Psi_m - \chi_i. \tag{2-9}$$

2.4.2 Electron Tunneling Through the Potential Barrier Presented by an Insulator between Blocking Contacts

If spacially separated blocking contacts are applied to an insulator, Schottky barriers form at the metal/insulator interfaces, and the energy band diagram for the structure is as shown in Fig. 2.9(a). When a bias voltage is applied, the negative charge on the cathode metal surface is increased, and that on the anode metal surface is decreased. Hence, the potential barrier at the cathode becomes greater, while that at the anode is diminished, (Fig. 2.9(b)). If the width of the barrier at the cathode is sufficiently thin, tunneling can take place [6] much the same as that described in Section 2.2.2.

2.4.3 Thermionic Emission of Electrons at Blocking Contacts

Consider again the structure of Fig. 2.9(b). If the potential barrier at the cathode is too thick to permit tunneling [6] or if the temperature is sufficiently high, current flow is limited principally by the rate at which electrons are thermally excited over the interfacial barrier and into the insulator conduction band.

In order [6] to determine the current flowing in the system, the lower limit of integration in eqn. 2-2 should be set to the interfacial barrier height, Φ_o at the cathode and $P(E_x)$

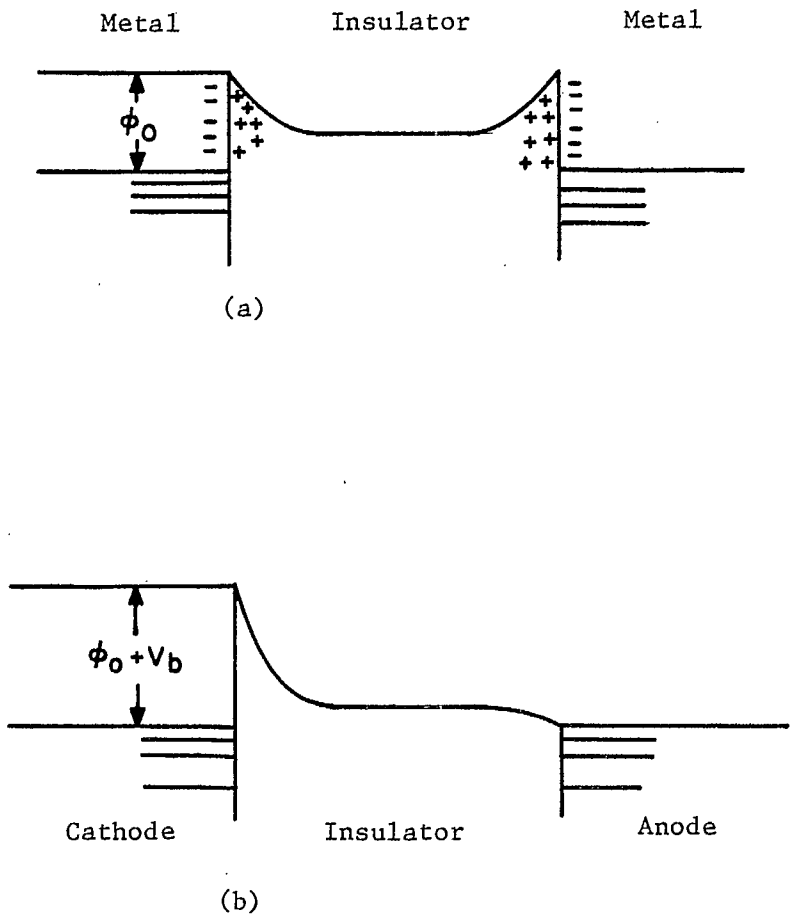

Fig. 2.9 Energy relationships at a structure formed by two blocking contacts separated by an insulator. (a) zero bias, (b) bias voltage, (V_b) applied.

should be set to unity. Integration then yields:

$$J = \frac{4\pi m e k_o^2 T^2}{h^3} \exp\left[\frac{-\Phi_o}{K_o T}\right] \qquad (2\text{-}10)$$

Image forces at the Schottky barrier, however, lower its height by an amount

$$\Delta\Phi = \left[\frac{(eV + \Psi_m - \Psi_i)e^7 N_d}{2(8\pi)^2 K^{3/4}}\right]. \qquad (2\text{-}11)$$

If $(\Phi_o - \Delta\Phi)$ is substituted for Φ_o in (2-10), the equation for current density becomes:

$$J = 120T^2 \exp\left\{\frac{-\Phi_o - 8.26\times10^{-6}\,[N_d(V+\Psi_m-\Psi_i)/K^3]^{1/4}}{K_o T}\right\} \text{A/cm}^2 \qquad (2\text{-}12)$$

where,

Φ_o, Ψ_m, Ψ_i and KT are in eV,

N_d is the donor impurity density (cm^{-3}) in the insulator (TYP $10^{15} < N_d < 10^{21}$)

K is the optical value of permittivity for the insulator.

K_o is Boltzman's constant

and V is applied bias voltage.

It should be noted that the conduction process is electrode limited, making the current density independent of insulator thickness. Eventually, however, at some transitional voltage, the process becomes bulk limited, and thickness dependent [6].

The exponential dependence of current density on applied voltage for thermionic emission is yet another potential source for passive intermodulation generation at metal-oxide-metal interfaces in multifrequency RF systems.

2.5 Metal/Semiconductor Contacts

Ohmic and blocking contacts can also be formed [3, 7] when a metal makes intimate contact with a semiconductor. For n-type semiconductors, energy relations for the different contacts are identical with those required at metal/insulator contacts. For p-type semiconductors however, relationships are reversed. That is, an ohmic contact is formed when the work function of the p-type semiconductor is lower than that of the metal. A blocking contact is formed when the semiconductor has a greater work function.

2.6 Summary

The second section of this chapter began by stating that an ohmic contact is formed when a metal makes intimate contact with an insulator, the work function of which is greater than that of the metal ($\Psi_i > \Psi_m$). It was shown that, at this type of contact, the electric field at the metal/insulator interface causes the energy bands in the insulator to bend downwards towards the interface, resulting in a metal/insulator potential barrier of magnitude $\Psi_m - \chi_i$.

Two types of nonlinear conduction in structures formed by an insulator between two ohmic contacts were discussed. Reference was made to works by Dubey [8] and Simmons [6], which show that tunneling through the potential barrier presented by the insulator could result in a nonlinear I-V characteristic. Dubey's tunneling equation was presented, and programmed in computer program TUNEL. Computations for tunneling through $Al/Al_2O_3/Al$ $Cu/Cu_2O/Cu$ structures showed that tunnel current density is a very sensitive inverse function of oxide thickness and a direct function of applied voltage. The I-V characteristic for tunneling was identified as being sufficiently nonlinear for passive intermodulation generation at hardware interfaces in UHF communications systems.

Section 2.2.3 was a discussion of space charge limited current flow between ohmic contacts to an insulator. References were made to papers by Lindmayer, Reynolds and Wrigley [11], and Simmons [6], which show the I-V characteristic for this phenomenon to be comprised of three regions. At low bias voltages, the characteristic is linear. If energy traps are present, a lesser quadratic region follows. Finally, at higher current the characteristic exhibits a more sensitive quadratic dependence on voltage. The I-V characteristic for space charge limited current flow ($.52\ mV \leq V \leq 208\ mV$) in a structure comprised of copper electrodes 10,000 square angstroms in area, separated by 10 Å of cuprous oxide (Cu_2O) was presented. It was noted that the dependence of this phenomenon on electron mobility in the insulator results in a lower probability of space charge limited conduction than that of tunneling in components of communications systems which are fabricated from metals upon which insulating oxides form. Further, the linear portion of the space charge limited characteristic for low voltages reduces the potential for passive intermodulation generation at power levels (200W) utilized in UHF systems.

Neutral contacts were considered next. This type of contact forms between a metal and an insulator which have equal work functions. At such contacts there is no space charge in the insulator, and therefore no distortion of the energy bands. The magnitude of the interfacial potential barrier is $(\Psi_m - \chi_i)$. Conduction is ohmic in structures formed by an insulator between neutral contacts until a threshold voltage is reached, beyond which current flow is electrode limited and non-linearly dependent upon

the bias-induced electric field in the insulator. Voltages developed at metal/insulator/metal interfaces in UHF communications systems, however, would be below those required for nonlinear conduction. Neutral contacts were therefore discounted as possible passive intermodulation generators.

Blocking, or Schottky barrier contacts were considered last. For this type of contact it is necessary that the insulator has a lower work function than that of the metal. When intimate contact is made, a positive charge accumulates in the insulator near the interface. This induces an electric field which results in an upward bending of energy bands in the insulator toward the metal contact. The magnitude of the contact potential is $\Psi_m - \chi_i$. In metal/insulator/metal sandwiches with blocking contacts, tunneling of the type encountered in structures with ohmic contacts can occur at the cathode-insulator barrier, providing the barrier is sufficiently thin. When the barrier is too thick to permit tunneling, thermionic emission becomes the dominant conduction mechanism. The I-V characteristic for this phenomenon shows a rapidly increasing nonlinear current response at low voltages (<2 V), leading to the conclusion that thermionic emission could contribute to passive intermodulation generation.

As a final note to this chapter, a comment should be added with regard to the symmetry of the metal/insulator/metal structures considered. In typical RF systems, it is probable that non-symmetrical structures are most prevalent as a result of interfaces between dissimilar metals, and impurities in naturally

occurring oxides. At the low voltages expected (Ch.III) at metal interfaces in UHF systems, however it has been reported [6, 27], that, at least for tunneling, the symmetry of the I-V characteristic is preserved even under conditions of dissimilar contacts, provided the contacts are of the same electric contact type.

CHAPTER III

The Generation of Passive Intermodulation Interference by Nonlinear Conduction Processes in Naturally Occurring Oxides at Inter-Metallic Contacts.

3.1 Introduction

A number of reports [1, 21] have cited experimental evidence that corrosion at metallic contacts leads to an increase in the passive generation of intermodulation product signals in multifrequency RF systems. It is the objective of work reported in this chapter to determine if the increased spurious signal generation could be the result of conduction through tunneling or space charge limited nonlinearities in structures in which ohmic contacts are made to naturally occurring metal oxides. Calculations are restricted to contacts of surface area similar to that of the inner and outer conductor contacts in a type N coaxial connector. Operation in the UHF (300-400 MHz) frequency band is assumed.

Section 3.2 details the development of a contact model similar to that used by Chapman and Darlington [3] for their tunneling calculations. An investigation into the generation of Passive Intermodulation signals by tunneling at the inner and outer contacts in RF connectors is reported in Section 3.3.

Section 3.4 discusses the possibility of passive intermodulation generation by space charge limited current flow. The chapter closes with a summary and discussion of results.

3.2 Development Of A Unit Equivalent Circuit For Use In Metal-Metal Contact Models.

Due to the unavoidable microscopic irregularities of all metallic surfaces, one can consider a metal/metal contact to be comprised of a random scattering of points ("A" spots) at which either actual metallic contact is made, or only a thin oxide layer separates the conductors interspersed with regions where the metals are separated by oxides of much greater thickness (Fig. 3.1). A single "A" spot [3, 22] might be modelled as shown in Fig. 3.2. Fig. 3.3 shows the equivalent electrical circuit. The inductance of the contact filament is represented by L. R(V) represents the nonlinear voltage controlled resistance of the thin oxide separating the filament ends. C_g and C_v respectively represent the capacitances of the thin oxide region (gap between filament ends) and the thick oxide (void) surrounding the contact filament.

Realistically, a random scatter of "A" spots covers the contact surface area. For simplicity in this study, however, a fixed geometrical pattern as shown in Fig. 3.4 will be assumed [3] In Fig. 3.2, let;

$r = 50\mathring{A}$ = radius of contact filament

A = contact spot area = $7854\mathring{A}^2$

$2T = 20\mathring{A}$ = thickness of oxide between filament ends

$\ell = 490\mathring{A}$ = contact filament length

$D = 1000\mathring{A}$ = width of void.

Then, values for the components of the unit equivalent circuit can be calculated as detailed below.

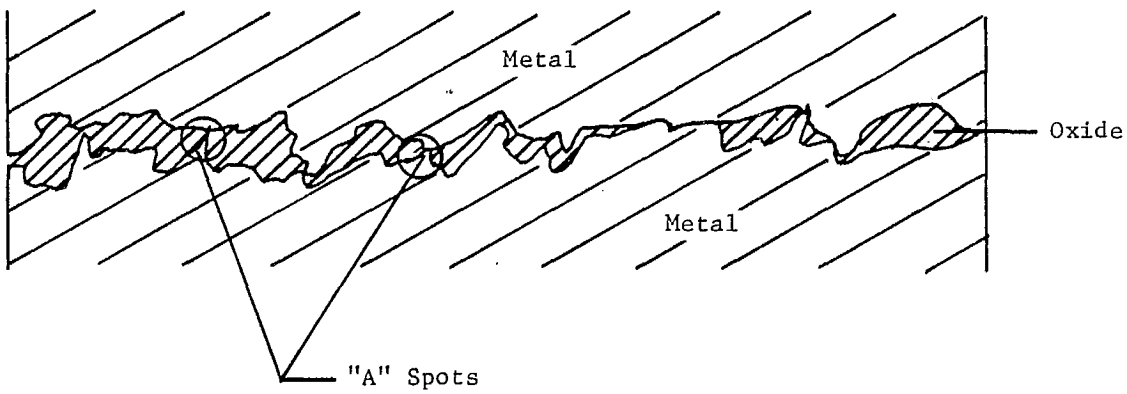

Fig. 3.1. Pictorial diagram of a contact between two oxidized metal surfaces.

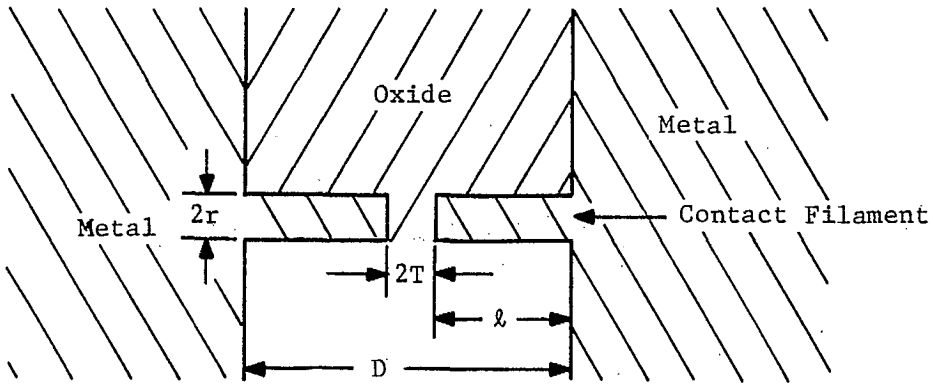

Fig. 3.2. Model of a single "A" spot.

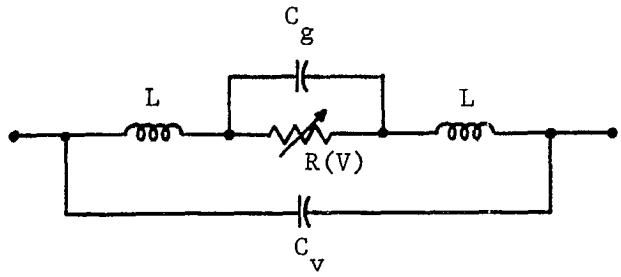

Fig. 3.3. Equivalent circuit for a single "A" spot, (From Chapman and Darlington [3]).

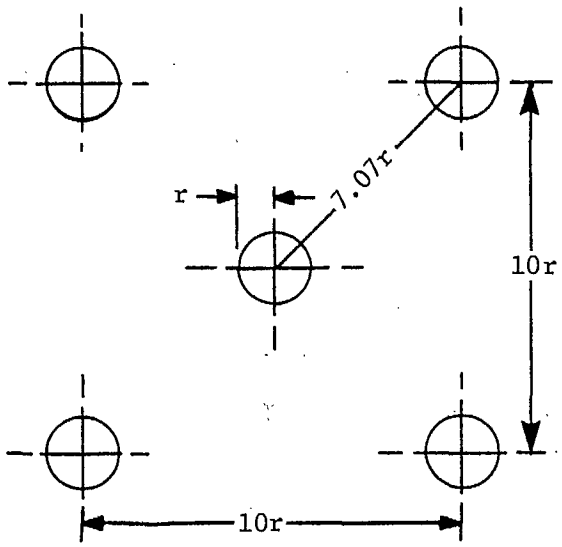

Fig. 3.4. Fixed geometry for the position of "A" spots at the metal/metal contact.

(i) Calculations for L:

From the Radio Engineering Handbook [23], the inductance at UHF of a straight round wire of length (ℓ) and diameter (d) is given by the equation:

$$L = 2 \times 10^{-3} \times \ell(\text{cm}) \left[2.303 \log_{10} \left(\frac{4\ell}{2r}\right) - 0.988\right] \mu H \qquad (3\text{-}1)$$

Substitution of the assumed dimensions yields

$$L = 1.95 + 10^{-14} \text{ H}$$

Then at 400 MHz, the inductive reactance of each contact filament is;

$$X_L = 4 \times 10^{-5} \text{ ohms}.$$

(ii) Calculations for C_g

Assuming a parallel plate geometriy,

$$C = \frac{\varepsilon(\text{Plate area})}{\text{width of gap between filament ends}}. \qquad (3\text{-}2)$$

For cuprous oxide, $\varepsilon_r = 12$, and for aluminum oxide $\varepsilon_r = 8\text{-}12$. These calculations will therefore use 12 as a standard value. Substitution in (3-2) gives;

$$C_g = 4.17 \times 10^{-18} \text{F}.$$

At 400 MHz,

$X_{c_g} = 9.54 \times 10^7$ ohms.

(iii) Calculations for C_v

The area of the void $= 50\ r^2 - \pi r^2 = 46.86\ r^2$.

Substitution in (3-2) gives;

$$C_v = 1.25 \times 10^{-18} F.$$

At 400 MHz.,

$$X_{c_v} = 3.20 \times 10^8 \text{ ohms.}$$

Since X_L is small in comparison with X_{c_g} and X_{c_v}, it can be omitted from the circuit model, which then reduces to R(V) in parallel with an equivalent capacitance, $C = (C_g + C_v)$, as in Fig. 3.5.

At 400 MHz,

$X_c = 7.35 \times 10^7$ ohms.

This "A" spot equivalent circuit will be used in the following sections as the basic unit in models for complete connector contact

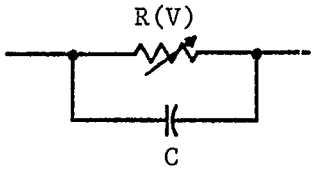

Fig. 3.5. Reduced equivalent circuit for an "A" spot at UHF.

surfaces.

3.3 Calculations Concerning the Power of Passive Intermodulation Signals That Could be Generated as a Result of Tunneling Phenomena in Coaxial Connectors

In this section, coaxial connectors similar in dimensions to a type N connector, and manufactured from (a) copper or (b) aluminum will be considered as circuit components which generate passive intermodulation in a two carrier test circuit. It will be assumed that the test circuit is comprised of a transmitter and receiver coupled through a duplexer and a single coaxial connector to a 50 ohm dummy load, as shown in Fig. 3.6.

Since copper and aluminum both have lower work functions than their respective oxides (Cu_2O* and Al_2O_3), metal/metal-oxide/metal structures with energy relationships as described in Section 2.2.1 of Chapter II could form in connectors manufactured from these materials. Under the proper conditions of energy and oxide thickness, tunneling could take place in metal/oxide/metal structures formed at the connector contact surfaces, with the possible generation of passive intermodulation signals due to multi-frequency excitation. Under the assumption that such spurious generation take place, the power of resulting passive intermodulation signals will be calculated. The maximum current density carried by each "A" spot (Fig. 3.5) of contact models for

---

* Pure Cu_2O is a p-type semiconductor. Impurities near the metal/oxide interface, however, make that region of oxide N type. This results in an ohmic contact.

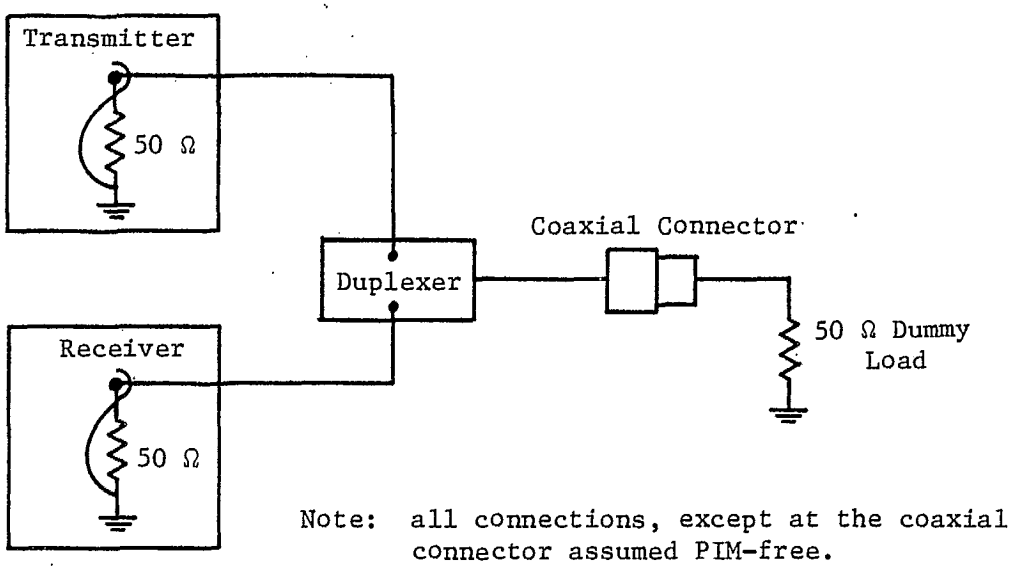

Fig. 3.6. Passive intermodulation test circuit block diagram.

connectors having estimated maximum and minimum contact areas is computed, and program TUNEL (Appendix A) is used to find tunnel voltages corresponding to current densities up to the calculated maximum. I-V characteristics for the total contact models are then formed by simply multiplying the single spot current densities by the total number of "A" spots on each contact. The I-V relationships are represented by least squares polynomial approximations, the coefficients of which are used in program IMPWR, [1] (Appendix A) leading to the calculation of intermodulation signal powers.

3.3.1 Connector Geometries and Contact Models

Figure 3.7 shows MIL Spec. drawings of RF type N male and female connectors. From lab measurements on RF connectors, the diameter of the centre conductor pin was found to be on the order of 0.0635 cm* (25 thousandths of an inch) and that of the outside of the female outer conducter contact ring was found to be 0.762 cm (308 thousandths of an inch). Due to the bevel on the connector contacts (Fig. 3.8) connection is not made over the entire contact surface, and contact area varies from connector to connector, and with wear. This report therefore deals with connectors which have contacts of lengths considered to be at the extremes. Section 3.3.2 is concerned with connectors which have

---

* The lab measurement of centre pin diameter was made and used in the analysis prior to receipt of the MIL Spec dimensions and is probably for a 75 ohm connector. The wide range assumed for possible contact lengths, however ensures that connectors with MIL Spec dimensions would generate Passive Intermodulation within the range computed for maximum and minimum area connectors.

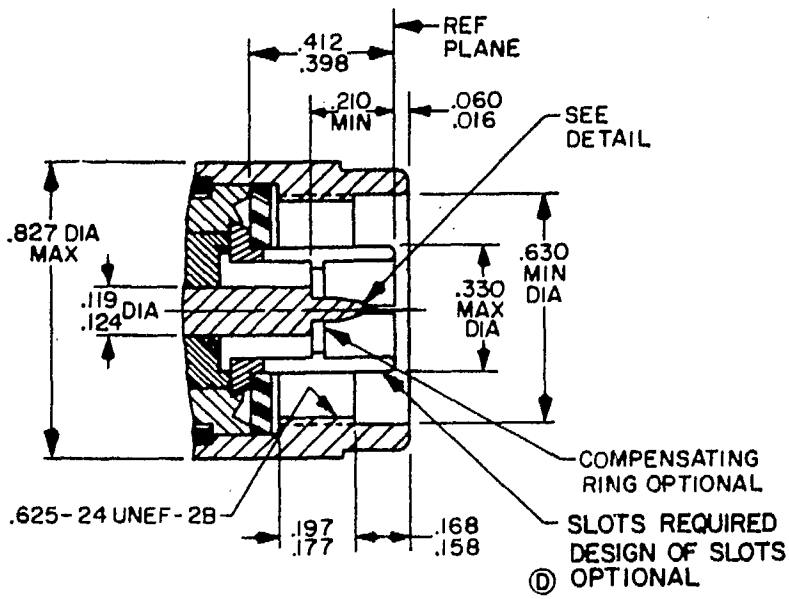

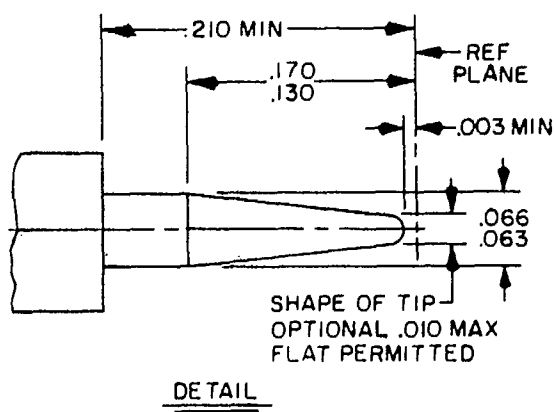

Fig. 3.7 (a) MIL Spec. drawing for a male type N RF connector (from MIL, C39012/1D)

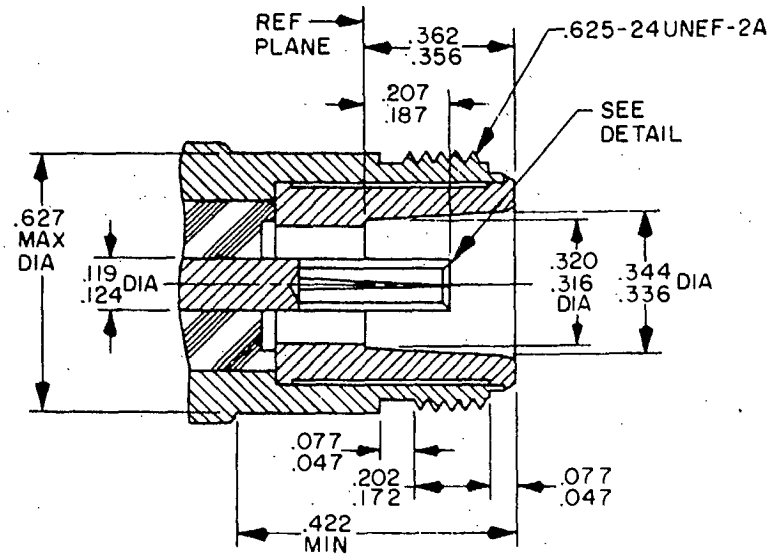

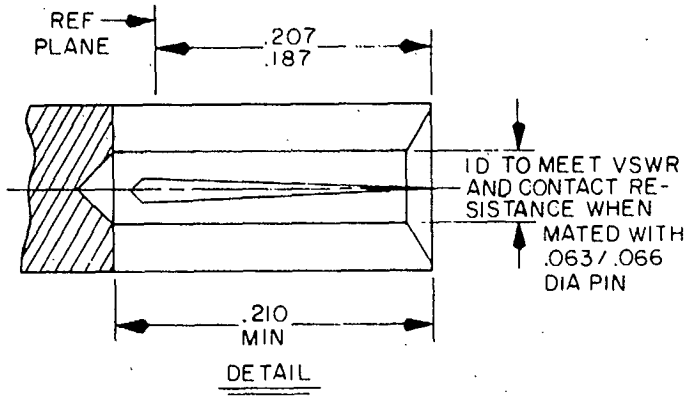

Fig. 3.7 (b) MIL Spec. drawing for a female type N RF connector (from MIL -C-39012/2D)

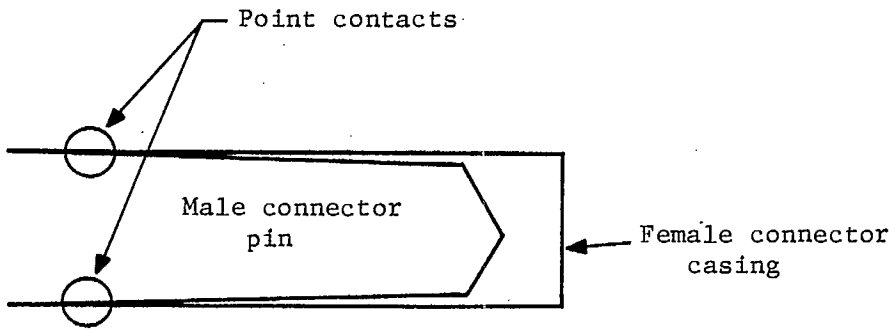

Fig. 3.8. Schematic representation of the centre contact in a mated RF connector pair. The figure shows that physical contact is made only over a very small fraction of the contact pin length as a result of the bevel on the centre conductor pin.

centre and outer contacts 0.254 cm (one hundred thousandths of an inch) long. Section 3.3.3 deals with connectors which have contacts of .0025 cm (one thousandth of an inch) in length.

For the centre pin of the long contact connector, the total contact area is:

$$AT_C = \pi d \ell = 0.1994 \text{ cm} \times 0.254 \text{ cm}$$
$$= 5.065 \times 10^{14} \text{ Å}^2$$

The area** of one "A" spot is

$$a = 50 \times (50)^2 \text{ Å}^2.$$
$$= 1.25 \times 10^5 \text{ Å}^2.$$

The total number of "A" spots on the long contact connector centre conductor contact is therefore 4×10^9. This contact can therefore be modelled as 4×10^9 "A" spot equivalent circuits in parallel.

The area of the outer conductor contact on the long contact connector is;

$$A_{To} = \pi \times 0.762 \text{ cm} \times 0.254 \text{ cm}$$
$$= 0.6 \text{ cm}^2$$

** Note that this area includes the area of the oxide region surrounding the contact filament cross-sectional area of 7,854 sq. Angstroms.

or 6.0×10^{15} $\mathring{A}^2$.

Division by the area of a single "A" spot gives the total number of parallel "A" spots in the outer conductor contact model for the long contact connector as 4.8×10^{10}.

The area of the centre conductor contact in the short contact connector is 1/100th that of the centre conductor contact area in the long contact connector. The number of "A" spot equivalent circuits in the short contact connector centre conductor contact model is therefore 4×10^7. Similarly, the number of "A" spot equivalent circuits in the outer conductor contact model for the short contact connector is $1/100 \times 4.8 \times 10^{10} = 4.8 \times 10^8$.

3.3.2 The Power of Passive Intermodulation Signals Generated by Tunneling in a Long Contact Copper Connector.

3.3.2(a) Passive Intermodulation Generated at A Long Contact Copper Connector Centre Conductor Contact

The current flowing through a RF connector to the load in a matched 50 ohm system may be calculated using the simple relationship

$$I = \left[\frac{P_T}{50}\right]^{1/2}, \qquad (3\text{-}3),$$

where P_T is the total transmit power.

If it is assumed for the present calculations that the maximum total power to be delivered to the load is 800 watts, the maximum centre conductor current is 4.0 Amps. Division by 4×10^9

spots gives a required maximum current density of 1 nA per spot.

Program TUNEL was used to find voltages corresponding to current densities up to the 1 nA maximum. Multiplication to obtain total tunnel currents then resulted in the I-V characteristic for the contact. This characteristic, with computed resistances, is shown in tabular* form in Table 3-1. An in-house CRC computer program was used to obtain a number of least squares polynomial representations for the I-V characteristic. The coefficients of the best fit (9th degree) polynomial are shown in Table 3-2. Table 3-3 shows a comparison of computed tunnel currents and those calculated using the least squares approximation at selected fixed tunnel voltages. The computed least squares coefficients were used in program IMPWR to compute intermodulation product currents for 3rd, 5th and 7th orders.

Since the average value of the nonlinear resistance (Table 3-1) is 3×10^{-4} ohms, the test circuit can be modelled as shown in Fig. 3.9. After converting the intermodulation generator to its Thevenin equivalent, the circuit becomes as in Fig. 3.10.

The Thevenin equivalent voltage for the intermodulation current source is given by:

$$V_{Th} = I_{IM} \times R_{NL}. \tag{3-4}$$

---

* The slight nonlinearity shown by this characteristic cannot be seen in any reasonably sized graphical presentation.

Table 3-1

I-V Characteristic Showing Nonlinear Resistance Values For Tunneling At A Long Contact Copper Connector Centre Conductor Contact (cuprous oxide thickness = 20 Å, contact area = 5×10^{14} Å^2)

TUNNEL VOLTAGE (VOLTS)	TUNNEL CURRENT (AMPS)	NONLINEAR RESISTANCE (OHMS)
-.900000D-03	-.327950D 01	.274432D-03
-.860000D-03	-.313360D 01	.274445D-03
-.820000D-03	-.298760D 01	.274468D-03
-.780000D-03	-.284170D 01	.274484D-03
-.740000D-03	-.269580D 01	.274501D-03
-.700000D-03	-.254990D 01	.274520D-03
-.660000D-03	-.240400D 01	.274542D-03
-.620000D-03	-.225820D 01	.274555D-03
-.580000D-03	-.211240D 01	.274569D-03
-.540000D-03	-.196660D 01	.274585D-03
-.500000D-03	-.182080D 01	.274604D-03
-.460000D-03	-.167500D 01	.274627D-03
-.420000D-03	-.152920D 01	.274653D-03
-.380000D-03	-.138350D 01	.274666D-03
-.340000D-03	-.123780D 01	.274681D-03
-.300000D-03	-.109210D 01	.274700D-03
-.260000D-03	-.946420D 00	.274719D-03
-.220000D-03	-.800760D 00	.274739D-03
-.180000D-03	-.655120D 00	.274759D-03
-.140000D-03	-.509520D 00	.274768D-03
-.100000D-03	-.363910D 00	.274793D-03
-.600000D-04	-.218340D 00	.274801D-03
-.200000D-04	-.727750D-01	.274820D-03
-.100000D-04	-.364090D-01	.274657D-03
-.200000D-05	-.729630D-02	.274111D-03

*

(1) The characteristic is symmetrical abour 0 volts.

(2) 100 points used for actual curve fit

(3) D Ox $\equiv 10^x$

Table 3-2

Coefficients of the Best Fit Least Squares Polynomial Representation* to the I-V Characteristic For Tunneling Through Cuprous Oxide 20 Å Thick ($T = 300^{o}$ K, $V \leq 900\mu V$)

a_0	-1.374×10^{-17}
a_1	3.693×10^{3}
a_2	1.933×10^{-10}
a_3	1.443×10^{7}
a_4	-2.804×10^{-4}
a_5	-2.666×10^{13}
a_6	7.689×10^{-1}
a_7	3.193×10^{19}
a_8	-4.535×10^{5}
a_9	-1.493×10^{25}

---

* $I = a_0 + a_1V + a_2V^2 + \ldots\ldots + a_nV^n$, where I has units of amps and V has units of volts.

Table 3-3

Comparison Of Computed Tunnel Currents For A Long Contact Copper Connector Centre Conductor Contact With Currents Calculated Using A 9th Degree Least Squares Polynomial Approximation To The Computed I-V Characteristic.

TUNNEL VOLTAGE (VOLTS)	TUNNEL CURRENT (AMPS)	LEAST SQUARES APPROXIMATE CURRENT (AMPS)	APPROXIMATION ERROR %
-.900000D-03	-.327950D 01	-.327936D 01	.412934D-02
-.860000D-03	-.313360D 01	-.313344D 01	.499115D-02
-.820000D-03	-.298760D 01	-.298751D 01	.306442D-02
-.780000D-03	-.284170D 01	-.284158D 01	.412788D-02
-.740000D-03	-.269580D 01	-.269568D 01	.452817D-02
-.700000D-03	-.254990D 01	-.254980D 01	.411405D-02
-.660000D-03	-.240400D 01	-.240394D 01	.265791D-02
-.620000D-03	-.225820D 01	-.225810D 01	.447655D-02
-.580000D-03	-.211240D 01	-.211228D 01	.573360D-02
-.540000D-03	-.196660D 01	-.196648D 01	.630416D-02
-.500000D-03	-.182080D 01	-.182069D 01	.597094D-02
-.460000D-03	-.167500D 01	-.167492D 01	.478260D-02
-.420000D-03	-.152920D 01	-.152917D 01	.212039D-02
-.380000D-03	-.138350D 01	-.138343D 01	.475631D-02
-.340000D-03	-.123780D 01	-.123772D 01	.631777D-02
-.300000D-03	-.109210D 01	-.109203D 01	.637471D-02
-.260000D-03	-.946420D 00	-.946364D 00	.592633D-02
-.220000D-03	-.800760D 00	-.800721D 00	.491272D-02
-.180000D-03	-.655120D 00	-.655099D 00	.316620D-02
-.140000D-03	-.509520D 00	-.509498D 00	.428154D-02
-.100000D-03	-.363910D 00	-.363914D 00	.113015D-02
-.600000D-04	-.218340D 00	-.218343D 00	.141955D-02
-.200000D-04	-.727750D-01	-.727801D-01	.704363D-02
-.100000D-04	-.364090D-01	-.363900D-01	.521616D-01
-.200000D-05	-.729630D-02	-.727800D-02	.250844D 00

Ibid. Table 3-1

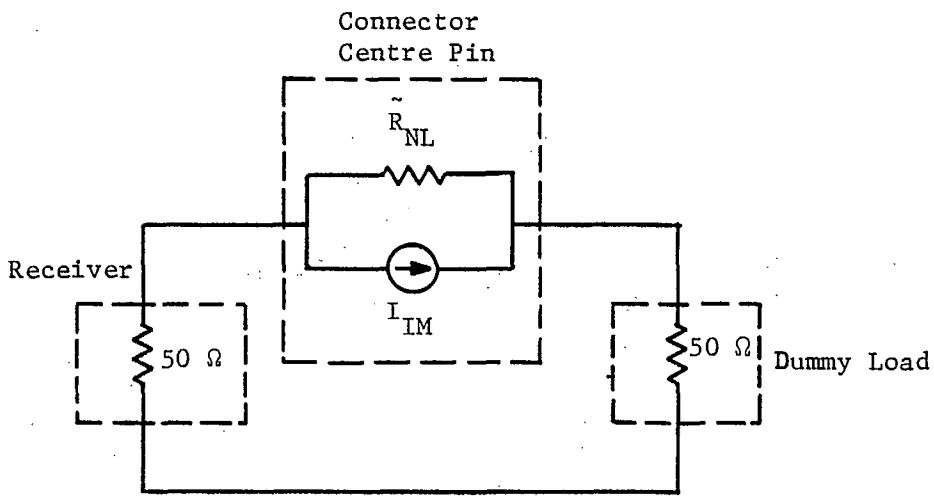

Fig. 3.9. Model for the assumed test circuit.

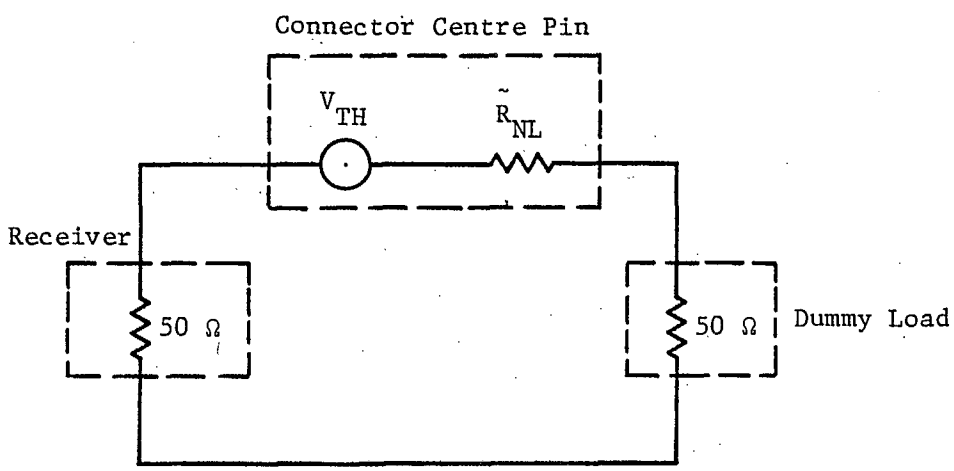

Fig. 3.10. Test circuit model with the IM generator (connector centre pin) replaced by its Thevenin equivalent circuit.

From Fig. 3.10, the intermodulation current in the receiver circuit is

$$I_{IMR} = \frac{I_{IM} \times R_{NL}}{R^2_{NL} + 100} \simeq \frac{I_{IM} \times RNL}{100} \qquad (3\text{-}4)$$

Therefore, the intermodulation power delivered to the receiver is

$$P_{IMR} = I^2_{IMR} \times 50 = \left(\frac{I_{IM} \times R_{NL}}{200}\right)^2 \qquad (3\text{-}5)$$

Equation 3-5 was used to calculate the power of 3rd, 5th and 7th order intermodulation signals generated by tunneling at the copper centre conductor contact for transmit powers ranging between 1 and 800 watts. These intermodulation power/drive power relationships are plotted in figures 3.11 to 3.13. The figures show an almost linear NdB/dB slope for each Nth order characteristic with minor deviations occurring at high transmit powers. Unlike the power characteristics for passive intermodulation generated in a commercial Schottky diode [1], the tunneling generated passive intermodulation power characteristics calculated for this contact are monotonic, and show no power minima.

3.3.2(b) Passive Intermodulation Generated at the Outer Conductor Contact in a Long Contact Copper Connector Outer Conductor Contact.

The current carried by the outer conductor in a closed coaxial system is equal to that carried by the inner conductor. For a maximum of 800 W transmit power in a 50 ohm system, the

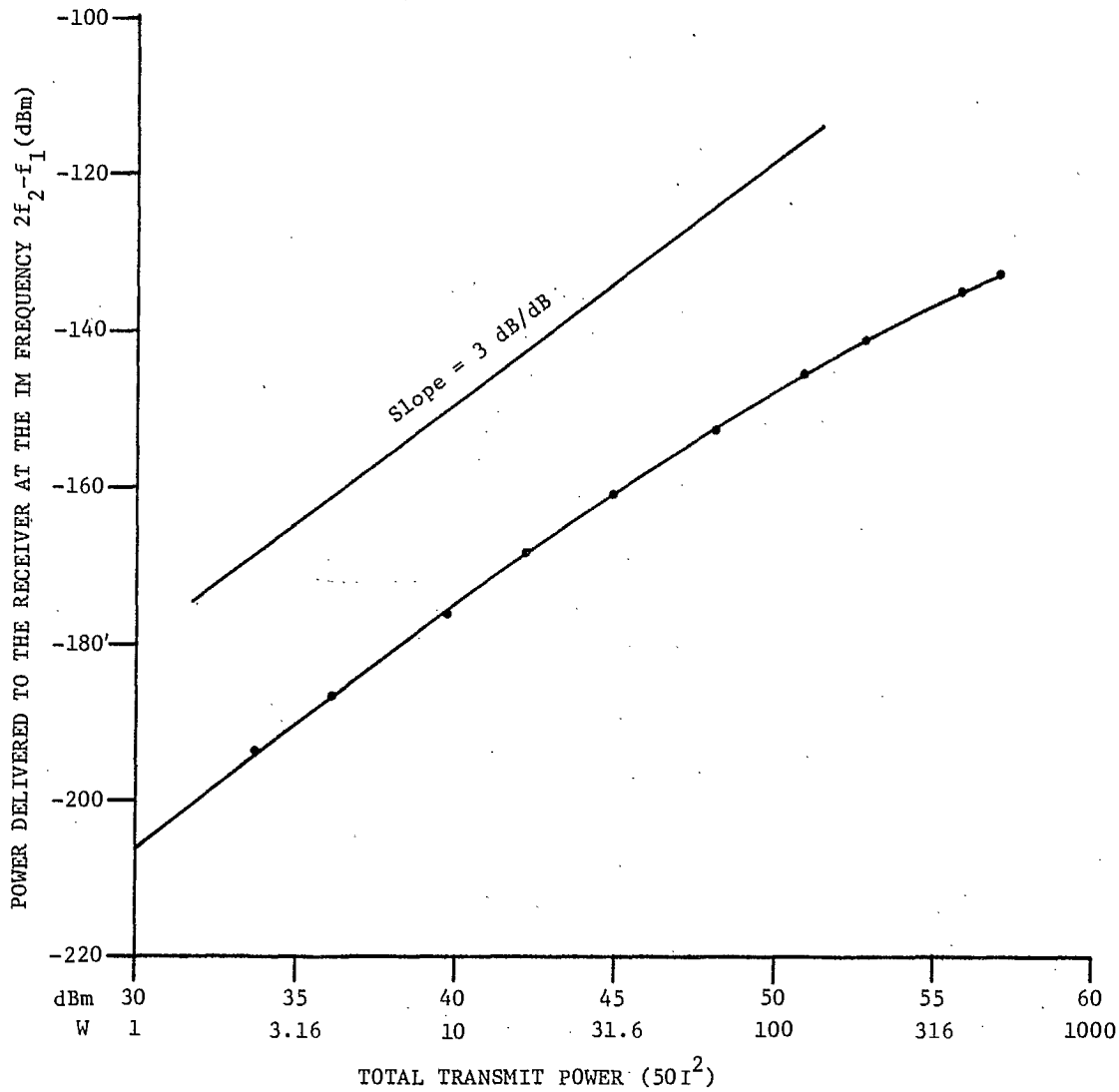

Fig. 3.11. Computed third order IM signal power dependence on total transmit power for IM signals generated by tunneling through 20 Å of cuprous oxide at a RF connector centre conductor contact. (contact area = 5×10^{14} Å^2).

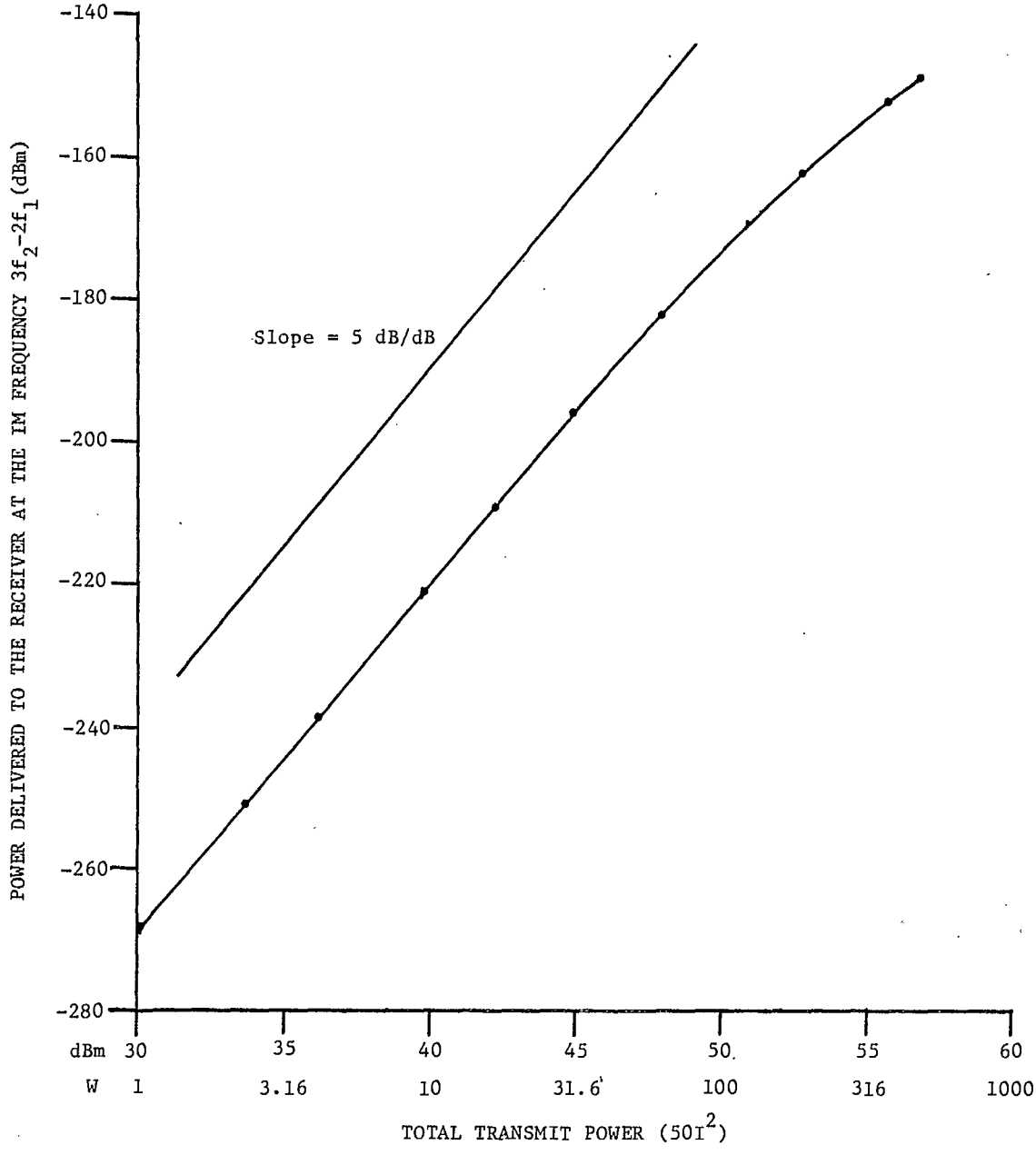

Fig. 3.12. Computed fifth order IM signal power dependence on total transmit power for IM signals generated by tunneling through 20 Å of cuprous oxide at a RF connector centre conductor contact, (contact area = 5×10^{14} Å^2).

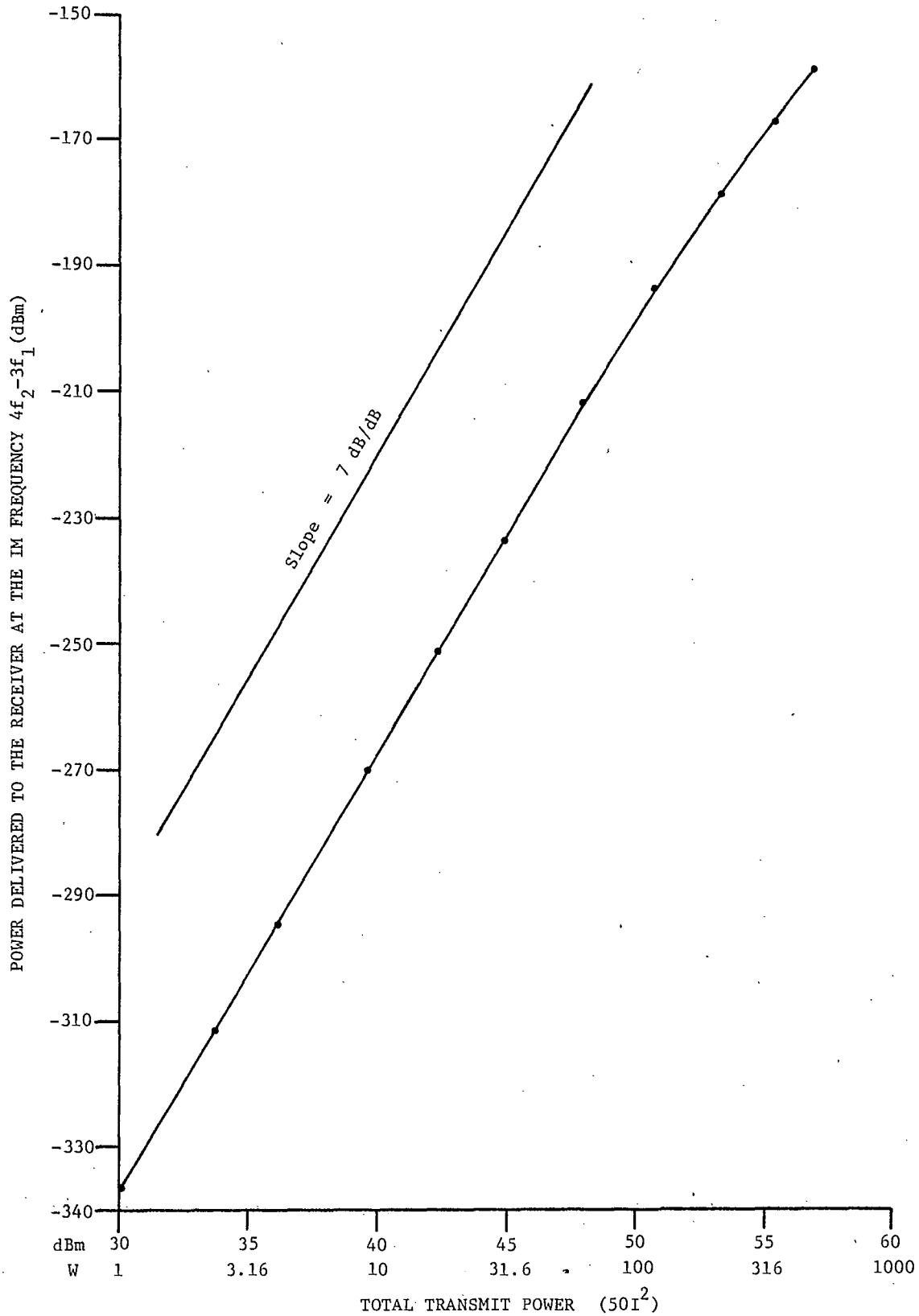

Fig. 3.13. Computed seventh order IM signal power dependence on total transmit power for IM signals generated by tunneling through 20 Å of cuprous oxide at a RF connector centre conductor contact, (contact area = 5×10^{14} Å^2).

maximum current is therefore 4.0 amps. This results in a current density of 0.0823 nA at each of the 4.86×10^{10} "A" spots on the long contact connector outer conductor contact.

An identical procedure to that in Section 3.3.2(a) was followed to compute the I-V characteristic for tunneling through a 20 Å copper oxide film at the outer conductor contact. The computed characteristic was found, however, to be a good deal more linear than that for tunneling at the centre conductor contact. An accurate polynomial approximation of degree greater than one or two could not be obtained. It was therefore concluded that any passive intermodulation generated at this contact would be at insignificant power levels.

3.3.3 The Power of Passive Intermodulation Signals Generated by Tunneling in a Short Contact Copper Connector.

3.3.3(a) Passive Intermodulation Generated at the Short Contact Copper Connector Centre Conductor Contact.

If a short contact connector centre conductor contact (3.3.1) is required to carry a maximum current of 4.0 amps (transmitter output power = 800 W), the maximum "A" spot current density for the geometry described in Section 3.3.1 is 100 nA. Program TUNEL was used as in Section 3.3.2(a) to find voltages corresponding to current densities up to a maximum of 100 nA per spot. The resulting I-V characteristic for the entire centre conductor contact is shown in Fig. 3.14. Tunnel resistances are tabulated in Table 3-4. The least squares computer program was again used to obtain several polynomial approximations to the tunneling characteristic. Coefficients of the best fit polynomial (9th degree) are shown in Table 3-5. Table 3-6 shows the polynomial approximation errors for selected voltages. The computed polynomial coefficiences were used in program IMPWR to compute Intermodulation product currents for 3rd, 5th and 7th orders.

The average value of the nonlinear tunnel resistance (Table 3-4) is 2.5×10^{-2}. Using this value in eqn. 3-5, the power of intermodulation signals as a function of total transmit power was calculated. The computed intermodulation power characteristics for 3rd, 5th and 7th orders are shown in figures 3.15 to 3.17.

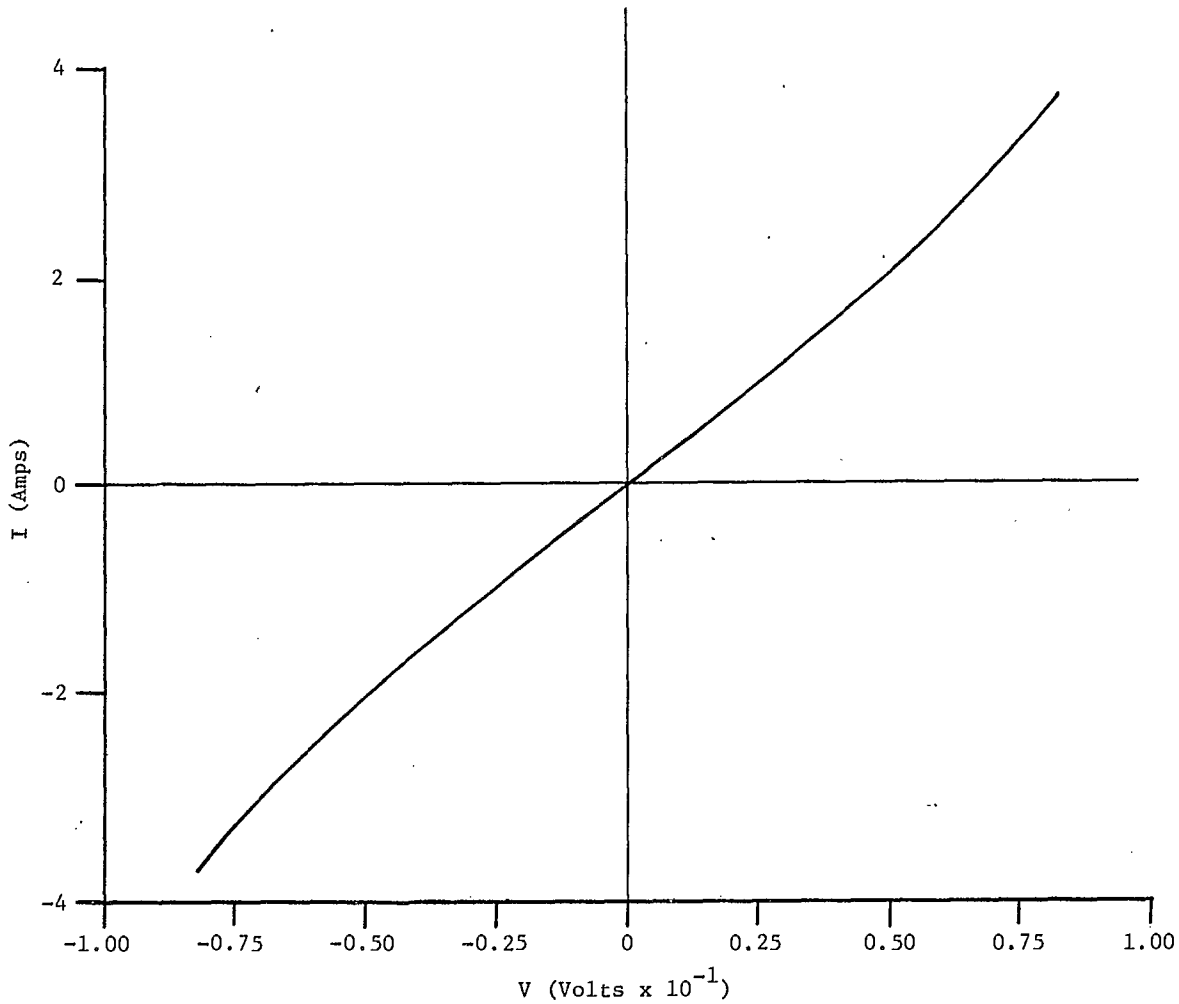

Fig. 3.14. Computed I-V characteristic for tunneling through 20 Å of cuprous oxide at a short contact copper connector centre conductor contact, (contact area = 5×10^{12} Å^2).

Table 3-4

I-V Characteristic Showing Nonlinear Resistance Values For Tunneling At A Short Contact Copper Connector Centre Conductor Contact (cuprous oxide thickness = 20 Å, contact area = 5×10^{12} Å^2).

TUNNEL VOLTAGE (VOLTS)	TUNNEL CURRENT (AMPS)	NONLINEAR RESISTANCE (OHMS)
-.820000D-01	-.369650D 01	.221832D-01
-.780000D-01	-.346600D 01	.225043D-01
-.740000D-01	-.324340D 01	.228156D-01
-.700000D-01	-.302710D 01	.231244D-01
-.660000D-01	-.281710D 01	.234283D-01
-.620000D-01	-.261310D 01	.237266D-01
-.580000D-01	-.241480D 01	.240186D-01
-.540000D-01	-.222180D 01	.243046D-01
-.500000D-01	-.203380D 01	.245845D-01
-.460000D-01	-.185040D 01	.248595D-01
-.420000D-01	-.167160D 01	.251256D-01
-.380000D-01	-.149690D 01	.253858D-01
-.340000D-01	-.132610D 01	.256391D-01
-.300000D-01	-.115900D 01	.258844D-01
-.260000D-01	-.995290D 00	.261230D-01
-.220000D-01	-.834790D 00	.263539D-01
-.180000D-01	-.677270D 00	.265773D-01
-.140000D-01	-.522530D 00	.267927D-01
-.100000D-01	-.370370D 00	.270000D-01
-.600000D-02	-.220590D 00	.271998D-01
-.200000D-02	-.730160D-01	.273913D-01
-.800000D-03	-.291470D-01	.274471D-01
-.600000D-03	-.218530D-01	.274562D-01
-.400000D-03	-.145640D-01	.274650D-01
-.200000D-03	-.727950D-02	.274744D-01

Table 3-5

Coefficients of the Best Fit Least Squares Polynomial Representation For the Tunneling I-V characteristic of the Short Contact Copper Connector Centre Conductor Contact ($T = 300^{o}$ K, $D = 20$ Å, $V_T \leq 82$ mV).

a_0	-1.896×10^{-6}
a_1	3.700×10^{1}
a_2	2.123×10^{-2}
a_3	2.030×10^{3}
a_4	-2.018×10^{1}
a_5	-3.236×10^{5}
a_6	5.407×10^{3}
a_7	4.727×10^{7}
a_8	-4.102×10^{5}
a_9	-2.604×10^{9}

* $I = a_0 + a_1V + a_2V^2 + \ldots\ldots + a_nV^n$, where I has units of amps, and V has units of volts.

Table 3-6

Comparison of Computed Tunnel Currents For A Short Contact Copper Connector Centre Conductor Contact With Currents Calculated Using a 9th Degree Least Squares Polynomial Approximation To The Computed I-V Characteristic

TUNNEL VOLTAGE (VOLTS)	TUNNEL CURRENT (AMPS)	LEAST SQUARES APPROXIMATE CURRENT (AMPS)	APPROXIMATION ERROR %
-.820000D-01	-.369650D 01	-.369542D 01	.292307D-01
-.780000D-01	-.346600D 01	-.346705D 01	.303217D-01
-.740000D-01	-.324340D 01	-.324362D 01	.690983D-02
-.700000D-01	-.302710D 01	-.302660D 01	.163824D-01
-.660000D-01	-.281710D 01	-.281634D 01	.269809D-01
-.620000D-01	-.261310D 01	-.261256D 01	.206567D-01
-.580000D-01	-.241480D 01	-.241471D 01	.359385D-02
-.540000D-01	-.222180D 01	-.222220D 01	.178133D-01
-.500000D-01	-.203380D 01	-.203447D 01	.331052D-01
-.460000D-01	-.185040D 01	-.185114D 01	.402518D-01
-.420000D-01	-.167160D 01	-.167195D 01	.206527D-01
-.380000D-01	-.149690D 01	-.149673D 01	.116589D-01
-.340000D-01	-.132610D 01	-.132540D 01	.524985D-01
-.300000D-01	-.115900D 01	-.115792D 01	.929812D-01
-.260000D-01	-.995290D 00	-.994195D 00	.110042D 00
-.220000D-01	-.834790D 00	-.834058D 00	.876659D-01
-.180000D-01	-.677270D 00	-.677253D 00	.256981D-02
-.140000D-01	-.522530D 00	-.523399D 00	.166370D 00
-.100000D-01	-.370370D 00	-.371998D 00	.439572D 00
-.600000D-02	-.220590D 00	-.222437D 00	.837313D 00
-.200000D-02	-.730160D-01	-.740179D-01	.137224D 01
-.800000D-03	-.291470D-01	-.296029D-01	.156421D 01
-.600000D-03	-.218530D-01	-.222023D-01	.159848D 01
-.400000D-03	-.145640D-01	-.148020D-01	.163425D 01
-.200000D-03	-.727950D-02	-.740191D-02	.168151D 01

Ibid. Table 3-1

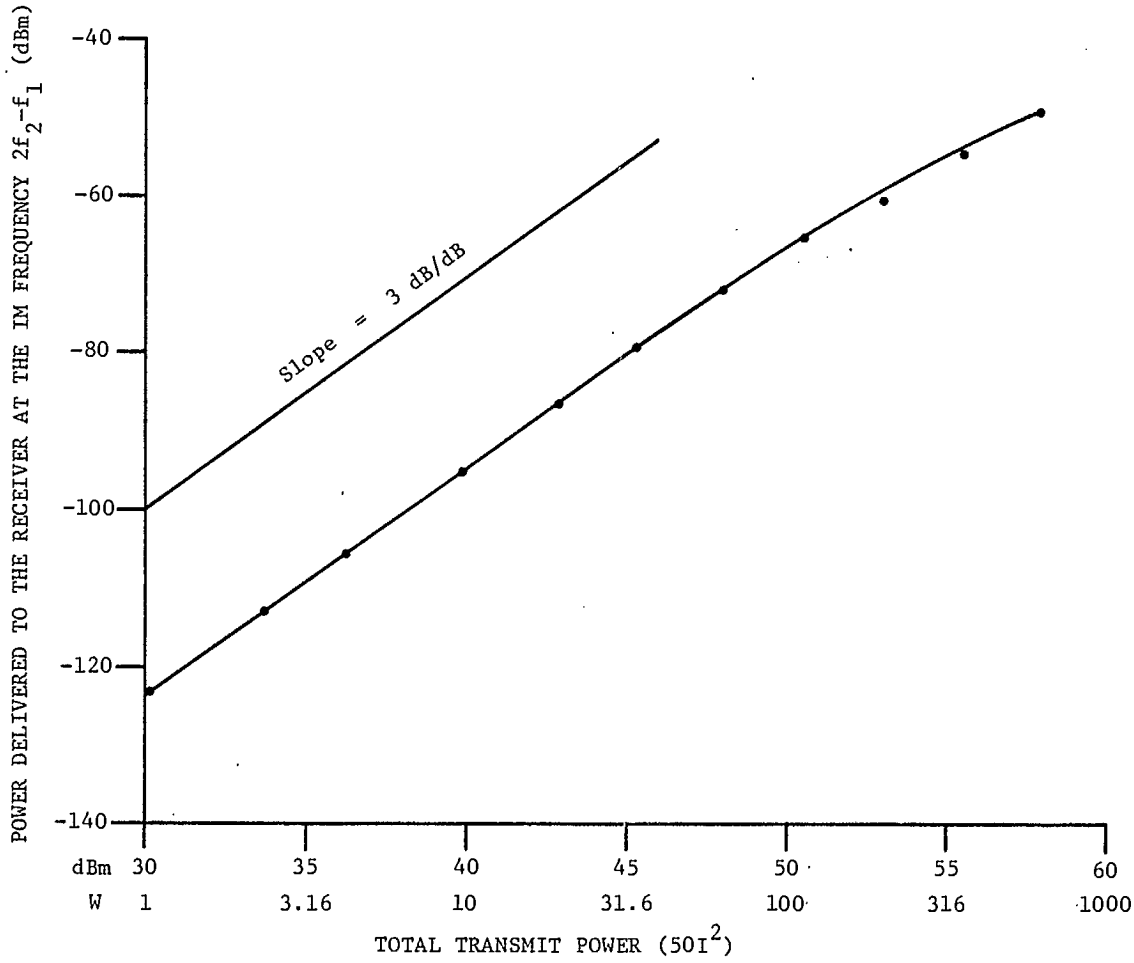

Fig. 3.15. Computed third order IM signal power dependence on total transmit power for IM signals generated by tunneling through 20 Å of cuprous oxide at a RF connector centre conductor contact, (contact area = 5×10^{12} Å^2).

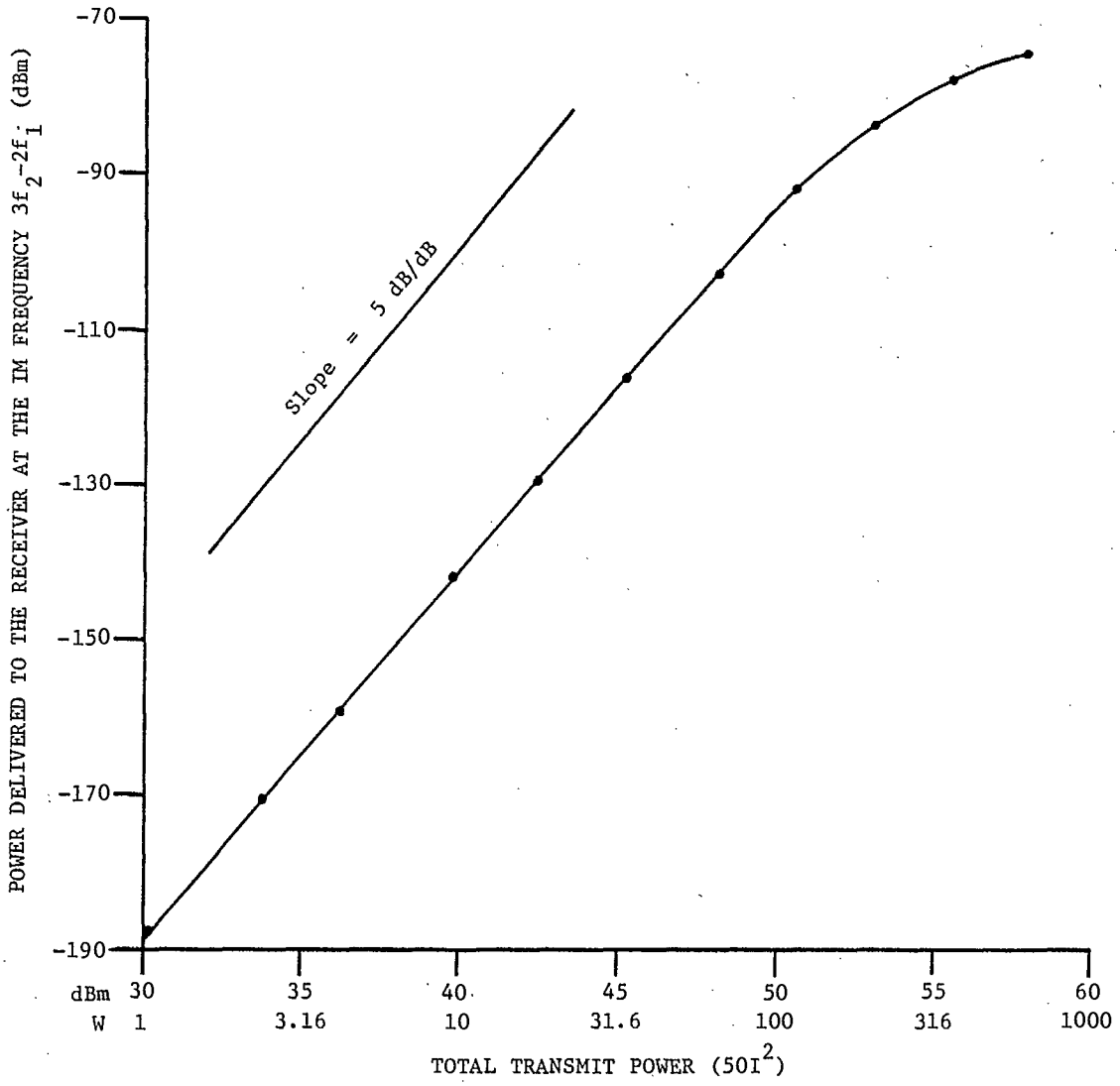

Fig. 3.16. Computed fifth order IM signal power dependence on total transmit power for IM signals generated by tunneling through 20 Å of cuprous oxide at a RF connector centre conductor contact, (contact area = 5×10^{12} Å^2).

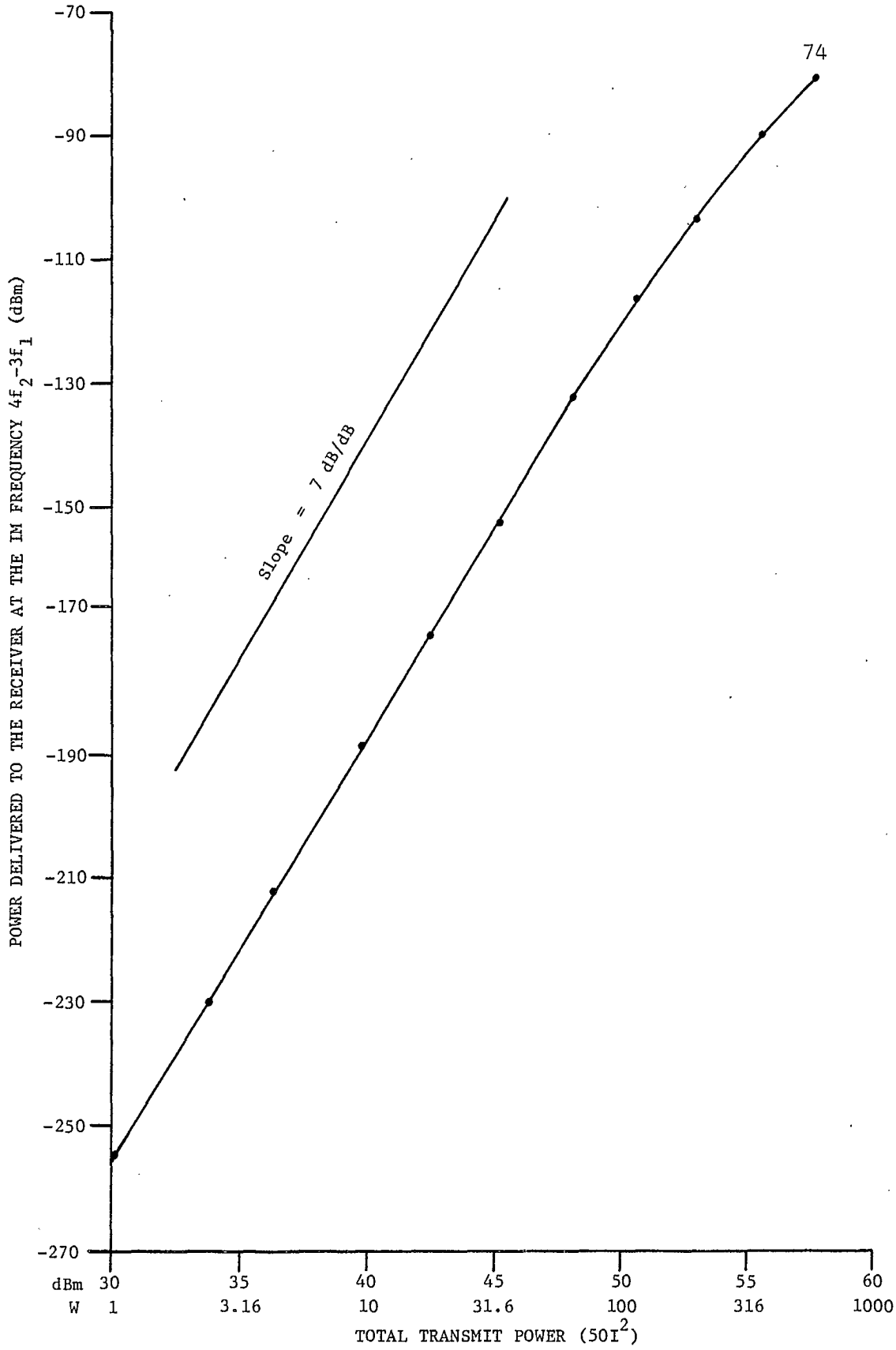

Fig. 3.17. Computed seventh order IM signal power dependence on total transmit power for IM signals generated by tunneling through 20 Å of cuprous oxide at a RF connector centre conductor contact, (contact area = 5×10^{12} Å^2).

Like the characteristics for the long contact connector, the curves shown in the referenced figures are monotonic and almost linear except at high transmit powers. Quantitative comparison shows that the power of passive intermodulation signals generated in the short contact connector is significantly greater (≈80 dB) than that generated in the long contact connector. This is a result of increased current density on the small area contact. Note also from Table 3-4 that the tunnel voltages are larger for the short contact connector. This corresponds to higher connector insertion loss.

3.3.3(b) Passive Intermodulation Generated at the Short Contact Copper Connector Outer Conductor Contact.

At the outer conductor contact in the short contact connector the maximum current density for 800 W is (4.0 amp/4.8 x 10^8 spots) or 8.3 nA/spot. Voltages corresponding to tunnel current densities up to this maximum were found with the aid of program TUNEL. The corresponding I-V characteristic with computed tunnel resistances may be seen in tabular form in Table 3-7. Table 3-8 shows the coefficients of the best fit (9th order) least squares polynomial approximation to the I-V characteristic, and approximation errors at selected tunnel voltages are shown in Table 3-9.

The average tunnel resistance of 2.2 x 10^{-3} ohms from Table 3-6 was used in conjunction with program TUNEL as described in Section 3.2 to calculate the intermodulation power/drive power data plotted in figures 3.18 to 3.20 for 3rd, 5th and 7th intermodulation products.

The figures show again that the intermodulation characteristics for tunneling are nearly linear and have slopes just slightly less than NdB/dB at Nth order. Comparison with figures 3.15 to 3.17 for passive intermodulation generated at the centre conductor contact in the short contact connector shows that passive intermodulation generated at the outer conductor contact is approximately 45 dB lower. This shows that the power of passive intermodulation signals generated by the outer conductor contact can be ignored regardless of the phase relationship of the generated signals with respect to those generated at the centre conductor contact.

Table 3-7

I-V Characteristic Showing Nonlinear Resistance Values For Tunneling At A Short Contact Copper Connector Outer Conductor Contact (cuprous oxide thickness = 20 Å, contact area = 6×10^{13} Å^2).

TUNNEL VOLTAGE (VOLTS)	TUNNEL CURRENT (AMPS)	NONLINEAR RESISTANCE (OHMS)
-.780000D-02	-.356800D 01	.218610D-02
-.620000D-02	-.282800D 01	.219236D-02
-.460000D-02	-.209200D 01	.219885D-02
-.300000D-02	-.136000D 01	.220588D-02
-.206000D-02	-.932700D 00	.220864D-02
-.178000D-02	-.805500D 00	.220981D-02
-.146000D-02	-.660300D 00	.221112D-02
-.114000D-02	-.515300D 00	.221230D-02
-.820000D-03	-.370500D 00	.221323D-02
-.755000D-03	-.341100D 00	.221343D-02
-.675000D-03	-.304900D 00	.221384D-02
-.610000D-03	-.275500D 00	.221416D-02
-.540000D-03	-.243900D 00	.221402D-02
-.460000D-03	-.207700D 00	.221473D-02
-.380000D-03	-.171600D 00	.221445D-02
-.300000D-03	-.135400D 00	.221566D-02
-.220000D-03	-.993000D-01	.221551D-02
-.175000D-03	-.789800D-01	.221575D-02
-.102000D-03	-.460300D-01	.221595D-02

Ibid. Table 3-1

Table 3-8

Coefficients of The Best Fit Least Squares Polynomial Approximation for the Tunneling Characteristic of the Short Conduct Copper Connector Outer Conductor Contact ($T = 300^{o}$ K, $D = 20\mathring{A}$, $V \leq 8$mV).

a_0	6.280×10^{-18}
a_1	4.518×10^{2}
a_2	-3.409×10^{-12}
a_3	2.352×10^{5}
a_4	5.352×10^{-7}
a_5	-6.095×10^{9}
a_6	-1.968×10^{-2}
a_7	9.788×10^{-13}
a_8	1.892×10^{2}
a_9	-5.922×10^{17}

---

* $I = a + a_1V + a_2V^2 + \ldots\ldots + a_nV^n$, where I has units of amps and V has units of volts.

Table 3-9

Comparison of Computed Tunnel Currents For A Short Contact Copper Connector Outer Conductor Contact With Currents Calculated Using a 9th Degree Least Squares Polynomial Approximation To The Computed I-V Characteristic.

TUNNEL VOLTAGE (VOLTS)	TUNNEL CURRENT (AMPS)	LEAST SQUARES APPROXIMATION CURRENT (AMPS)	APPROXIMATION ERROR %
-.780000D-02	-.356800D 01	-.356833D 01	.911443D-02
-.620000D-02	-.282800D 01	-.282783D 01	.607006D-02
-.460000D-02	-.209200D 01	-.209234D 01	.161833D-01
-.300000D-02	-.136000D 01	-.136047D 01	.346408D-01
-.206000D-02	-.932700D 00	-.932553D 00	.157719D-01
-.178000D-02	-.805500D 00	-.805427D 00	.906464D-02
-.146000D-02	-.660300D 00	-.660321D 00	.311428D-02
-.114000D-02	-.515300D 00	-.515389D 00	.172464D-01
-.820000D-03	-.370500D 00	-.370603D 00	.278798D-01
-.755000D-03	-.341100D 00	-.341209D 00	.318730D-01
-.675000D-03	-.304900D 00	-.305036D 00	.447279D-01
-.610000D-03	-.275500D 00	-.275651D 00	.547584D-01
-.540000D-03	-.243900D 00	-.244009D 00	.445263D-01
-.460000D-03	-.207700D 00	-.207851D 00	.725472D-01
-.380000D-03	-.171600D 00	-.171697D 00	.564438D-01
-.300000D-03	-.135400D 00	-.135546D 00	.108028D 00
-.220000D-03	-.993000D-01	-.993984D-01	.991009D-01
-.175000D-03	-.789800D-01	-.790662D-01	.109127D 00
-.102000D-03	-.460300D-01	-.460839D-01	.117003D 00

?

Ibid. Table 3-1

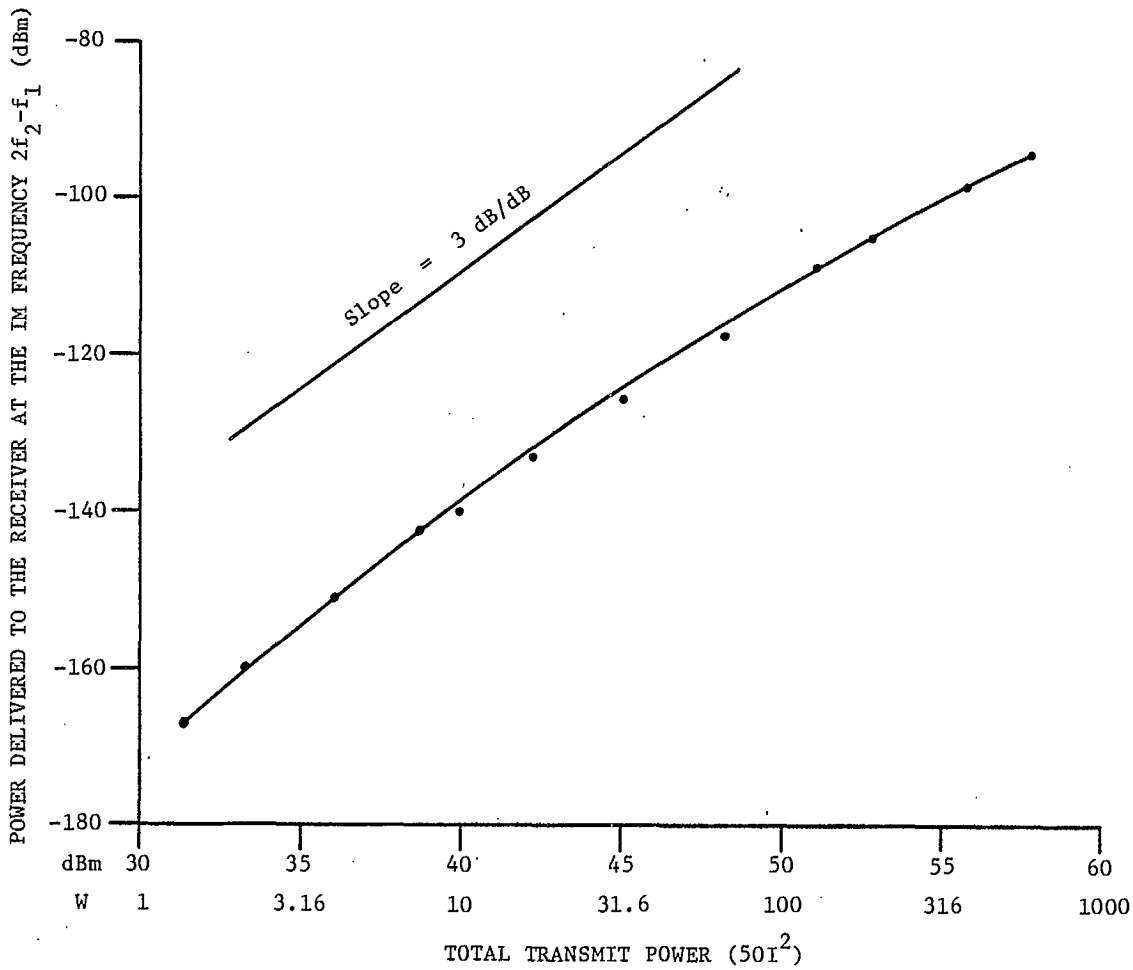

Fig. 3.18. Computed third order IM signal power dependence on total transmit power for IM signals generated by tunneling through 20 Å of cuprous oxide at a RF connector centre conductor contact, (contact area = 6.28×10^{13} Å^2).

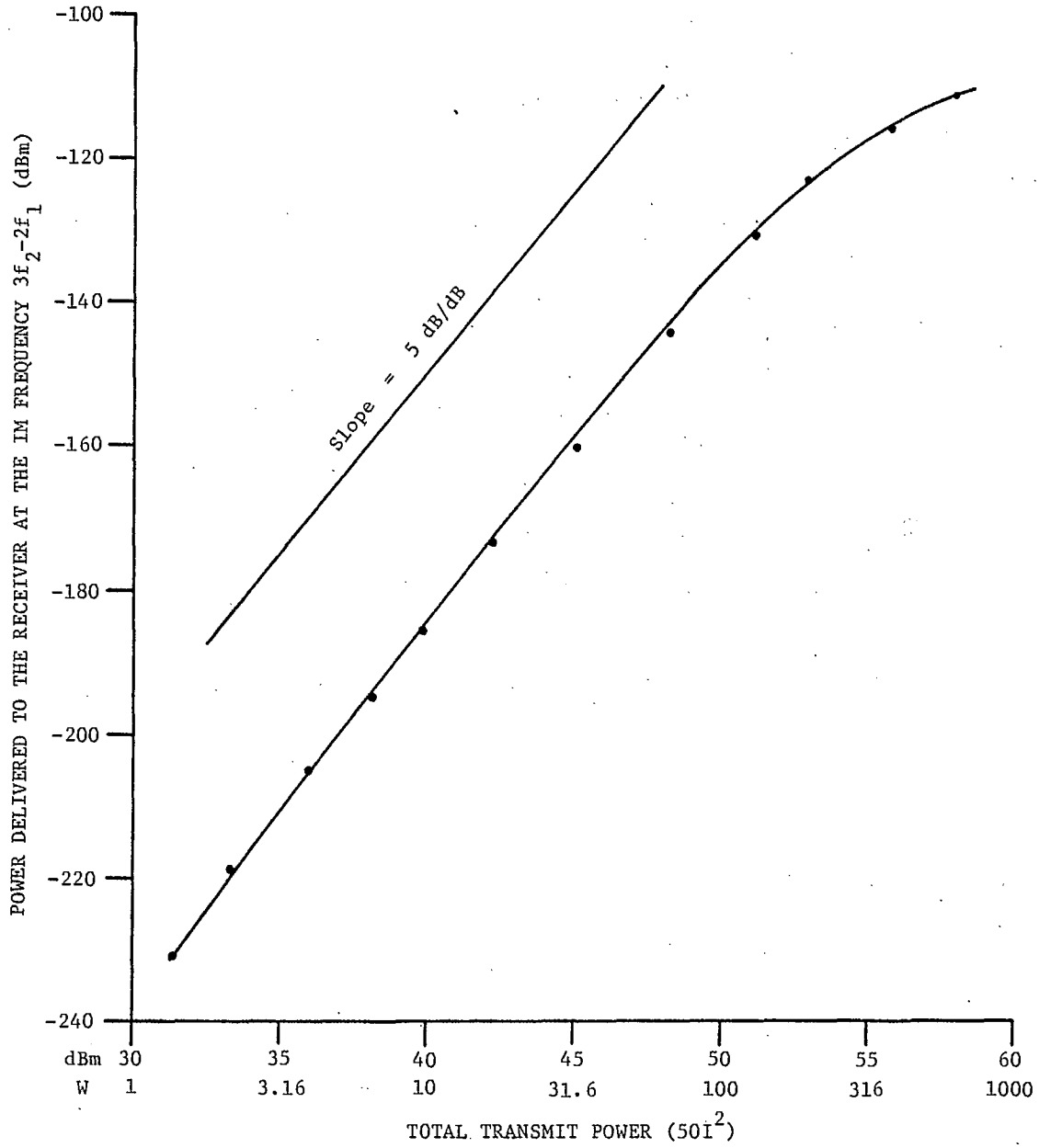

Fig. 3.19. Computed fifth order IM signal power dependence on total transmit power for IM signals generated by tunneling through 20 Å of cuprous oxide at a RF connector centre conductor contact, (contact area = 6.28×10^{13} Å^2).

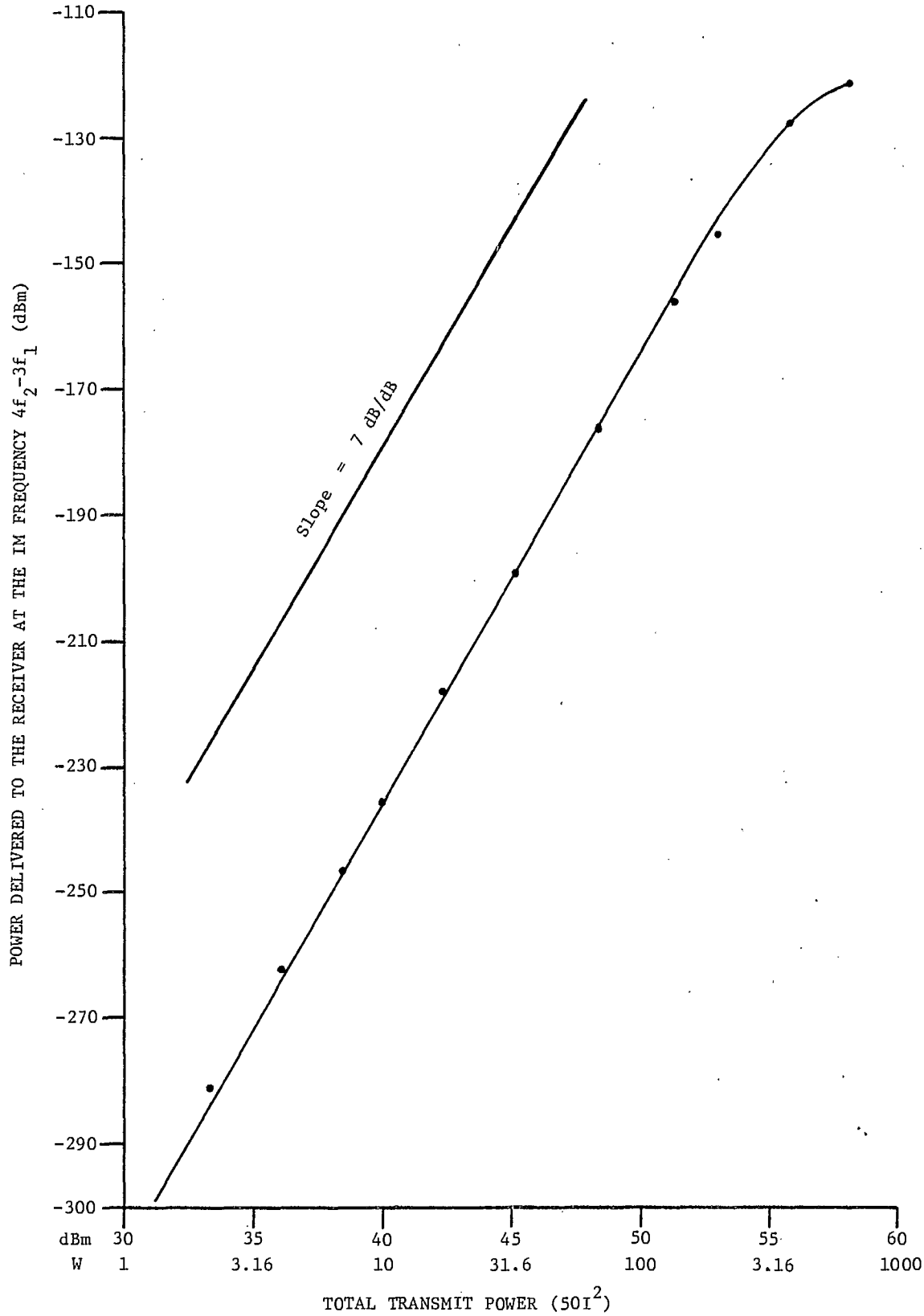

Fig. 3.20. Computed seventh order IM signal power dependence on total transmit power for IM signals generated by tunneling through 20 Å of cuprous oxide at a RF connector centre conductor contact, (contact area = 6.28×10^{13} Å^2).

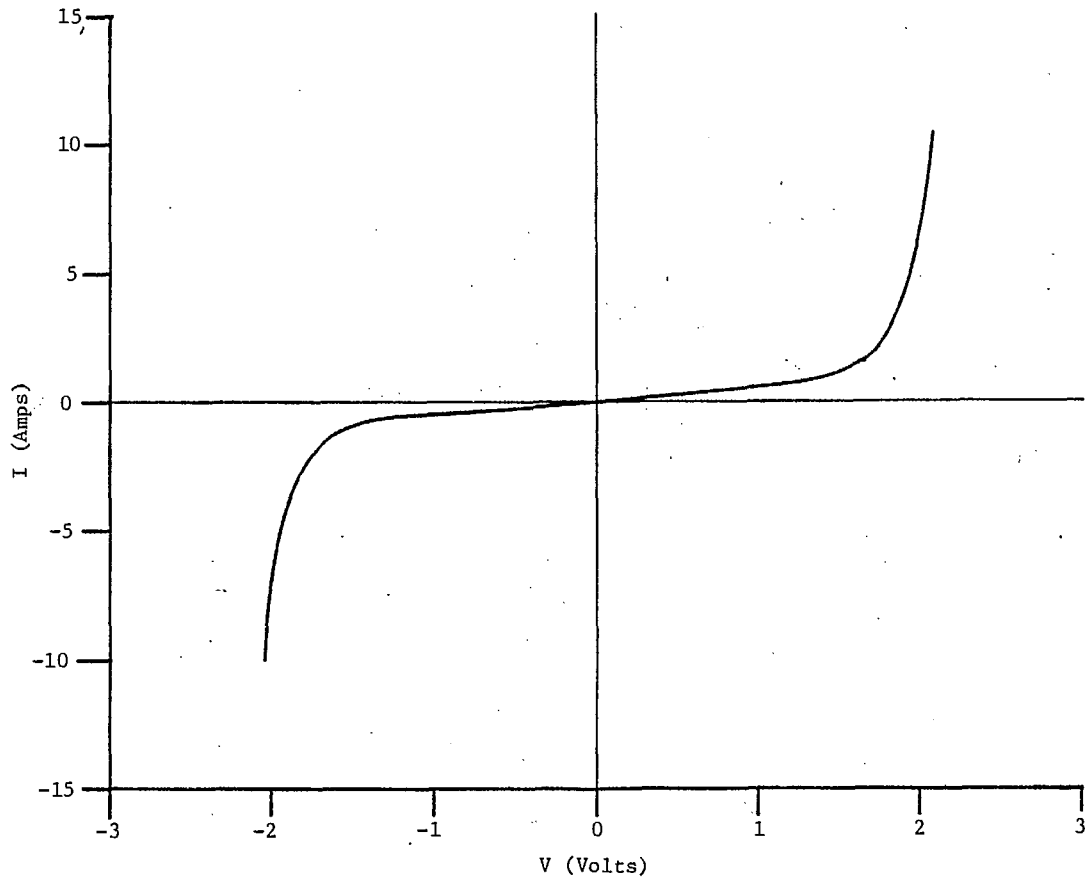

Fig. 3.21. Computed I-V characteristic for tunneling at a short contact aluminum connector centre conductor contact. (aluminum oxide thickness = 20 Å, contact area = 5×10^{-12} Å^2)

3.3.4 The Power of Passive Intermodulation Signals Generated by Tunneling in Aluminum Connectors

An identical contact model to that used for copper connector contacts was used to model contact surfaces in long and short contact aluminum connectors. In all contact cases, (centre and outer conductor contacts for long and short contact connectors), it was found that the tunneling I-V characteristic for aluminum/aluminum-oxide/aluminum structures remains very linear until relatively large tunnel voltages are reached. Tables 3-10 and 3-11 show computed data for the tunneling I-V characteristic at a short contact aluminum connector centre conductor contact. The characteristic has been drawn in Fig. 3.21.

The high tunnel voltages predicted by the computed characteristics are not reasonable values for the potential expected between mated contacts in a RF connector. Such results can be interpreted in two manners.

If it is assumed that the contact model used in the calculations is an adequate representation of geometries at two mating aluminum surfaces, calculations show that the power dissipation at currents near the beginning of the nonlinear conduction region would be excessive. This would lead to the destruction of the oxide at the metal/oxide/metal interface, and the establishment of a clean metal/metal contact at which no passive intermodulation could be generated. For example, Fig. 3.21 shows that in a 200 W/50 ohm system, (2 A on the centre conductor) the tunnel voltage would be 1.8 Volts. This corresponds to a power dissipation of 3.6 Watts at the $Al/Al_2O/Al$ interface. Although no

Table 3-10

I-V Characteristic and Resistance Values For Tunneling At The Centre Conductor Contact Of A Short Contact Aluminum Connector
(0V < V < 1 mV, oxide thickness = 20 Å)

AREA = 7854.00

VOLTS	AMPS	R
.00000000D 00	.00000000D 00	.00000000D 00
.50000002D-04	.27210888D-04	.18374996D 01
.10000000D-03	.54421733D-04	.18375006D 01
.15000001D-03	.81632606D-04	.18375006D 01
.20000001D-03	.10884355D-03	.18374996D 01
.24999931D-03	.13605428D-03	.18374996D 01
.29999972D-03	.16326505D-03	.18375006D 01
.34999964D-03	.19047593D-03	.18375006D 01
.39999955D-03	.21768683D-03	.18374996D 01
.44999947D-03	.24489756D-03	.18375006D 01
.49999938D-03	.27210847D-03	.18374996D 01
.54999930D-03	.29931916D-03	.18375006D 01
.59999921D-03	.32653008D-03	.18375006D 01
.64999913D-03	.35374099D-03	.18374996D 01
.69999904D-03	.38095168D-03	.18375006D 01
.74999896D-03	.40816260D-03	.18374996D 01
.79999887D-03	.43537351D-03	.18374996D 01
.84999879D-03	.46258443D-03	.18374996D 01
.89999870D-03	.48979511D-03	.18374996D 01
.94999862D-03	.51700603D-03	.18374996D 01
.99999853D-03	.54421672D-03	.18375006D 01
.10499984D-02	.57142763D-03	.18374996D 01

Table 3-11

I-V Characteristic and Resistance Values For Tunneling At The Centre Conductor Contact Of A Short Contact Aluminum Connector. (100 mV < V < 2V, oxide thickness = 20 Å).

VOLTS	AMPS	R
.10000002D 00	.54421782D-01	.18374996D 01
.20000005D 00	.10884356D 00	.18374996D 01
.30000007D 00	.16326523D 00	.18375006D 01
.40000010D 00	.21768713D 00	.18374996D 01
.50000012D 00	.27210927D 00	.18374968D 01
.60000014D 00	.32653189D 00	.18374929D 01
.70000017D 00	.38095605D 00	.18374825D 01
.80000019D 00	.43538463D 00	.18374557D 01
.90000021D 00	.48982656D 00	.18373852D 01
.10000000D 01	.54431069D 00	.18371859D 01
.10999994D 01	.59893721D 00	.18365850D 01
.11999989D 01	.65407473D 00	.18346510D 01
.12999983D 01	.71120936D 00	.18278694D 01
.13999977D 01	.77019405D 00	.18177304D 01
.14999971D 01	.86210203D 00	.17399292D 01
.15999966D 01	.10721216D 01	.14923639D 01
.16999960D 01	.15984430D 01	.10635319D 01
.17999954D 01	.27140656D 01	.66320997D 00
.18999949D 01	.47340965D 01	.40134263D 00
.19999943D 01	.80613356D 01	.24809712D 00
.20999937D 01	.13219885D 02	.15885109D 00

quantitative information is available, it is anticipated that this power dissipation would be more than adequate to destroy 20 Å of oxide.

The second interpretation that can be made is that the contact model is unrealistic. If the contact surfaces, for example, were more regular than was assumed, greater total currents would flow through the increased number of contact spots due to the smoother surface, resulting in lower, more reasonable tunnel voltages for a particular total current. It is clear that metallurgical as well as electrical experimentation is required before conclusions can be drawn with regard to the validity of the contact model for aluminum connectors. This is left as a topic for further investigation.

Passive intermodulation calculations based on data with such uncertain validity as the I-V characteristics computed for tunneling in aluminum connectors would have little meaning until the contact model can be substantiated. Intermodulation power computations for aluminum connectors have therefore been omitted from this report.

3.4 Passive Intermodulation Signal Generation Due To Space Charge Limited Current Flow in Naturally Occurring Oxides At Metal/Oxide/Metal Interfaces

Space charge limited current flow (Ref. Section 2.2.2) is another phenomenon that can take place when two spacially separated ohmic contacts are made to an insulating material. This nonlinear mechanism could be a source for the production of passive intermodulation in structures where the oxide thickness is too great to permit tunneling.

From Section (2.2.2) the relationship between current density and normalized [11] current (5) for space charge limited current flow is:

$$J_{scl} = \frac{\delta \varepsilon \mu \ (KT/q)^2}{d^3} \quad A/cm^2 \qquad (3\text{-}6)$$

where,

δ is normalized current

μ is electron mobility in the insulator

d is the insulator thickness (cm)

and the other symbols have their usual meanings.

Consider a short contact copper connector (Section 3.3.3(a)) inner conductor contact. The current density on the connector contact corresponding to a transmit power of 800 Watts applied to a 50 ohm load was calculated to be 1nA per spot, the equivalent of 1270 A/cm^2. For 20 Å of cuprous oxide (μ = 210 cm^2/V sec) and this current density,

$$\delta = \frac{1.27 \times 10^{3} \times (20 \times 10^{-8})^{3}}{8.75 \times 8.854 \times 10^{-14} \times 210 \times (.026)^{2}}$$

$$= 9.23 \times 10^{-5}$$

For this range of δ, the voltage developed across the metal/oxide/metal/structure [11] can be determined from the equation;

$$\delta = 3V_b (q/KT) \qquad (3\text{-}7)$$

Substitution in (3-6) therefore gives

$$J_{scl} = \frac{\varepsilon\mu (KT/q) V_b}{d^3} \qquad (3\text{-}8)$$

It is clear from this equation that space charge limited current is a linear function of the voltage developed across the structure in this region of operation. Space charge phenomenon in copper oxide would result in sufficient nonlinearity to generate passive intermodulation only under conditions where much higher current densities are present. This would correspond with a smaller overall contact surface area, on more irregular contact surfaces, which would result in the establishment of fewer contact "A" spots.

Although the work function relationships in aluminum/aluminum oxide/aluminum structures would permit the establishment of a space charge, it is highly unlikely that significant currents would flow by the space charge limited mechanism in such structures,

as electron mobility is so low in aluminum oxide that it is normally considered to be a perfect insulator. The lack of readily available mobility data has precluded a quantitive study of space charge limited conduction for aluminum contacts in this report. It is believed, however, that results would show that there is little probability of passive intermodulation generation.

3.5 Summary and Discussion

This chapter began with the development of a unit equivalent circuit for use in modelling metal/metal contacts at UHF following the method of Chapman and Darlington [3]. Next the anticipated maximum and minimum inner and outer conductor contact areas in a coaxial connector with dimensions similar to those of a type-N connector were calculated. The maximum and minimum area contacts were then modelled by the number of parallel unit equivalent circuits required to cover their surface areas.

Passive intermodulation calculations for tunneling at the modelled contacts began by considering the generation of intermodulation signals at the centre conductor of a copper connector with contacts of maximum surface area. A computation format was developed in which single spot current densities corresponding to a total of 800 W transmit power were calculated, and used in the tunnel equation program (TUNEL) to find the voltage range of interest. From these calculations I-V characteristics for tunneling at the contact surfaces were derived. Least squares polynomial approximations were applied to the I-V characteristics. The resulting polynomial coefficients were then used as input data for program (IMPWR) for the computation of intermodulation product currents following the method of Sea [5]. Equations were developed for relating intermodulation currents to intermodulation power delivered to the receiver in a simple test circuit model. Application of the calculated intermodulation currents in the circuit model equations led to the calculation of intermodulation power/drive power response characteristics for passive

intermodulation generated at the centre conductor contact in the maximum area contact copper connector. Identical procedures were used to calculate the power of passive intermodulation signals attributable to tunneling at the maximum contact area copper connector outer conductor contact, a minimum contact area copper connector inner and outer conductor contacts, and for aluminum connectors. The investigation then proceeded to similar analyses for passive intermodulation generated by space charge limited current flow at coaxial connector contact surfaces.

The most obvious result of the calculations is that the power of intermodulation signals generated as a result of tunneling is a very sensitive function of current density. In the case of the long contact (maximum area contact) copper connector, it was computed that intermodulation product signals at the level of -141 dBm could be generated at 200 W transmit power by the centre conductor contact, whereas the outer conductor contact which had an area 11.8 times larger was found to have a linear I-V characteristic which would result in the absence of any passive intermodulation. In the case of the short (minimum area) contact connector, passive intermodulation generated by the outer conductor contact was 45 dB lower than that generated at the smaller centre conductor contact. Comparison of the power of passive intermodulation signals generated by the centre contact of the short contact connector and the power of those generated at the contact surfaces in the long contact connector shows that passive intermodulation signal powers decrease by 4 dB for every dB decrease in current density, or

$P_{IM} \alpha J^{2.5}$ at all orders. From these calculations it was concluded that the centre conductor contacts in coaxial connectors are the major contributors to tunneling-generated passive intermodulation. In comparison, passive intermodulation signals generated at the outer conductor contacts are at insignificant powers, regardless of their phase relative to those generated at the centre conductor contacts.

With regard to the signatures, or shapes of the tunneling generated passive intermodulation drive power/intermodulation power characteristics, it was noted that in all cases, monotonic relationships with slopes of approximately N dB/dB at Nth order resulted. This is in contrast with previously reported [1] characteristics for a commercial Schottky diode which exhibited frequent slope changes and very distinct minima. It is beleived that the difference in intermodulation response characteristics is due to the difference in the shapes of the I-V characteristics for the two phenomena. The nonlinear tunneling I-V relationship for copper/copper-oxide interfaces is characterised by a very slow increase in current in response to voltage increments, resulting in a smooth, but distinctly nonlinear shape. The Schottky diode I-V relationship on the other hand is an exponential, which exhibits a more abrupt knee, at which point the current rises rapidly as a function of voltage.

Work presented in this chapter also shows that for identical contact models, tunneling in a copper connector follows a nonlinear conduction characteristic, beginning at very low tunnel

voltages, whereas tunneling in an aluminum connector is characterized by a relationship which is linear over a range extending to voltages in excess of 1 volt. This is a result of the difference in contact potentials that exist when copper and aluminum are in contact with their respective oxides. The contact potential for a Cu/CuO_2 contact is 0.42 eV. For an Al/Al_2O_3 interface, the contact potential is 1.34 eV.

Finally, in this chapter an investigation was made of the possible generation of passive intermodulation as a result of space charge limited current flow where ohmic contacts are made to naturally occurring metal oxides in coaxial connectors. Using the same metal/metal contact model as that assumed for tunneling, it was found that the space charge limited characteristic in copper oxide is not sufficiently nonlinear for passive intermodulation generation. Further, it can be shown that even at oxide thicknesses five times as great in the same geometrical model, the I-V characteristic is still linear. Much higher current densities would be required for space charge limited phenomenon in copper oxide to become a significant passive intermodulation generator. No calculations were made for passive intermodulation resulting from space change limited phenomena in aluminum oxide due to the lack of quantitative information concerning mobilities. Electron mobility is, however, known to be extremely low in aluminum oxide, leading to the conclusion that space charge limited current flow would probably not take place.

CHAPTER IV

Intermodulation Power Signatures

4.1 Introduction

In a previous report [1] it was postulated that the drive power response of intermodulation signals generated by different nonlinearities would take distinct forms. It was further suggested that these intermodulation power "signatures" could be useful as an aid in the identification of intermodulation generators in functioning RF systems.

In this chapter the results of an investigation of the power response characteristics of intermodulation "signals" generated by selected arbitrary nonlinearities is presented. Particular attention is given to two characteristics; the power of intermodulation signals as a function of total transmit power, and the relationship between the power of intermodulation signals of different order at fixed total transmit powers. Recent laboratory measurements at CRC and reported computer results [1] have shown the slope of the later characteristic to be much lower than expected, and in some instances non-monotonic.

Section 4.2 discusses the computed characteristics of intermodulation signals resulting from the simulated application of two sinusoidal carriers to a symmetrical I-V characteristic similar in shape to that of a current limiter. The nonlinearity

discussed in Section 4.3 is identical to that of Section 4.2 for positive voltages, but is linear in the negative voltage region. The linearization was performed to permit the study of passive intermodulation generated by non-symmetrical nonlinearities. The non-linearity of Section 4.4 is symmetrical and is such that the current rises rapidly with an increase in voltage. Section 4.5 deals with the semi-linearized form of the I-V characteristic studied in Section 4.4. The results of the investigation are discussed in Section 4.6.

4.2 The Characteristics of Intermodulation Signals Generated In A Symmetrical Nonlinear I-V Characteristic In Which The Current Remains Constant After Reaching A fixed Maximum.(Symmetrical Current Limiter)

An arbitrary symmetrical nonlinear I-V characteristic covering a similar operating range to those discussed in Chapter III was sketched in cartesian coordinates. Data points corresponding to the arbitrary curve were then used in the CRC-in-house least squares polynomial approximation program (LSQPOLY) to generate a polynomial representation for the characteristic. Since the originally sketched curve was chosen arbitrarily, an acurate representation was not required, allowing a 20th degree polynomial fit to be requested. Table 4-1 shows the polynomial coefficients. Figure 4.1 shows a plot of the characteristic generated using the computed coefficients in the polynomial of eqn. 1-4.

By using the computed polynomial coefficients in computer program IMPWR, (Appendix A) intermodulation currents were calculated for use in computing intermodulation signal powers in the manner* described in Section 3.3.2(a) of Chapter III.

The computed intermodulation power/transmit power relationships for 3rd, 5th and 7th order intermodulation products are shown in figures 4.2, 4.3 and 4.4. Figure 4.5 shows the relationship between the power of intermodulation products of consecutive order at four different fixed total transmit powers.

---

* An average nonlinear resistance value of .02 ohms was used for all intermodulation power calculations in this chapter.

Table 4-1

Coefficients of The Power Series Polynomial* Used To Generate The Arbitrary I-V Characteristic of Figure 4.1

a_0	-1.035×10^{-17}
a_1	6.558×10^{1}
a_2	-4.073×10^{-13}
a_3	-2.091×10^{4}
a_4	-4.165×10^{-10}
a_5	2.375×10^{7}
a_6	3.402×10^{-6}
a_7	-1.847×10^{10}
a_8	-4.297×10^{-3}
a_9	8.533×10^{12}
a_{10}	2.507×10^{0}
a_{11}	-2.411×10^{15}
a_{12}	-8.157×10^{2}
a_{13}	4.219×10^{17}
a_{14}	1.571×10^{5}
a_{15}	-4.467×10^{19}
a_{16}	-1.780×10^{7}
a_{17}	2.623×10^{21}
a_{18}	1.097×10^{9}
a_{19}	-6.559×10^{22}
a_{20}	-2.842×10^{10}

* $I = a_0 + a_1V + a_2V^2 + \ldots\ldots + a_nV^n$, where I has units of Amps, and V has units of Volts.

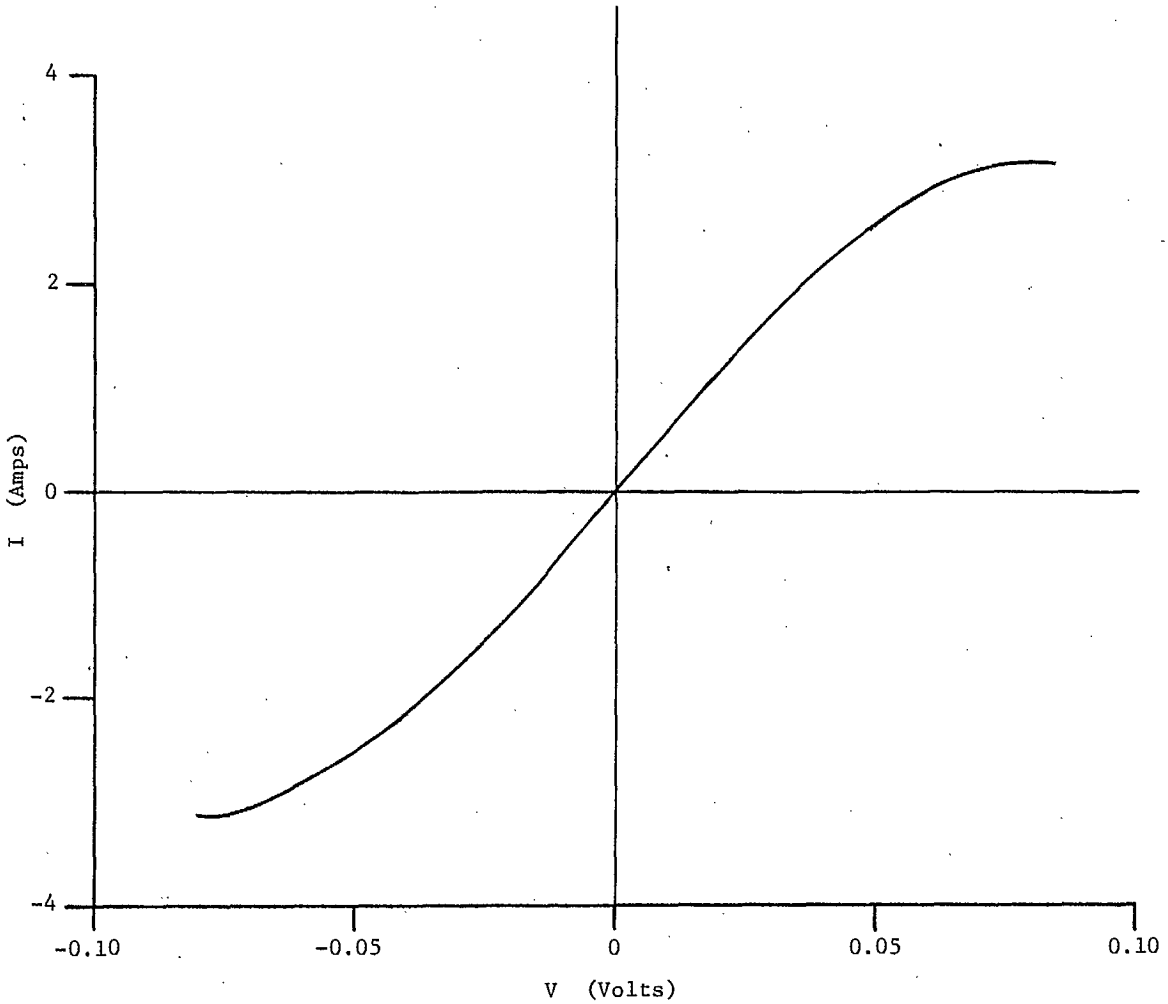

Fig. 4.1. Symmetrical "limiter-type" I-V characteristic computed using the polynomial coefficients of Table 4-1 in Equation 1-4.

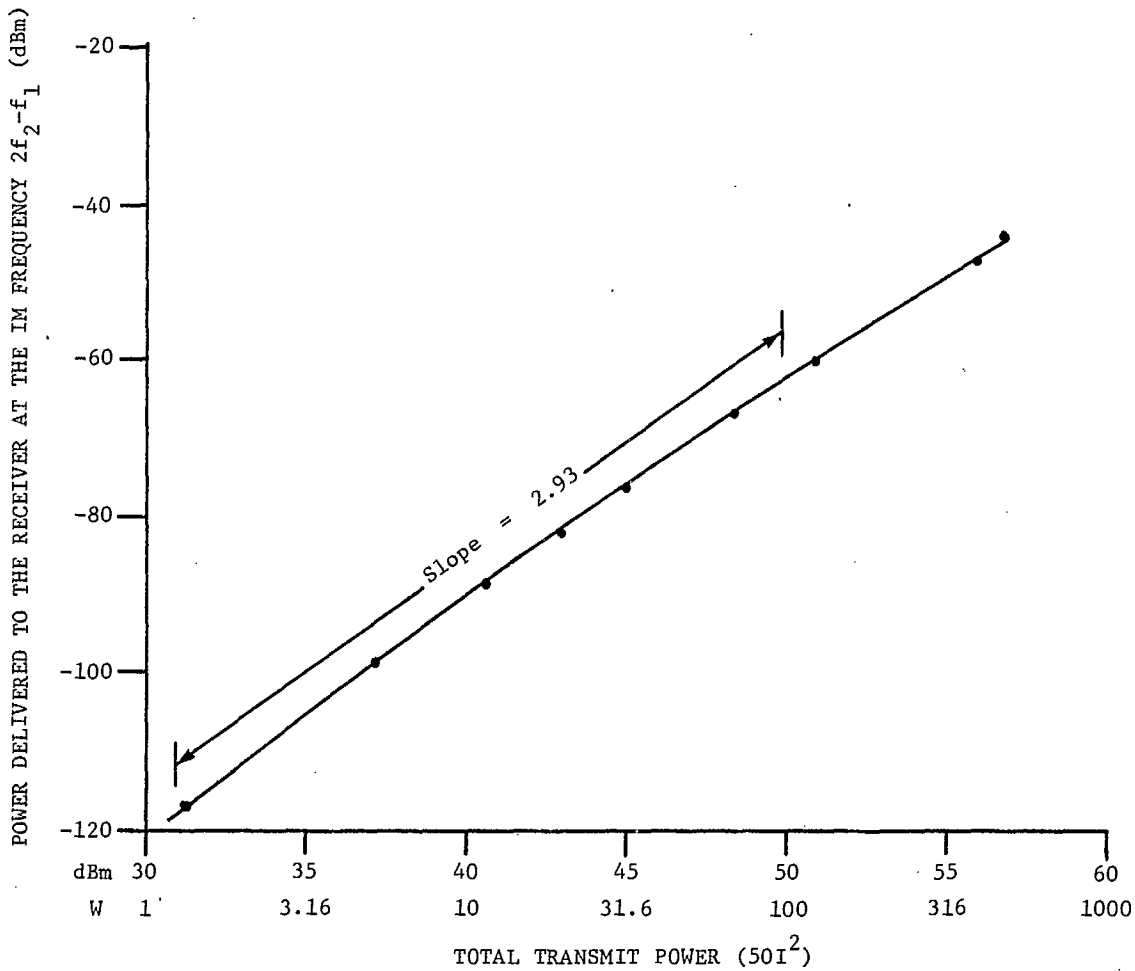

Fig. 4.2. Computed third order IM signal power dependence on total transmit power for IM signals generated by application of a two frequency signal to the symmetrical "current limiter-type" I-V characteristic of Fig. 4.1.

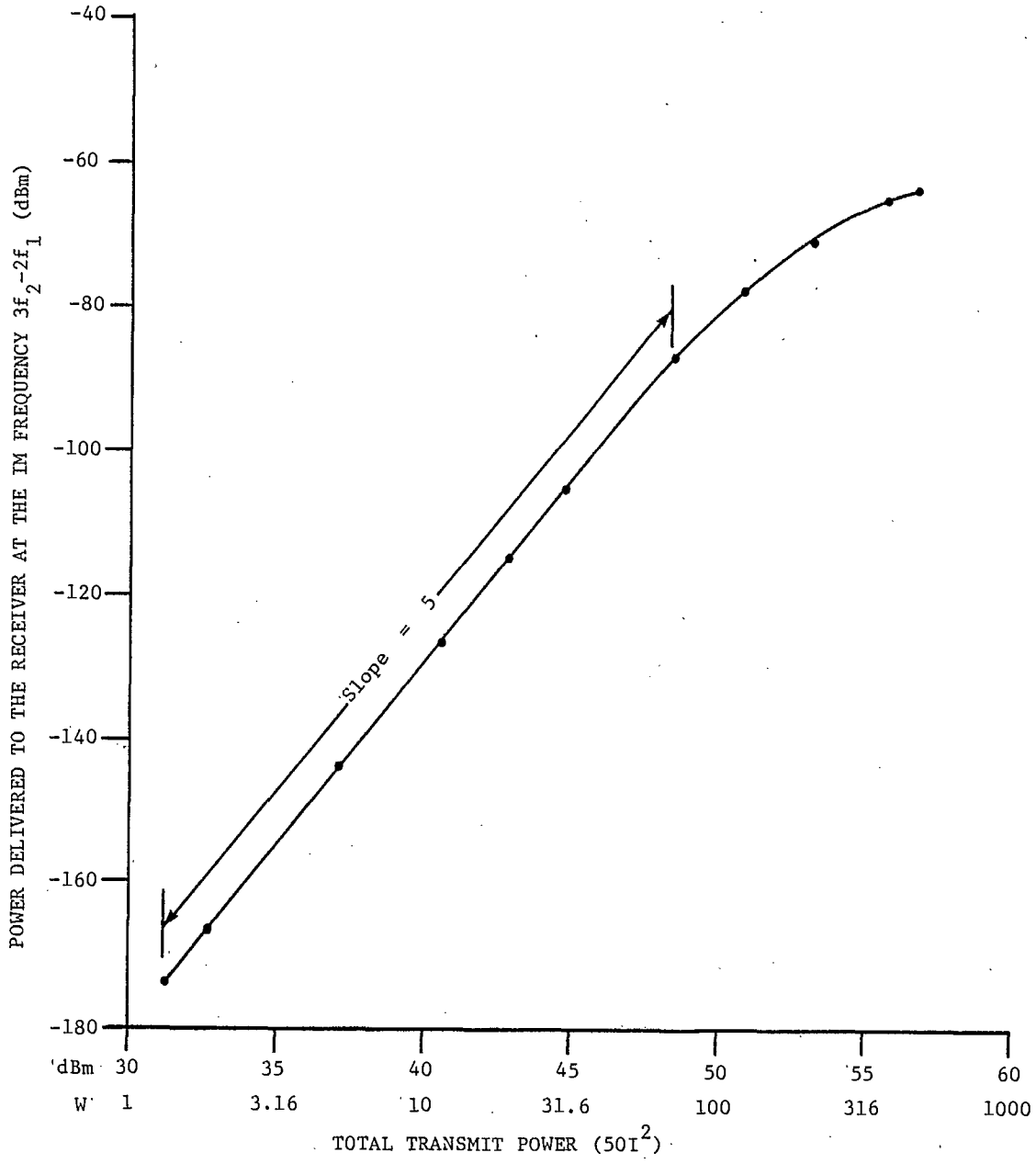

Fig. 4.3 Computed fifth order IM signal power dependence on total transmit power for IM signals generated by application of a two frequency signal to the symmetrical "current limiter-type" I-V characteristic of Fig. 4.1.

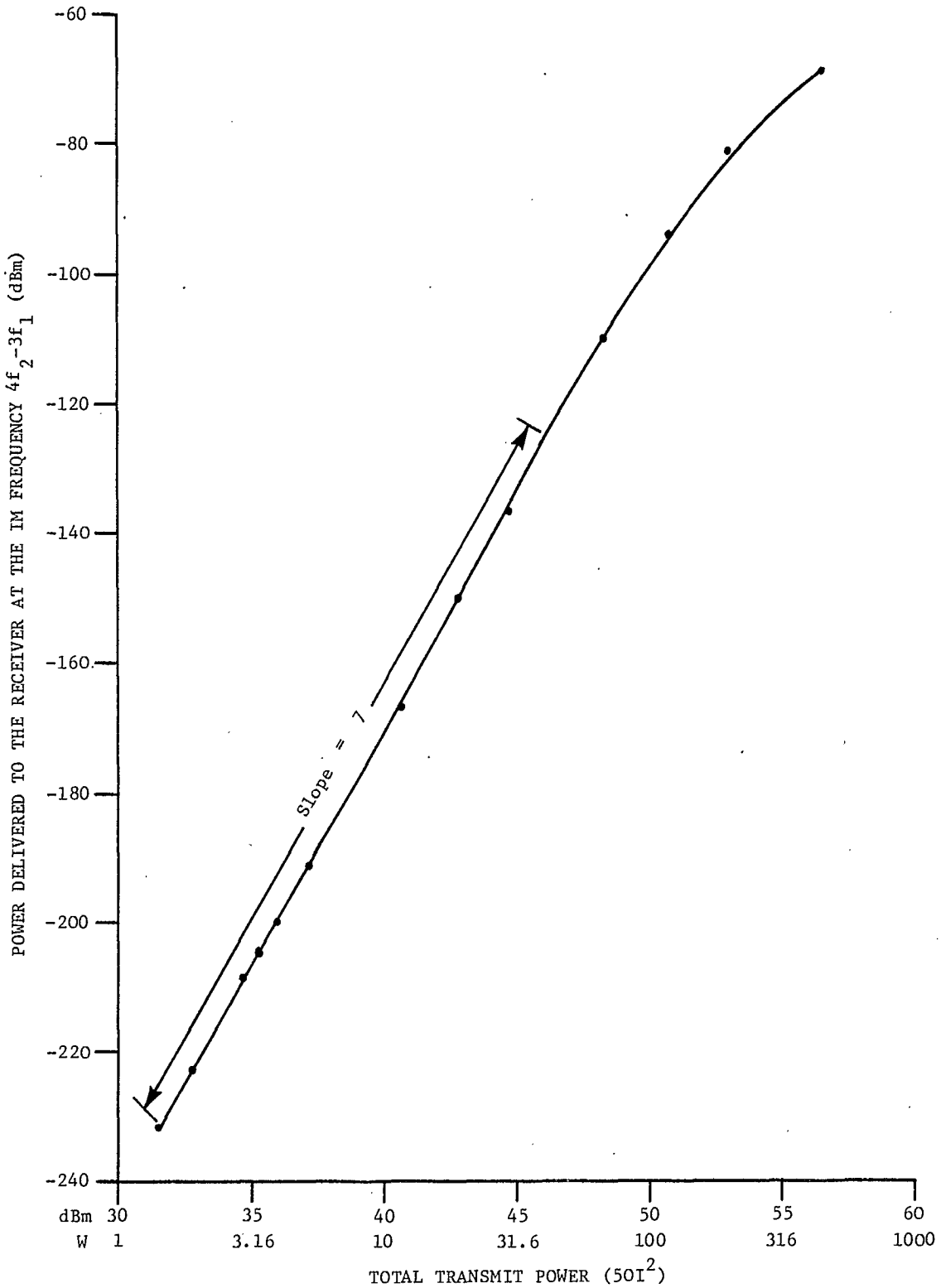

Fig. 4.4. Computed seventh order IM signal power dependence on total transmit power for IM signals generated by application of a two frequency signal to the symmetrical "current limiter-type" I-V characteristic of Fig. 4.1.

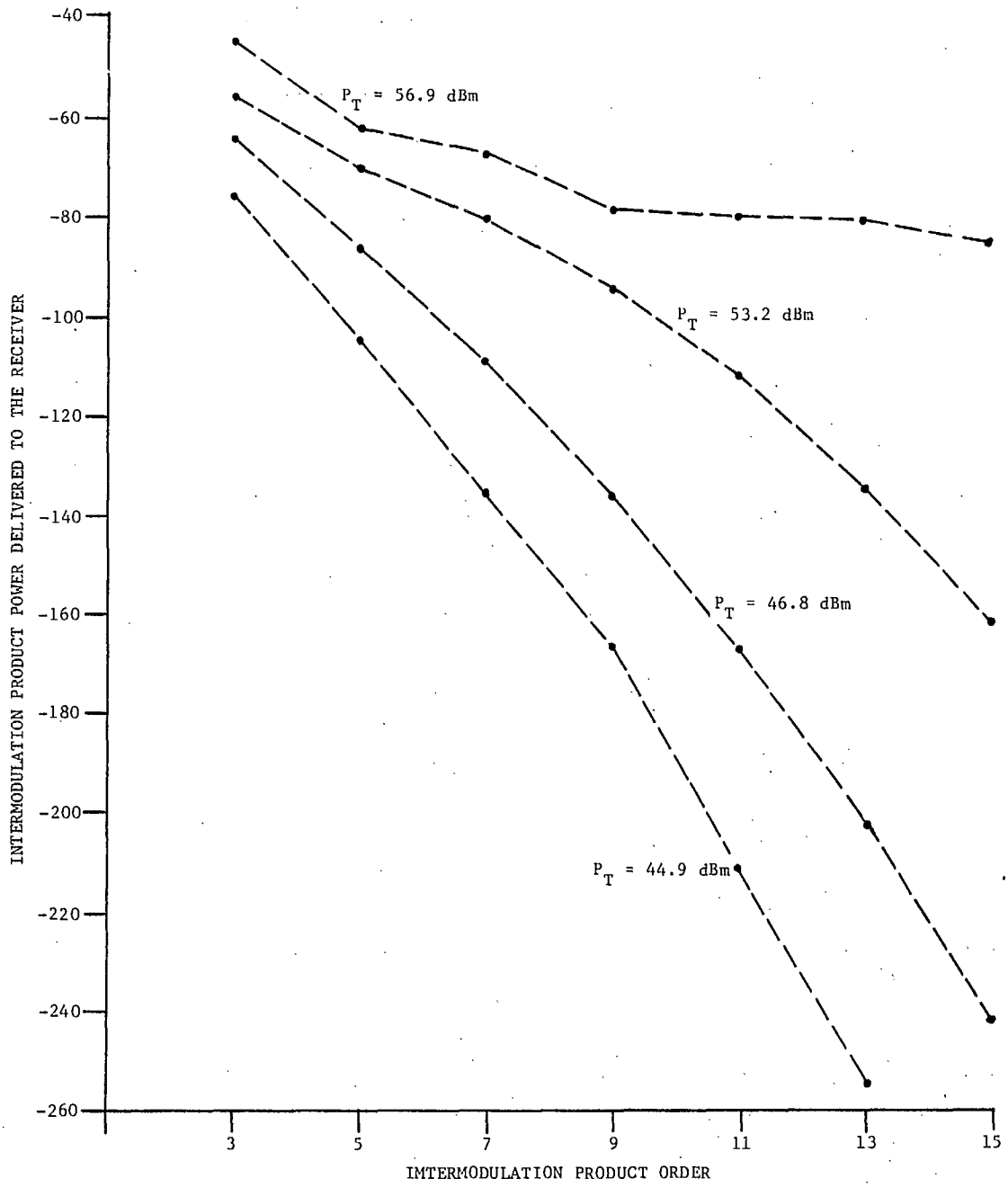

Fig. 4.5. The computed relative power of IM signals of consecutive order generated by the application of two frequency signals of different total power to the symmetrical "current limiter-type" I-V characteristic of Fig. 4.1.

The intermodulation power/transmit power curves are notably free from minima of the type found during a previous study [1]. The figures also show a nearly NdB/dB slope, at Nth order, except for high powers, where the polynomial approximation is less accurate.

Figure 4.5 shows that the relationship between the power of intermodulation products of different order is dependent upon total transmit power, but is monotonic. The curves show decreasing slopes as transmit power is increased.

4.3 The Characteristics of Intermodulation Signals Generated by A Non-Symmetrical Nonlinearity In Which Positive Currents Remain Constant After Reaching a Fixed Maximum and Negative Currents Vary Linearly As A Function of Voltage (Semilinearized Current Limiter)

The symmetrical I-V characteristic studied in Section 4.2 was altered by linearizing the characteristic for negative currents and voltages. Numerical data from the semi-linearized I-V characteristic was input to CRC in-house computer program LSQPOLY to obtain a representative least squares polynomial approximation. Table 4-2 shows coefficients of the computed 20th degree polynomial. Figure 4.6 is a plot of the I-V relationship obtained by substitution of the computed polynomial coefficients in eqn. 1-4.

Intermodulation power/drive power relationships are shown in figures 4.7 to 4.9. Figure 4.10 is a plot of the relative power of intermodulation signals of consecutive order at fixed transmit powers.

The figures show that, as for the symmetrical "current limiter", there are no minima in the intermodulation power/drive power relationships. The relative magnitude plot for intermodulation products of consecutive order is identical, except for magnitudes, to the corresponding plot for the symmetrical characteristic.

Table 4-2

Coefficients of The Power Series Polynomial* Used To Generate The Arbitrary I-V Characteristic of Figure 4.4

a_0	-3.393×10^{-4}
a_1	6.612×10^{1}
a_2	-1.335×10^{2}
a_3	-1.042×10^{4}
a_4	-1.699×10^{5}
a_5	1.173×10^{7}
a_6	3.332×10^{8}
a_7	-8.997×10^{9}
a_8	-3.134×10^{11}
a_9	4.066×10^{12}
a_{10}	1.666×10^{14}
a_{11}	-1.109×10^{15}
a_{12}	-5.392×10^{16}
a_{13}	1.838×10^{17}
a_{14}	1.087×10^{19}
a_{15}	-1.785×10^{19}
a_{16}	-1.339×10^{21}
a_{17}	9.129×10^{20}
a_{18}	9.241×10^{22}
a_{19}	-1.805×10^{22}
a_{20}	-2.741×10^{24}

* $I = a_0 + a_1V + a_2V^2 + \ldots\ldots + a_3V^3$, where I has units of Amps and V has units of Volts.

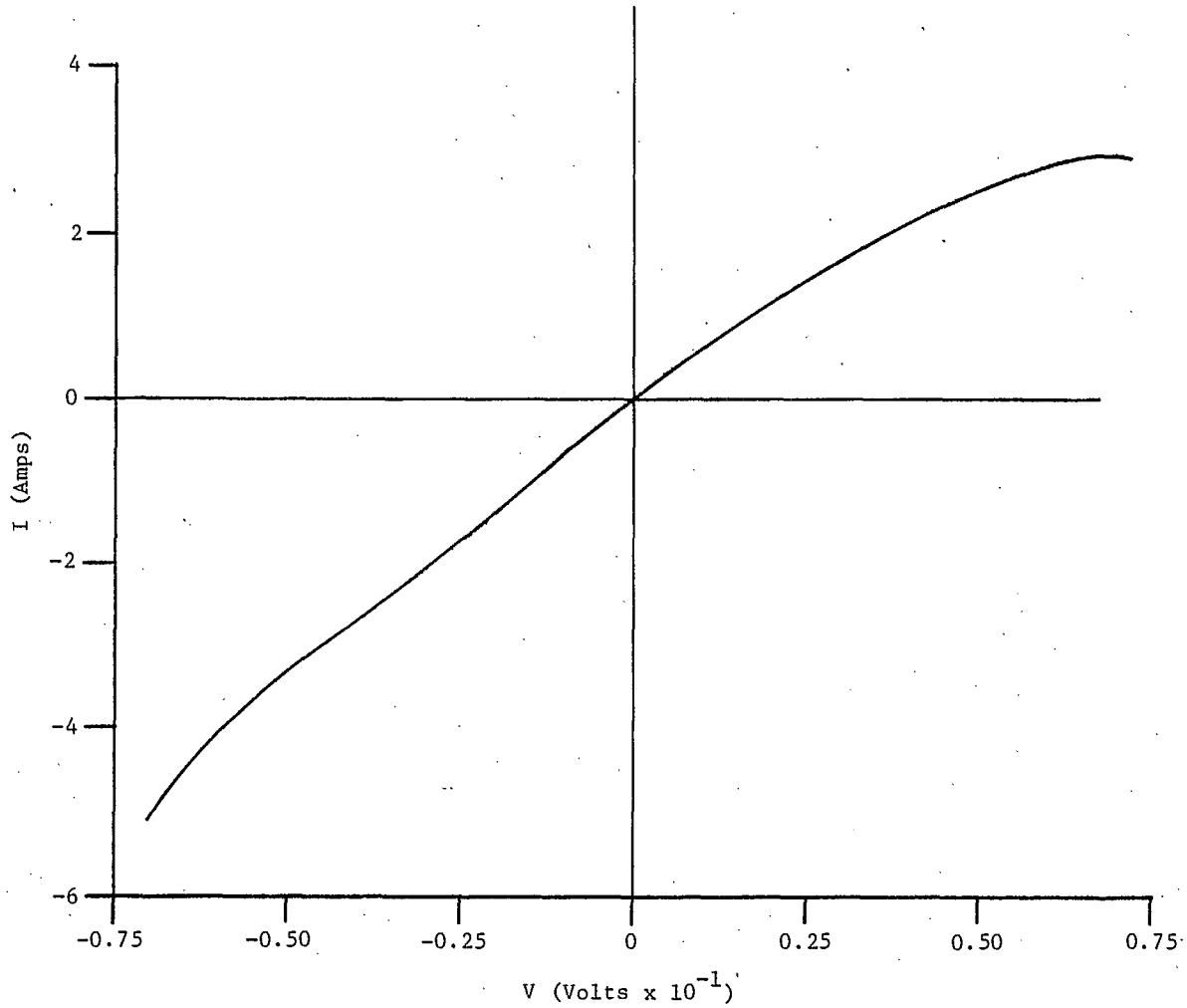

Fig. 4.6. Semilinearized "limiter-type" I-V characteristic computed using the coefficients of Table 4-2 in Equation 1-4.

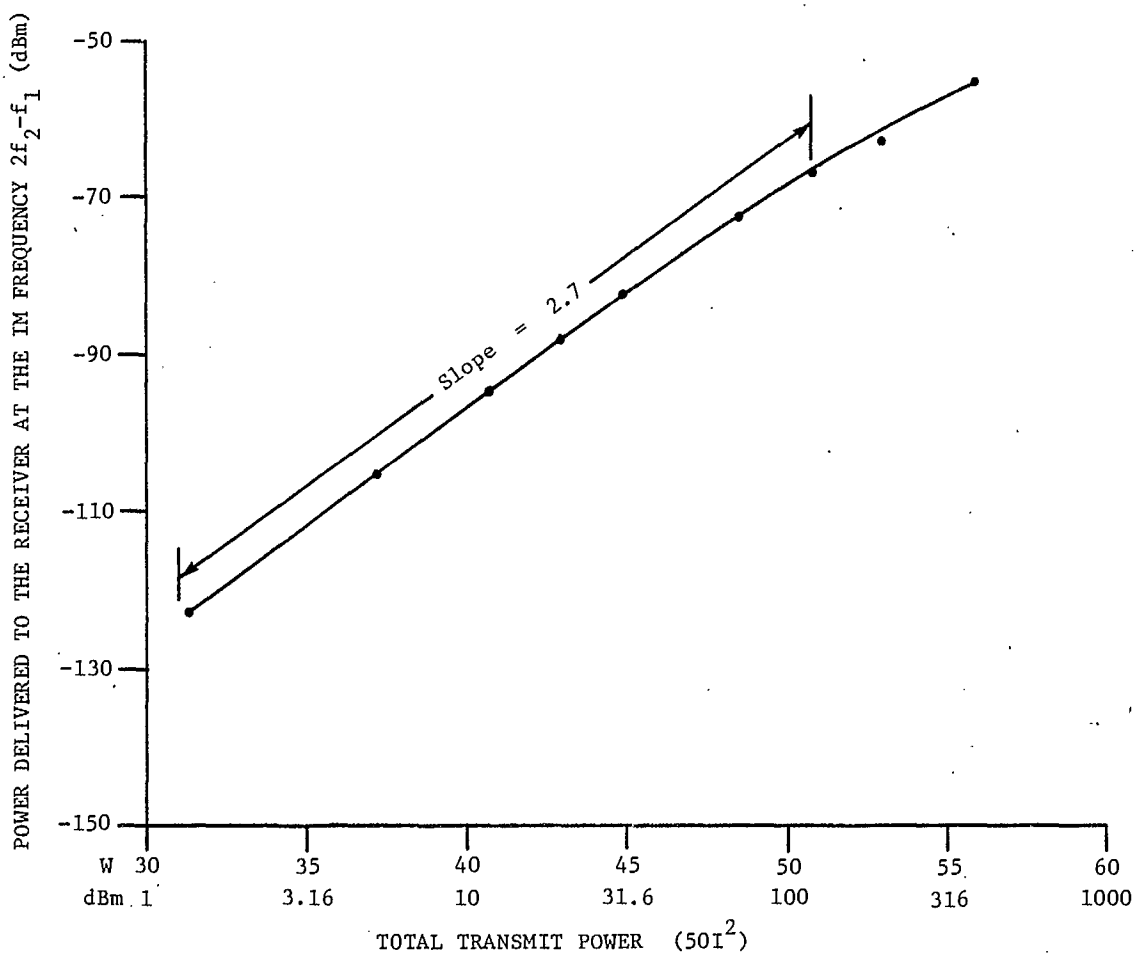

Fig. 4.7. Computed third order IM signal power dependence on total transmit power for IM signals generated by application of a two frequency signal to the semilinearized "current limiter-type" I-V characteristic of Fig. 4.6.

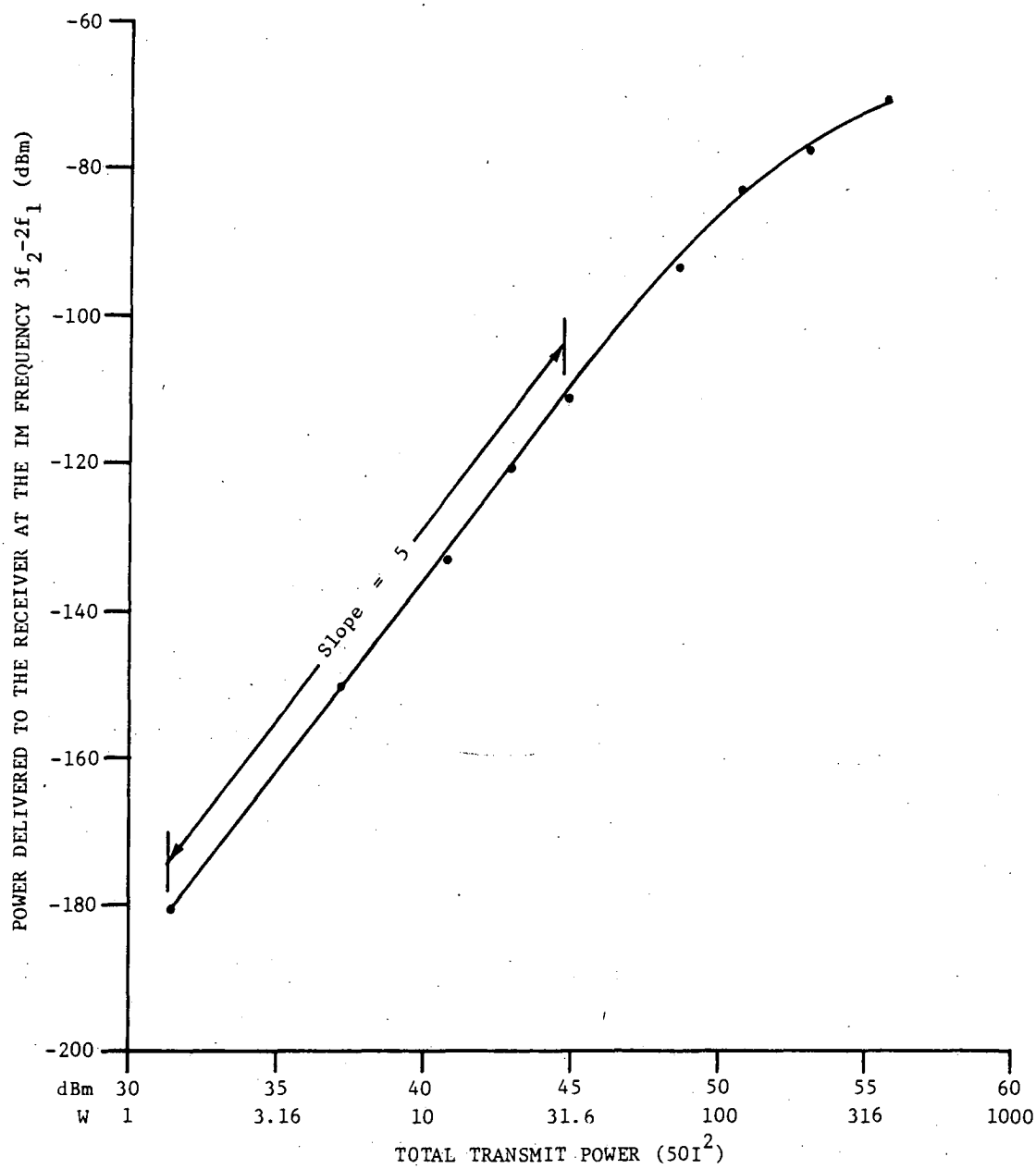

Fig. 4.8. Computed fifth order IM signal power dependence on total transmit power for IM signals generated by application of a two frequency signal to the semi-linearized "current limiter-type" I-V characteristic of Fig. 4.6.

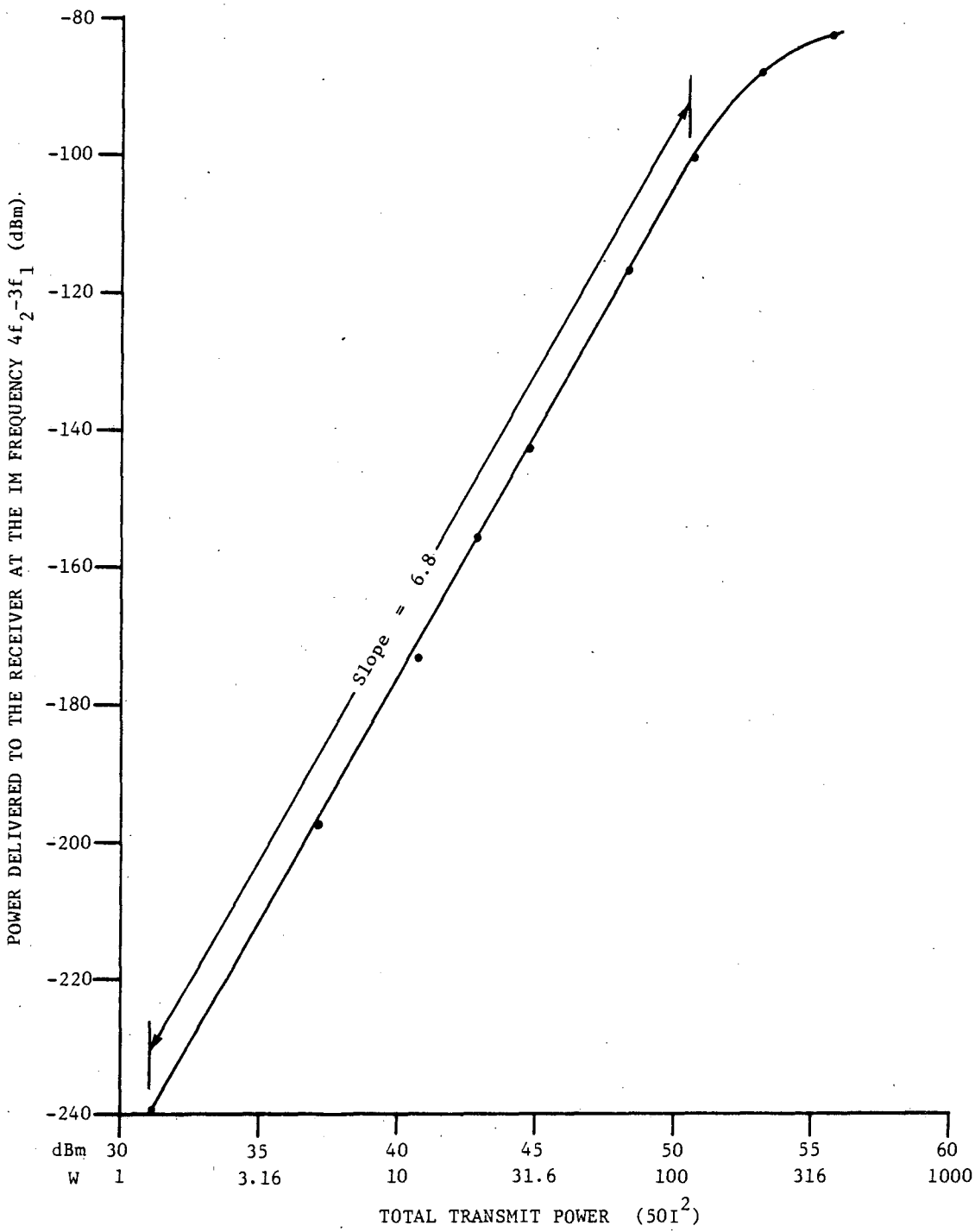

Fig. 4.9. Computed seventh order IM signal power dependence on total transmit power for IM signals generated by application of a two frequency signal to the semi-linearized "current limiter-type" I-V characteristic of Fig. 4.6.

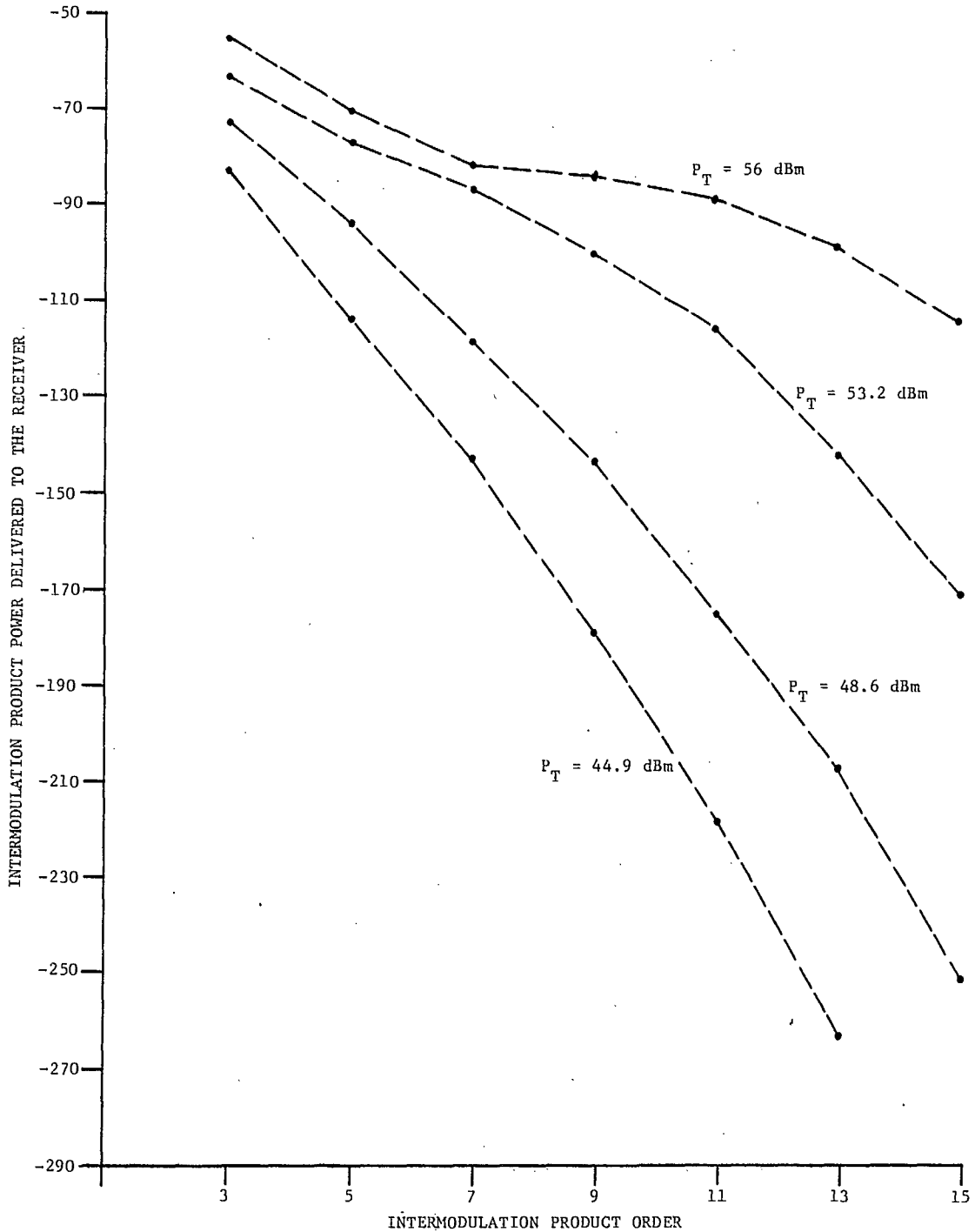

Fig. 4.10. The computed relative power of IM signals of consecutive order generated by the application of two frequency signals of different total power to the semilinearized "current limiter-type" I-V characteristic of Fig. 4.6.

4.4 The Characteristics of Intermodulation Signals Generated in a Symmetrical Nonlinearity In Which Current Rises Rapidly as a Function of Voltage (Symmetrical "current expander")

An arbitrary symmetrical I-V characteristic in which current increases very rapidly (positively and negatively) as a function of applied voltage was sketched in cartesian coordinates. Currents and voltages in a region of operation similar to that represented by the characteristics studied in Chapter III were chosen. Data from the sketch were used in program LSQPOLY to obtain a least squares polynomial representation. The coefficients of the computed 15th degree* polynomial are shown in Table 4-3. Figure 4.11 is a plot of the current and voltage data generated by the substitution of the computed coefficients in eqn. 1-4.

The method described in Section 3.2 of Chapter III was used to compute intermodulation signal powers as a function of total transmit power. Figures 4.12 to 4.14 show 3rd, 5th and 7th order intermodulation product power dependence upon total transmit power. Figure 4.15 shows the relative power of intermodulation signals of consecutive orders at four different fixed total transmit powers.

The most significant feature of the intermodulation signal/drive power relationships for this symmetrical "current expander" is the occurrence of deep intermodulation power minima

---

* Very poor fits were obtained for higher order polynomials.

Table 4-3

Coefficients of The Power Series Polynomial Used To Generate The Arbitrary I-V Characteristic of Figure 4.11*

a_0	-9.306×10^{-17}
a_1	3.781×10^{01}
a_2	1.103×10^{-12}
a_3	-6.371×10^{03}
a_4	-2.223×10^{-09}
a_5	2.081×10^{07}
a_6	9.247×10^{-07}
a_7	-2.119×10^{10}
a_8	1.544×10^{-04}
a_9	1.039×10^{13}
a_{10}	-1.608×10^{-01}
a_{11}	-2.575×10^{15}
a_{12}	3.199×10^{01}
a_{13}	3.156×10^{17}
a_{14}	-2.037×10^{03}
a_{15}	-1.524×10^{19}

* $I = a_0 + a_1V + a_2V^2 + \ldots\ldots + a_{15}V^{15}$, where I has units of Amps and V has units of Volts.

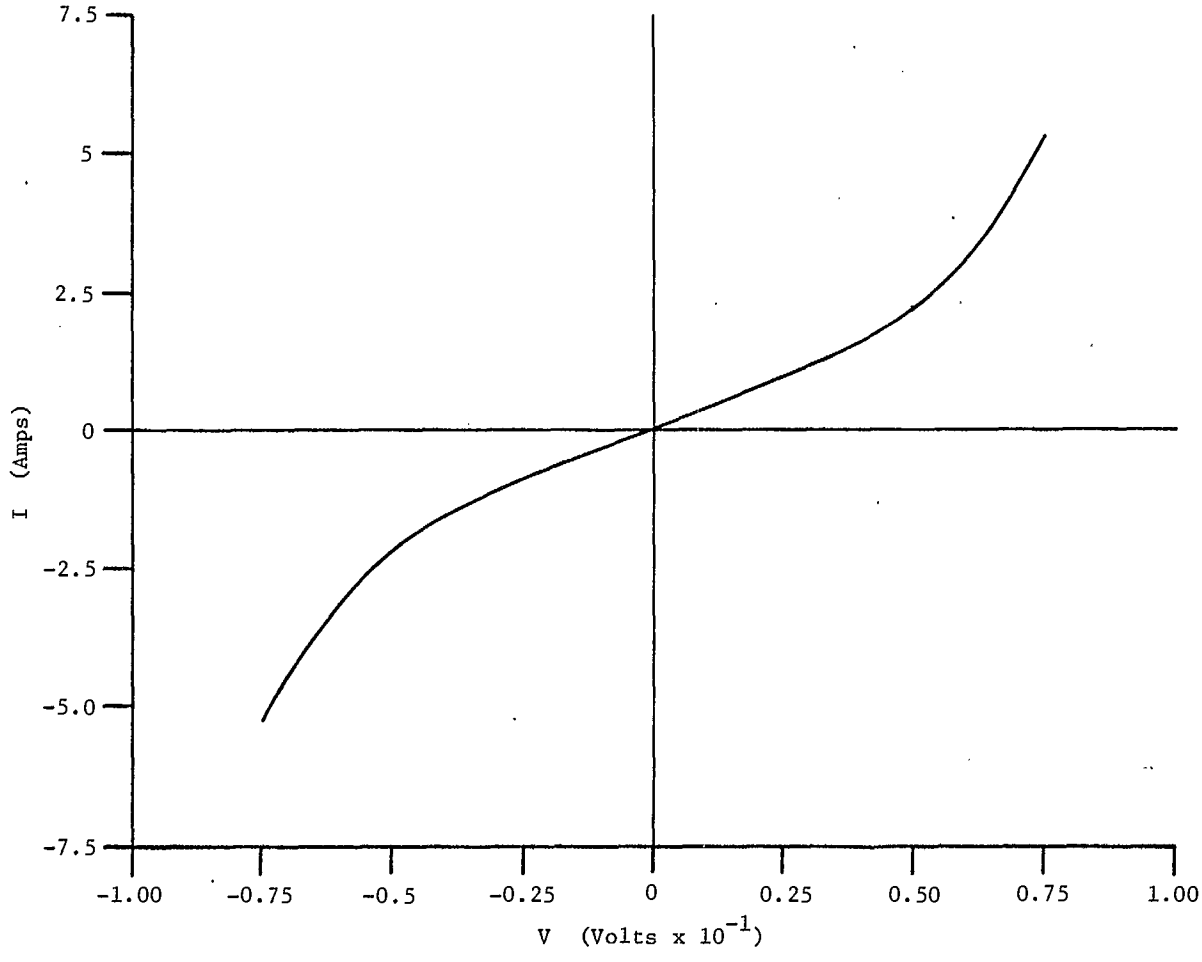

Fig. 4.11. Symmetrical "expander-type" I-V characteristic computed using the coefficients of Table 4-3 in Equation 1-4.

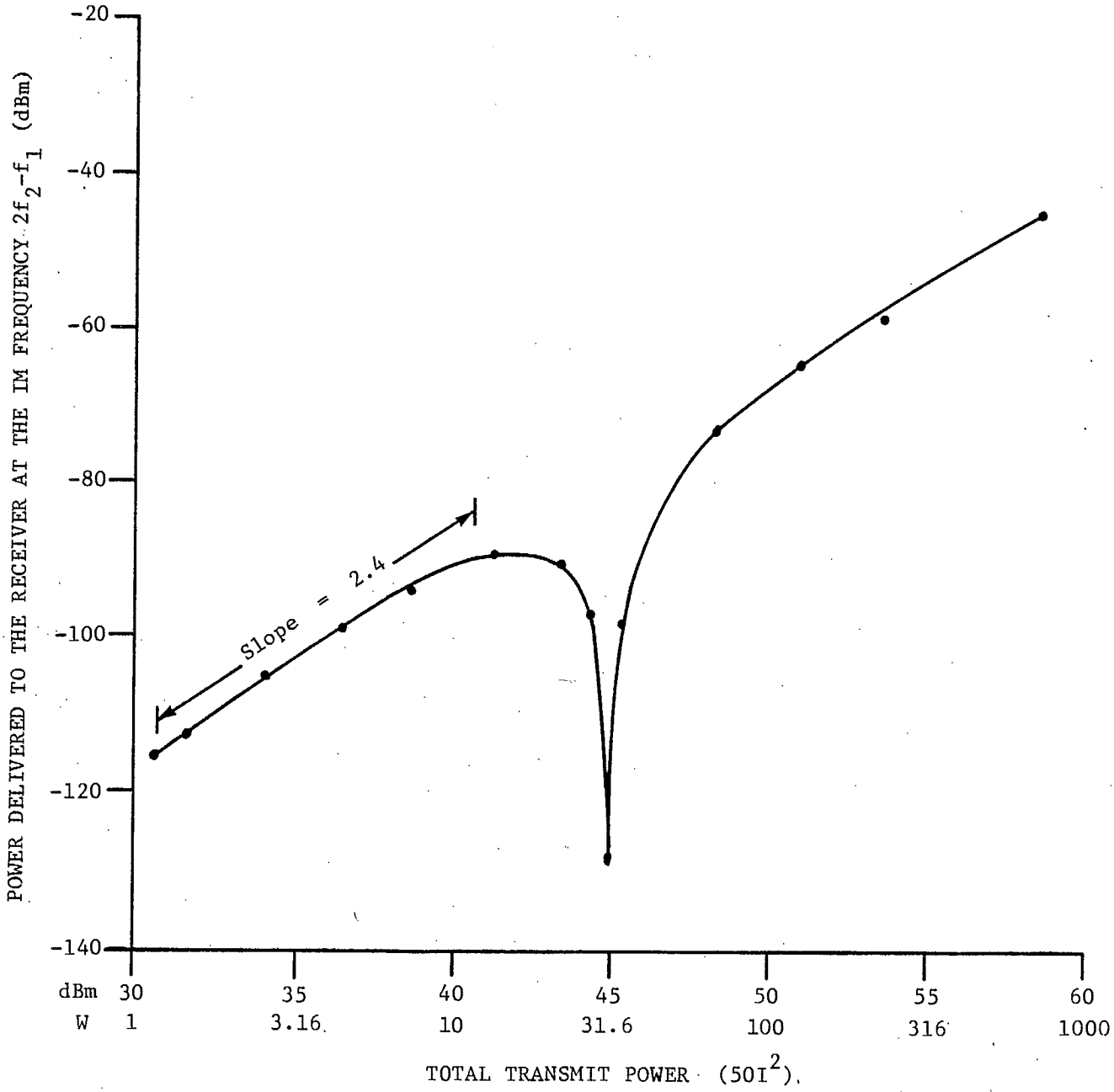

Fig. 4.12. Computed third order IM signal power dependence on total transmit power for IM signals generated by application of a two frequency signal to the symmetrical "current expander-type" I-V characteristic of Fig. 4.1.

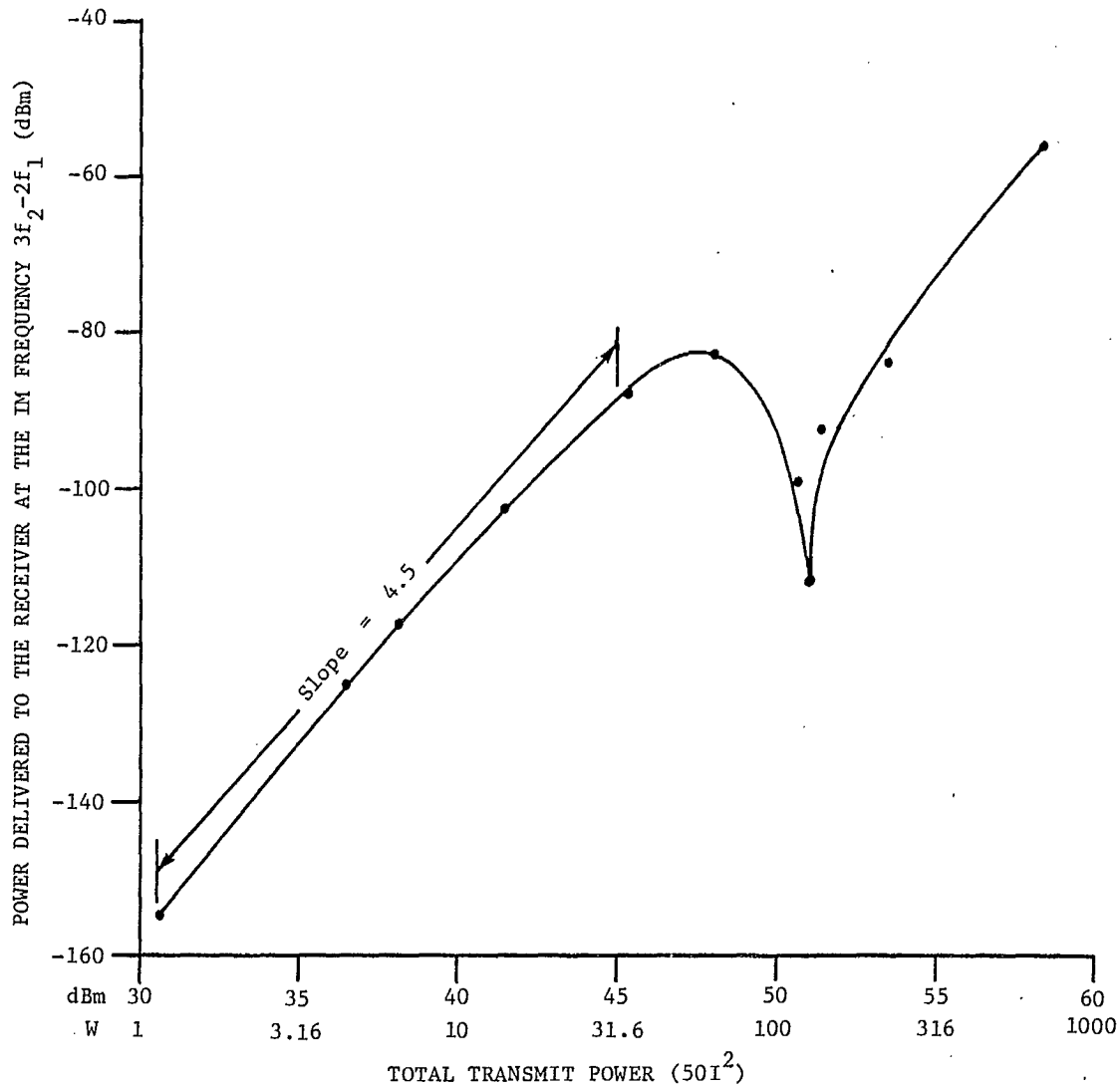

Fig. 4.13. Computed fifth order IM signal power dependence on total transmit power IM signals generated by application of a two frequency signal to the symmetrical "current expander-type" I-V characteristic of Fig. 4.11.

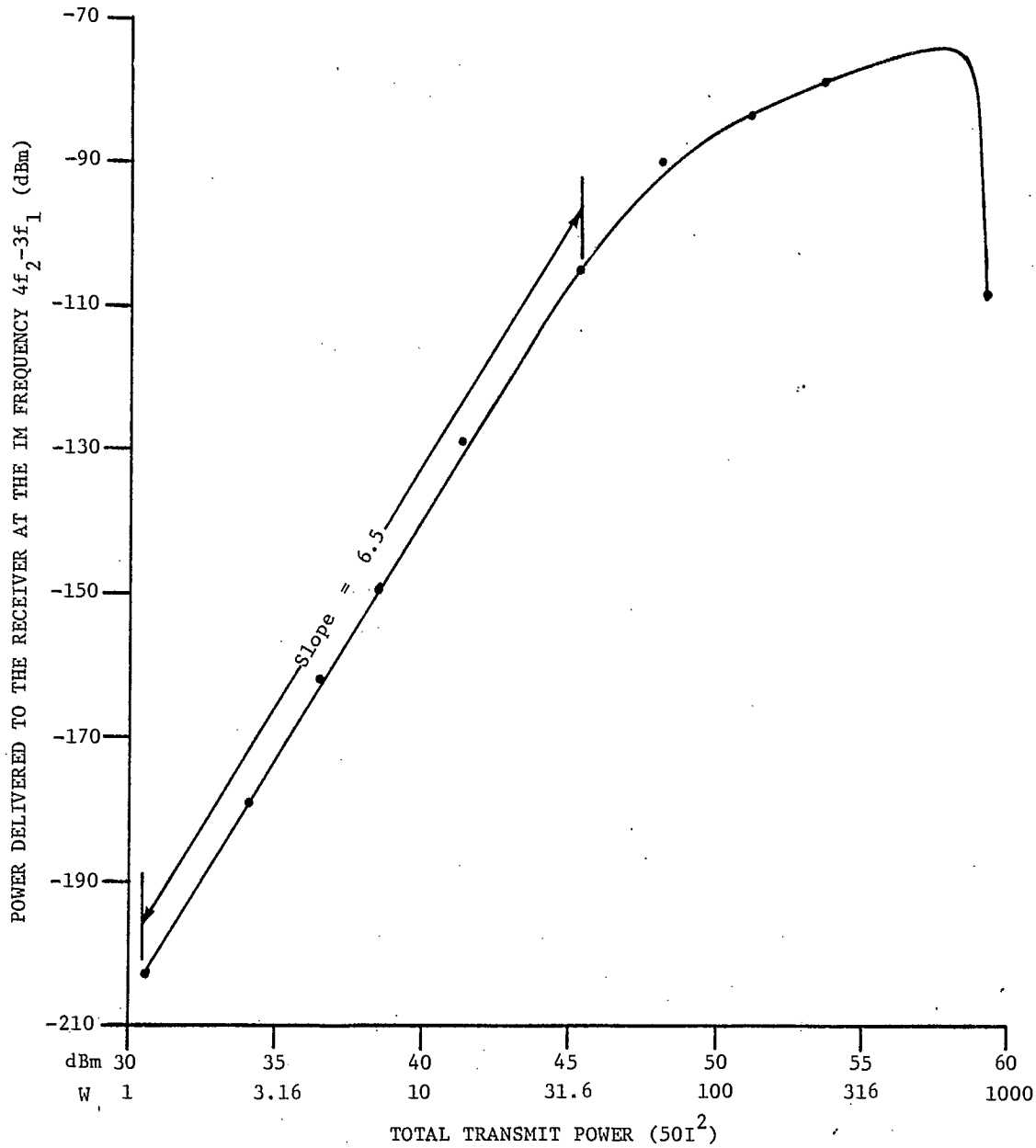

Fig. 4.14. Computed seventh order IM signal power dependence on total transmit power for IM signals generated by application of a two frequency signal to the symmetrical "current expander-type" I-V characteristic of Fig. 4.11.

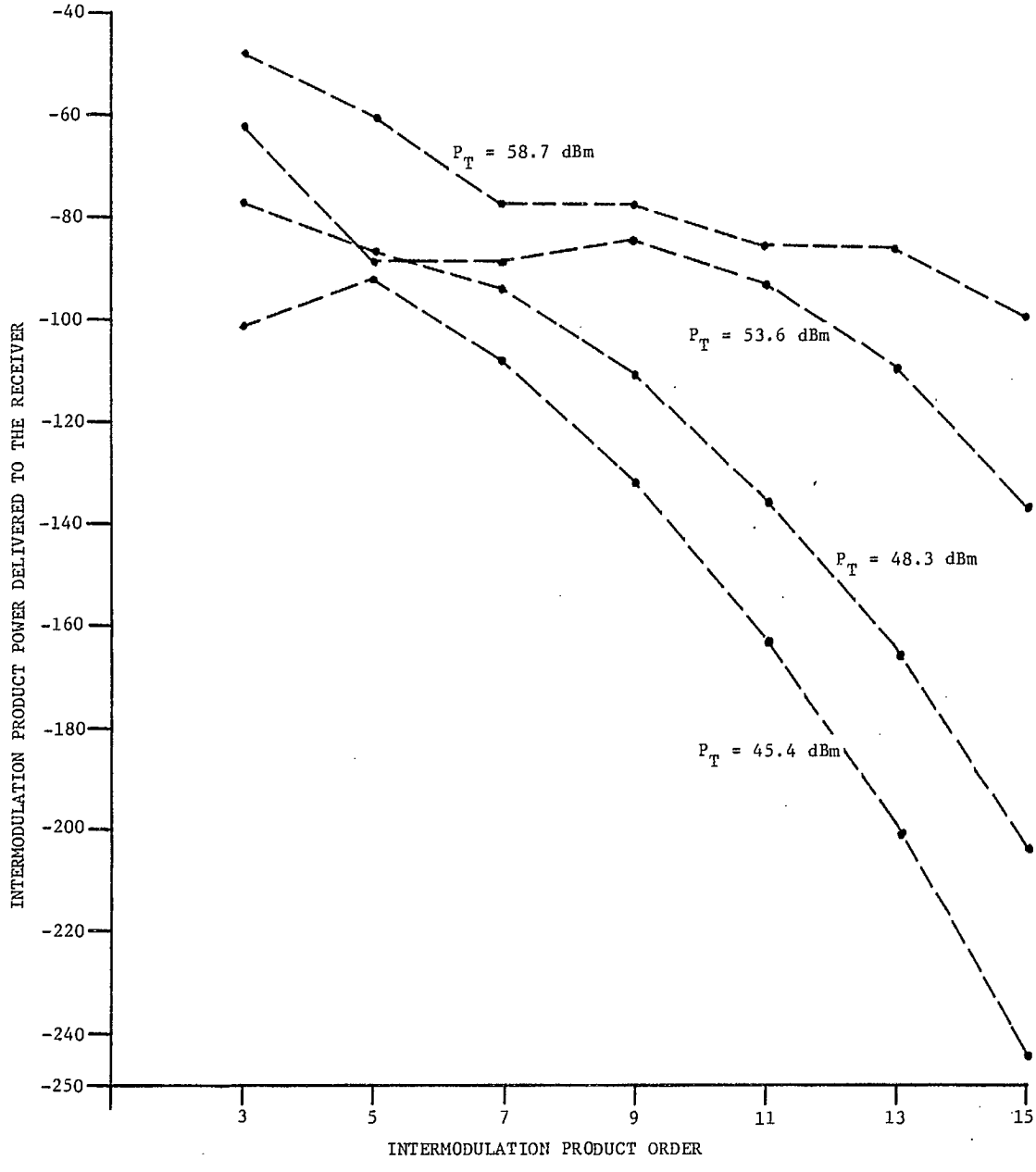

Fig. 4.15. The computed relative power of IM signals of consecutive order generated by the application of two frequency signals of different total power to the symmetrical "current expander-type" I-V characteristic of Fig. 4.11.

for all orders. The deepest minimum occurs in the third order characteristic, and the minima become more shallow and at higher transmit powers for higher orders. The second notable feature is that the slopes of the curves are significantly less than NdB/dB (N is intermodulation order) in their most linear regions. Finally, it should be noted that as a direct result of the minima in the intermodulation signal/drive power characteristics, the power/order relationships are non-monotonic.

4.5 The Characteristics of Intermodulation Signals Generated in a Non-Symmetrical Nonlinearity In Which Current Rises Rapidly As A Function of Voltage In The Positive Voltage Region, and Is An Almost Linear Function of Voltage In the Negative Voltage Region (Semilinearized "Current Expander")

The symmetrical I-V characteristic of Section 4.4 was altered by linearizing the characteristic for negative currents and voltages. The least squares polynomial program (LSQPOLY) was then applied to data from the semi-linearized characteristic. Table 4-4 shows the coefficients of the resultant 15th degree polynomial. Figure 4.16 is a plot of I-V characteristic obtained by using the computed characteristic in eqn. 1.4.

The method of Section 3.2 in Chapter III was again used to compute intermodulation signal powers as a function of total transmit power. Figures 4.17, 4.18 and 4.19 show the 3rd, 5th and 7th order characteristics respectively. Figure 4.20 shows the relative power of intermodulation signals of consecutive order at four different fixed total transmit powers.

Like the characteristics for the symmetrical "current expander", the intermodulation signal/drive power curves for the semi-linearized expander studied in this section show intermodulation power minima. For this characteristic, however, the relationship between the depth of the minima and intermodulation product order is absent, although the minima still occur at higher transmit powers for higher orders. The slopes of the most linear portions of the curves are significantly less than NdB/dB. The intermodulation power/order relationships are again non-monotonic as a result of the minima in the drive power response curves.

Table 4-4

Coefficients of The Power Series Polynomial Used To Generate The Arbitrary I-V Characteristic of Figure 4-16

a_0	9.735×10^{-4}
a_1	3.727×10^{1}
a_2	-5.163×10^{1}
a_3	-1.554×10^{3}
a_4	1.804×10^{5}
a_5	9.336×10^{6}
a_6	-2.064×10^{8}
a_7	-9.953×10^{9}
a_8	1.054×10^{11}
a_9	4.965×10^{12}
a_{10}	-2.512×10^{13}
a_{11}	-1.240×10^{15}
a_{12}	2.873×10^{15}
a_{13}	1.526×10^{17}
a_{14}	-1.269×10^{17}
a_{15}	-7.382×10^{18}

* $I = a_0 + a_1V + a_2V^2 + \ldots\ldots + a_{15}V^{15}$, where I has units of Amps and V has units of Volts.

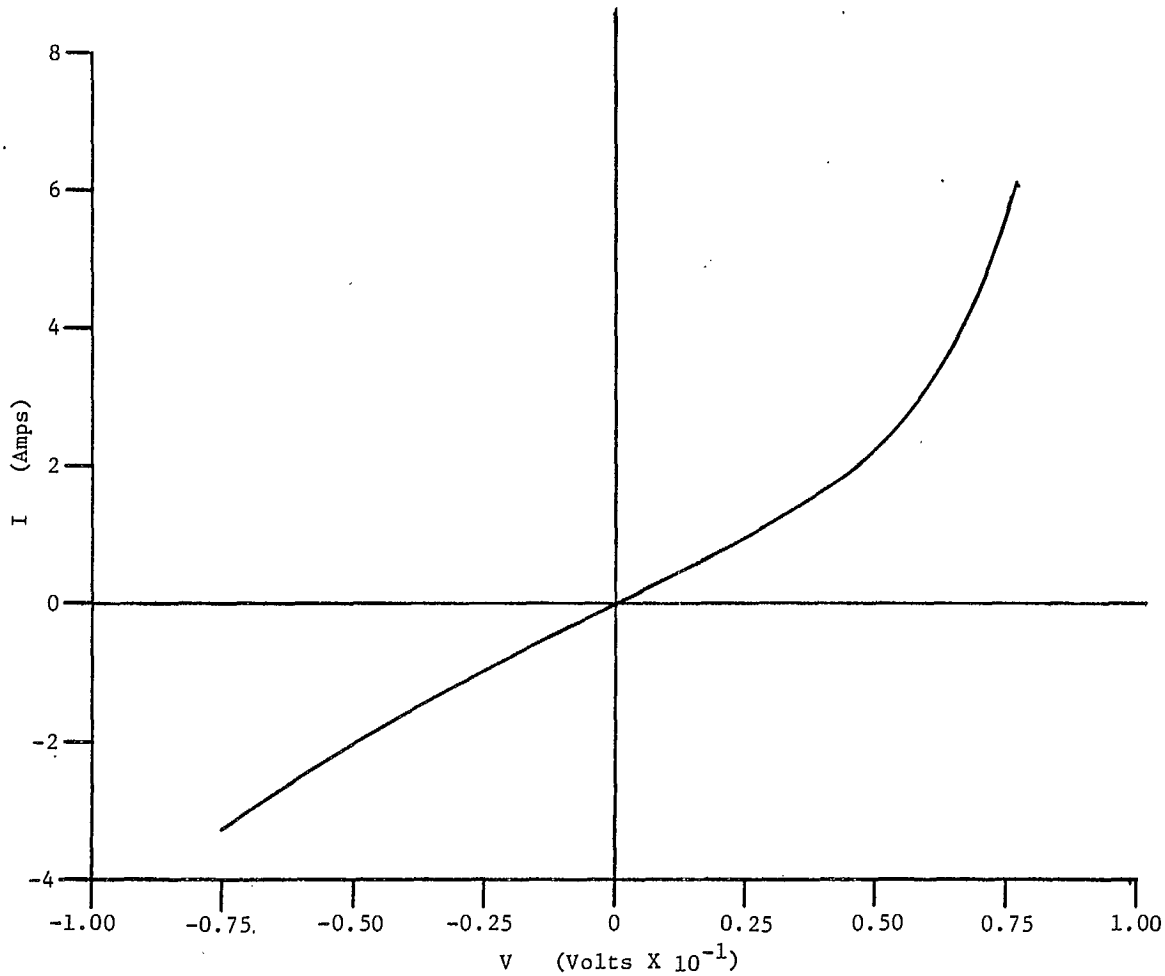

Fig. 4.16. Semilinearized "expander-type" I-V characteristic computed using the coefficients of Table 4-4 in Equation 1-4.

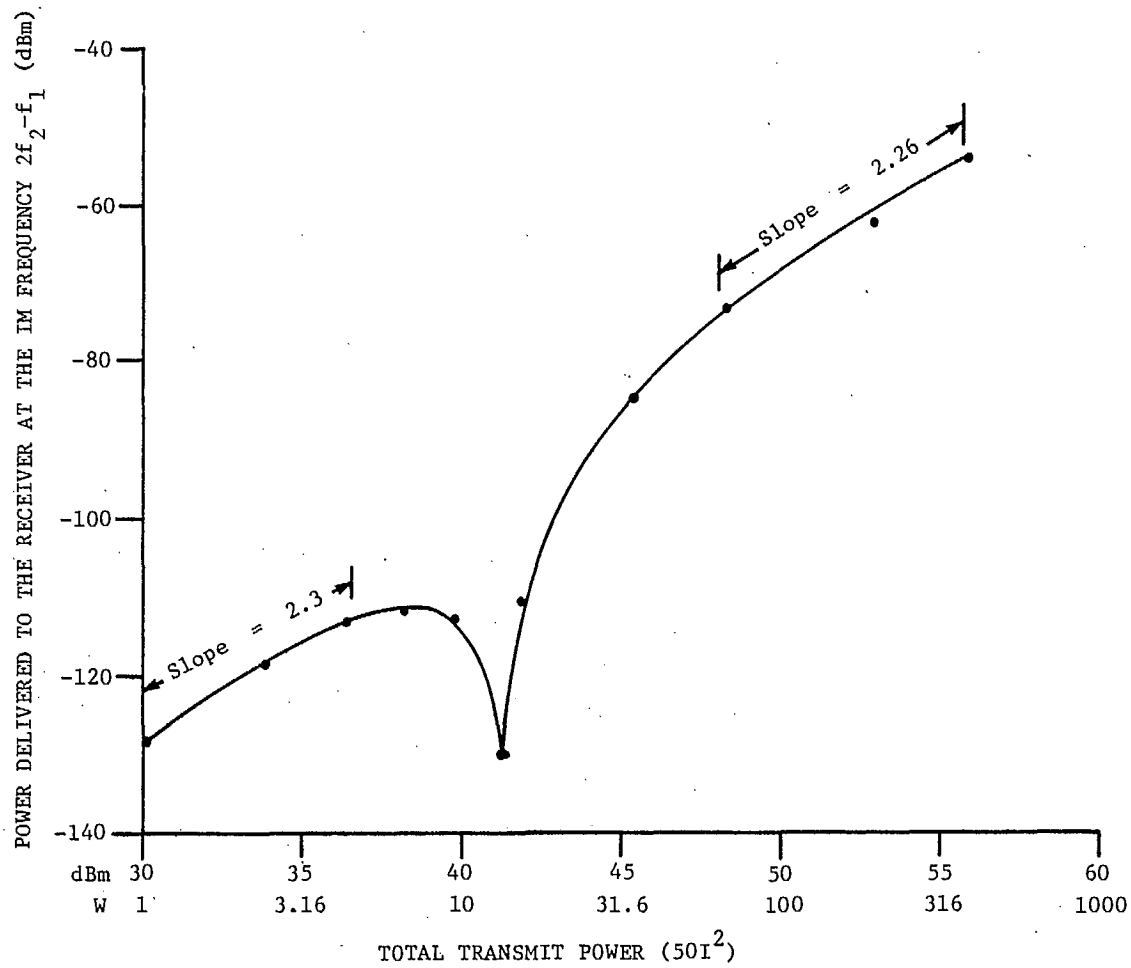

Fig. 4.17. Computed third order IM signal power dependence on total transmit power for IM signals generated by application of a two frequency signal to the semi-linearized "current expander-type" I-V characteristic of Fig. 4.16.

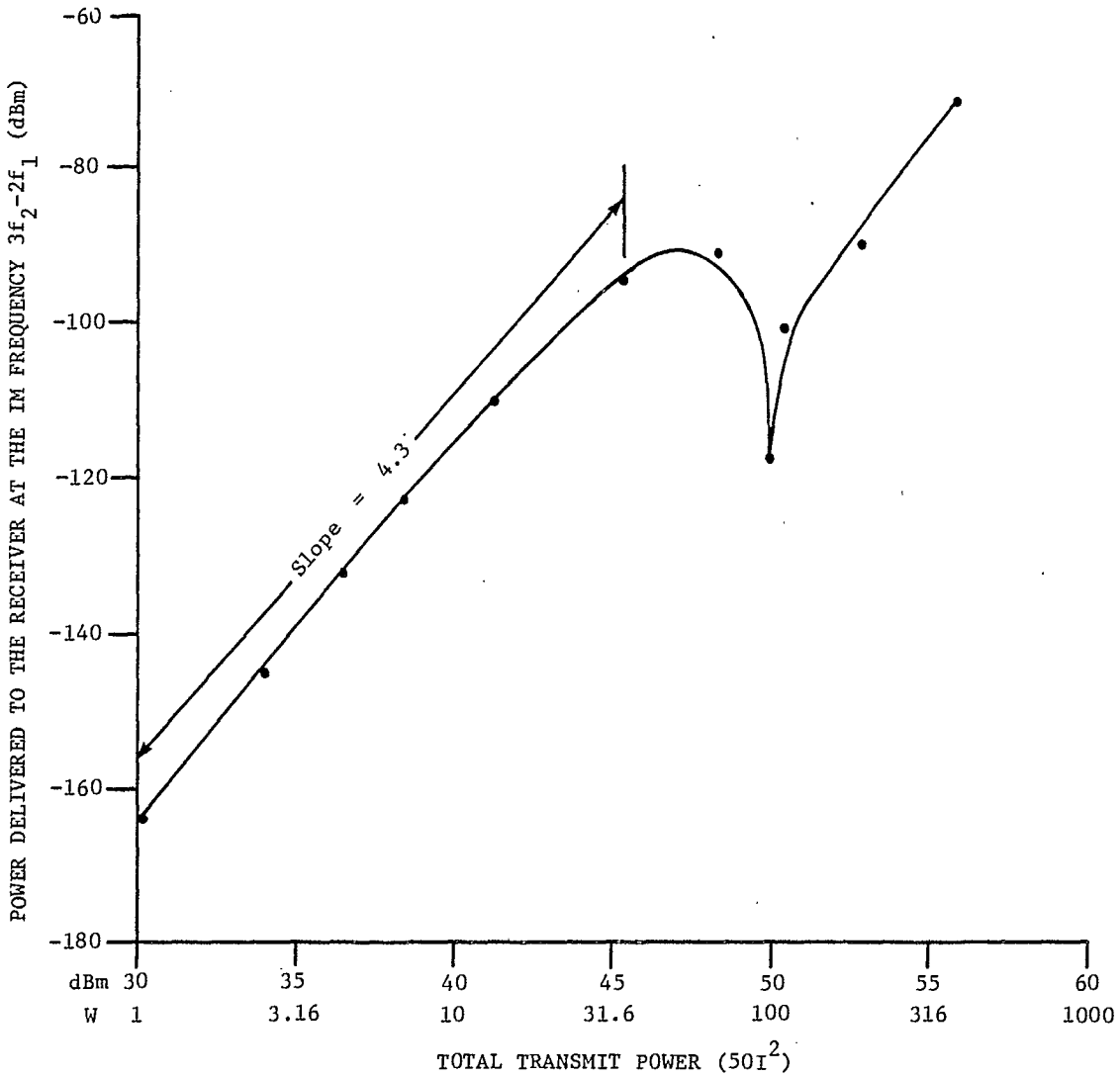

Fig. 4.18. Computed fifth order IM signal power dependence on total transmit power for IM signals generated by application of a two frequency signal to the semilinearized "current expander-type" I-V characteristic of Fig. 4.16.

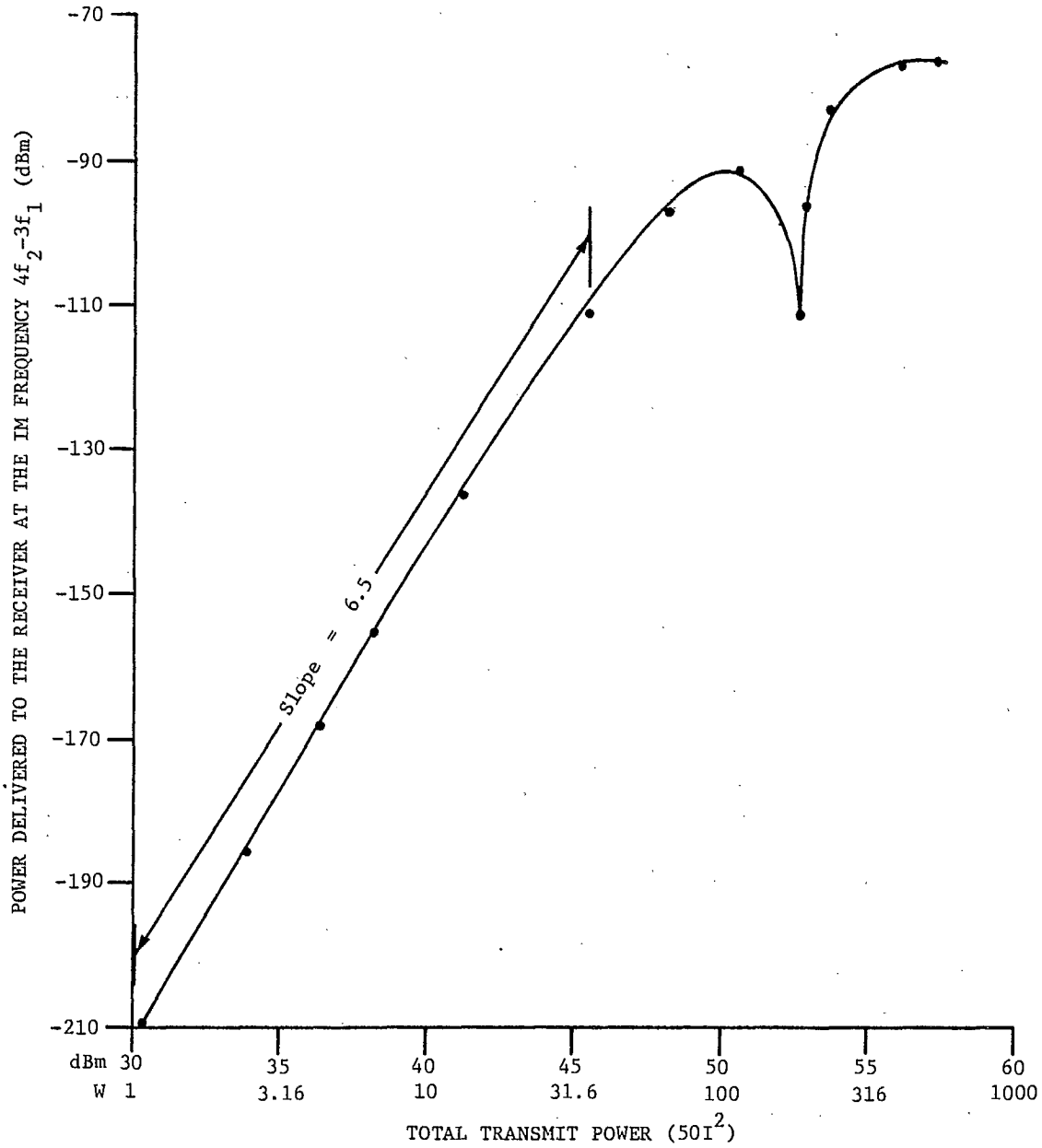

Fig. 4.19. Computed seventh order IM signal power dependence on total transmit power for IM signals generated by application of a two frequency signal to the semilinearized "current expander-type" I-V characteristic of Fig. 4.16.

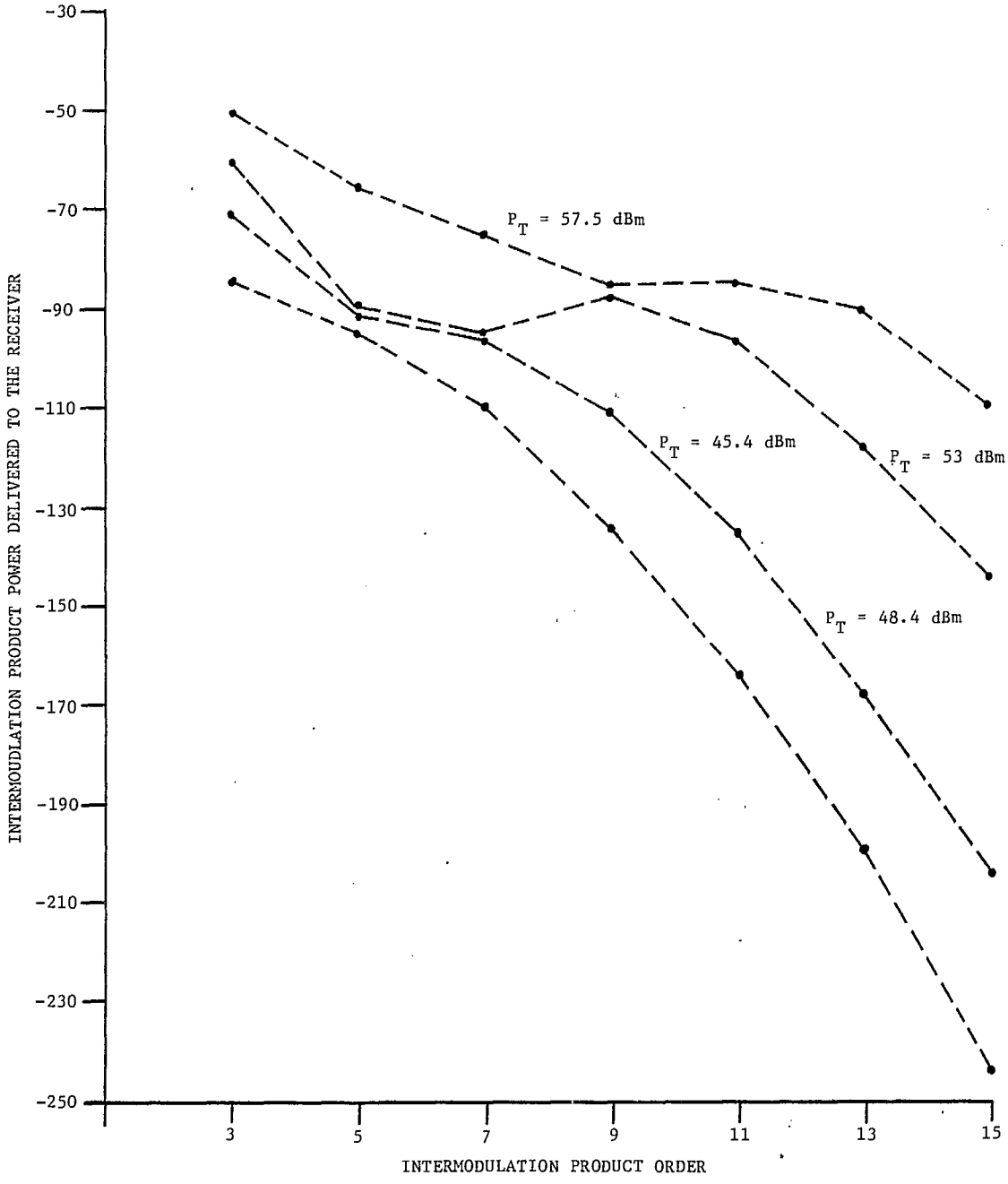

Fig. 4.20. The computed relative power of IM signals of consecutive order generated by the application of two frequency signals of different power to the semi-linearized "current expander-type" I-V characteristic of Fig. 3.16.

4.6 Discussion

The purpose of work reported in this chapter has been to compare the shapes of the power response characteristics of intermodulation signals generated by I-V nonlinearities of different forms. Intermodulation power response curves for symmetrical and non-symmetrical "current limiter" and "current expander" type I-V characteristics were drawn from computed data.

Table 4-5 shows a comparison of computed results for "current limiter" and "current expander" type characteristics. The major difference between results is that the intermodulation power response curves for the expander type characteristics show distinct minima, regardless of symmetry. These minima are not exhibited by the intermodulation power response curves for the current limiter, whether symmetrical or non-symmetrical. Measured and computed results [1] for passive intermodulation generated by a Schottky diode expander type nonlinearity and computed results for space charge limited current flow, [25] which also has an expander type nonlinearity are in agreement with this finding. The expander type nonlinearities computed in Chapter III for tunneling at the contact surfaces in RF connectors, however, result in passive intermodulation signals which have monotonic power response curves. This apparent discrepancy may be the result of the smoothly curving nature of the tunneling nonlinearities as compared with the relatively abrupt slope changes exhibited by the arbitrary curves studied in this chapter. Of lesser significance, and as a direct result of the intermodulation power minima, the intermodulation power/order relationships for the expander characteristics are non-monotonic, the slopes of the intermodulation power/drive power relationships are significantly lower than N dB/dB at Nth order, and the intermodulation product power dynamic

Table 4-5

Comparison of Results For "Limiter" and "Expander" Type I-V Characteristics

Subject of Comparison	Limiter	Expander
Intermodulation Power Minima	No	Yes
Intermodulation Power/Order relationship	Monotonic-general trend toward decreasing slope for higher transmit powers	Non-monotonic, but still exhibits general trend towards decreasing slope for higher transmit powers
Average dynamic range of passive intermodulation powers generated by symmetrical and non-symmetrical I-V characteristics	3rd order: 70 dB 5th order: 111 dB 7th order: 165 dB	3rd order: 70 dB 5th order: 91 dB 7th order: 130 dB
Intermodulation power/drive power slopes at Nth order	approximately N dB/dB	Significantly less than N dB/dB
Symmetry	No difference between the behavior of intermodulation signals generated by symmetrical characteristics and that of intermodulation signals generated by non-symmetrical characteristics was noted in either the "limiter" or "expander" cases.	

range for the same range of transmit powers is lower at 5th and 7th orders than the corresponding power range of intermodulation signals generated by the limiter type nonlinearity.

The differences noted in the intermodulation power response characteristics confirm that there is a relationship between intermodulation power signatures and the form of the intermodulation generating nonlinearity. Further, this relationship can aid in the identification of intermodulation generators in functioning RF systems. For example, if measured intermodulation power response curves, or intermodulation power/order relationships for a particular system are monotonic, space charge limited current flow, thermionic emission, and naturally formed Schottky junctions can all be discounted as sources for observed intermodulation interference.

Table 4-6 is a summary of polynomial characteristics for the nonlinearities studied in this chapter. Examination of the table shows that there is no apparent difference between the polynomial coefficients of the expander and limiter type nonlinearities that can account for the noted differences in response characteristics. There is also a trend in the intermodulation power/order relationships for the nonlinearities studied toward decreasing slopes as transmitter power is increased that cannot be readily explained. The explanations for these intermodulation signal characteristics are left as topics for further research.

Table 4-6

Summary of Polynomial Characteristics for The Arbitrary Nonlinear I-V Characteristics Chosen For Investigation

		Limiter	Expander
Symmetrical	a) coefficient sign	12 -Ve, 8 +Ve	8 -Ve, 7 +Ve
	b) periodic sign change	No	No
	c) coefficient magnitudes	even - small odd - large monotonic increase with increasing index	even - small odd - large
	d) dc coefficient	insignificant (-Ve)	insignificant (-Ve)
Non-Symmetrical	a) coefficient sign	12 -Ve, 8 +Ve	8 -Ve, 7 +Ve
	b) periodic sign change	No	No
	c) coefficient magnitudes	even and odd coefficients same order of magnitude/monotonic increase with increasing index	even and odd coefficients same order of magnitude/monotonic increase with increasing index
	d) dc coefficient	significant (-Ve)	significant (+Ve)

CHAPTER V

Summary, Conclusions, and Recommendations

5.1 Summary

There were three primary and equally important objectives of the investigation covered by this report. The first objective was to review the types and electrical conduction characteristics of electrical contacts between metals and naturally occurring metal oxides, and to assess the potential of such structures for the generation of passive intermodulation in multifrequency RF systems. The second objective was to compute the magnitude of intermodulation interference that could be generated by electron tunneling and space charge limited current flow through metal/metal-oxide/metal interfaces in copper and aluminum RF connectors. The third objective was to determine if there is a relationship between the form, or shape, of the nonlinear I-V characteristic of a passive intermodulation generator and the signature, or intermodulation response characteristic of the generated passive intermodulation. The purpose of work carried out toward the latter objective was to ascertain the viabilility of the use of intermodulation signal power signatures for intermodulation source identification.

The subject of metal/metal-oxide/metal contacts was approached via a study of available literature concerning metal/insulator contacts and electrical conduction through metal/insulator/metal structures. It was noted that three basic types of electrical contact can be made with an insulating material. These include ohmic contacts, which are made when the work function of the metal (ψ_m) is lower than that of the insulator (ψ_i), neutral contacts which form when $\psi_m = \psi_i$, and blocking contacts which form when $\psi_m > \psi_i$. For structures in which spacially separated ohmic contacts are made to an insulator it was found that two nonlinear conduction mechanisms could take place. When very thin insulators are sandwiched between ohmic contacts, electrons can tunnel through the energy barrier presented by the insulator. The current-voltage relationship for tunneling is extremely nonlinear, even within the range of low voltages expected to be developed across metal/oxide/metal structures in UHF hardware. Tunneling was therefore identified as a possible passive intermodulation generator. The second reported nonlinear mechanism for conduction through an insulator between ohmic contacts is space charge limited current flow. The I-V characteristic for this conduction process consists of a linear region at very low applied voltages followed by two quadratic regions of different sensitivity. Space charge limited current flow was assessed as having a potential for intermodulation generation, provided applied signal voltages exceed the range of the initial linear region on the I-V characteristic. It was noted, however, that unlike tunneling, space charge limited

current flow has a direct dependance on insulator conductivity. This would lower the probability of occurrence of this type of conduction in metal oxides such as aluminum oxide which exhibit low electron mobility. When spacially separated neutral contacts are made to an insulating material it was found that conduction is linear until the thermionic saturation current is reached. Voltages corresponding to this threshold for nonlinear conduction, however, were considered to be far in excess of those which could be developed across hardware junctions in UHF systems with transmit powers in the 200 watt range. Two types of non-linear conduction were noted to be possible at blocking contacts. In structures with only a thin insulator between blocking contacts, tunneling is possible at the cathode - insulator interface. Tunneling in this type of structure was also considered to have a potential for passive intermodulation generation. When the potential barrier presented at the cathode-insulator interface is too thick to permit tunneling, thermionic emission can take place. For this conduction mechanism current has an exponential dependence upon voltage. Passive intermodulation generation as a result of thermionic emission was considered possible. Table 5-1 is a summary of conclusions regarding the possibility of passive intermodulation generation by nonlinear conduction phenomena studied in this investigation.

It was noted that when metallic contact is made to an n-type semiconductor, interfacial energy relations required for each type of electrical contact are identical with those at metal/insulator interfaces. For metal/p-type semiconductor

Table 5-1

Summary of The Possibility of Passive Intermodulation Generation by Nonlinear Conduction Phenomena Studied In This Investigation

Electric Contact Type	Nonlinear Conduction Phenomenon	Potential for Passive Intermodulation Generation in 200 W UHF Systems	Anticipated Probability of occurrence in Structures Of:	
			$CU/CUO_2/CU$	$Al/Al_2O/Al$
ohmic ($\psi_m < \psi_i$)	tunneling	yes	high	high
	space-charge-limited current flow	yes	high/intermediate	low
neutral ($\psi_m = \psi_i$)	thermionic emission	no	nil	nil
blocking ($\psi_m > \psi_i$)	Tunneling	yes	nil	nil
	thermionic emission	yes	nil	nil

junctions, however, required energy (work function) relationships for ohmic and blocking contacts are reversed.

Since metal oxides can normally be classed as insulators or semiconductors [10,24] the general theory reviewed in Chapter II concerning conduction processes in metal/insulator/metal structures was considered applicable in the investigation of conduction nonlinearities in contacts between metals and naturally occurring metal-oxides. The information contained in Chapter II was therefore applied in a study of the intermodulation generating potential of tunneling and space charge limited nonlinearities at metal/metal-oxide/metal interfaces in RF connectors. To begin, a unit equivalent electrical circuit model was developed to represent a single electrical contact between two oxidized extremeties on microscopically irregular mating metal surfaces. After measuring the dimensions of the inner and outer conductor contacts of a type N coaxial connector, estimates were made of the minimum and maximum contact surface area expected for both inner and outer conductors in a mated coaxial connector. Minimum and maximum contact area connectors were then modelled by adding the number of parallel unit equivalent circuits required to cover the estimated connector contact surface areas. The nonlinear resistances of the connector contact models were first assumed to be tunneling nonlinearities. This allowed the application of the tunneling equations of Chapter II to compute I-V characteristics for the modelled connectors. From these, intermodulation signal powers were calculated through the use of the coefficients of polynomial representations for the computed I-V characteristics

in an algebraic computation routine reported by Sea [5]. Intermodulation power response characteristics and intermodulation power/order relationships were computed for intermodulation signals generated at the inner and outer conductor contacts in maximum and minimum contact area copper and aluminum connectors. Comparisons were made, resulting in conclusions regarding the passive intermodulation generation potential of electron tunneling at metal/metal-oxide/metal interfaces. Next, the nonlinear resistances in the connector contact models for the copper connector were assumed to be the result of space charge limited conduction phenomena. Following the procedures used for the calculation of the power of intermodulation signals generated by tunneling, it was quickly found that for the contact model and operating conditions assumed, operation is over the initial linear range of the space charge limited nonlinearity and no passive intermodulation could be generated. Since the probability of space charge limited conduction is low, in aluminum/aluminum-oxide structures, the passive intermodulation generation potential for this mechanism in aluminum connectors was also considered to be low.

The work conducted in relation to the study of intermodulation power signatures was reported in Chapter IV. Four different arbitrary I-V characteristics covering operating ranges similar to that of the tunneling characteristics of Chapter III were chosen as a basis for intermodulation signal power calculations. Included were an I-V characteristic with a shape similar to that of a symmetrical current limiter, one in which

current rises rapidly and symmetrically in positive and negative voltage regions as a function of voltage, and modified versions of these symmetrical characteristics, which had linear slopes in the negative voltage region. Intermodulation power response curves and intermodulation power/order relationships for each of the characteristics corresponding to two frequency sinusoidal excitation with transmit powers between 1 W and 800 W applied to the dummy load in the test circuit model of Fig. 3.6 (RF connector replaced by assumed nonlinearity) were calculated. Results for each nonlinearity were compared with each other, with the results for tunneling in Chapter III and with previously measured [1] and computed intermodulation power signatures.

5.2 Conclusions

Since it is possible to classify metal oxides as semiconductors, or insulators, nonlinear conduction phenomena at oxidized metallic interfaces in communications system hardware can be expected to be similar to conduction through structures formed by insulators or semiconductors sandwiched between metal electrodes. Reasonably extensive research has been performed over the last several decades on the electrical properties of metal/insulator/metal and metal/semiconductor/metal junctions, and a variety of nonlinear conduction mechanisms have been found to be possible. Depending upon energy relations at the electrode interfaces with the insulator or semiconductor, metal-insulator, or metal-semiconductor contacts are broadly classified as ohmic, neutral, or blocking. At ohmic contacts, electron tunneling and space charge limited current flow, both of which exhibit nonlinear I-V characteristics are possible. Conduction through structures which have ohmic contacts is linear until current reaches the thermionic saturation value. For currents greater than this limit, tunneling can take place. Where there are blocking contacts, electron tunneling or the exponentially nonlinear conduction process of thermionic emission over the interfacial energy barrier between the cathode and the insulator/semiconductor can take place.

The probability of the formation of each type of electrical contact between metals normally used for UHF hardware and their naturally occurring oxides was not considered in detail. The objective was instead to assume the existence of

each contact type and assess its potential for passive intermodulation generation under the operating conditions typical of UHF communications systems with transmit powers in the 200W range. Without conducting detailed numerical studies, it was possible to draw the following conclusions.

1) When metal/oxide/metal interfaces are formed with ohmic contacts, the nonlinearity which is characteristic of electron tunneling in this type of structure can be considered as a potential source for intermodulation generation. Space charge limited current flow also has a nonlinearity which presents a threat of intermodulation interference. For this mechanism, however, junction voltages for nonlinear conduction would have to be greater than those required for nonlinear conduction due to tunneling.

2) Where ohmic contacts are formed, passive intermodulation generation is not probable, as junction voltages required for nonlinearity in structures with ohmic contacts are far in excess of those expected at metallic interfaces in UHF hardware.

3) For structures in which blocking junctions are formed tunneling and thermionic emission are both mechanisms which could generate passive intermodulation in 200W UHF systems.

Detailed calculations were made to assess the potential of intermodulation generation by conduction mechanisms at ohmic contacts with dimensions similar to those of the contacts in a

type N connector. Nonlinearities at copper/copper and aluminum/aluminum interfaces were studied, leading to the following conclusions:

4) The power of intermodulation signals generated as a result of electron tunneling is a very sensitive function of current density. Computed intermodulation product signal powers at 3rd, 5th and 7th orders were found to increase by 4 dB for every dB increase in current density. That is, intermodulation power is directly proportional to $J^{2.5}$.

5) In coaxial connectors, the major contribution to passive intermodulation generated by tunneling is from the centre conductor contact. In comparison, passive intermodulation generated by the outer conduct of contact is negligible (on the order of 45 dB lower for the minimum contact area connector studied in this investigation).

6) For the copper connector model, calculations show that the power of passive intermodulation signals generated by tunneling in a 200W UHF system ranges between -60 dBm and -141 dBm. Calculations for an aluminum connector model with identical dimensions operating with the same transmit powers showed that the I-V characteristic for aluminum/aluminum oxide junctions is extremely linear up to power levels of approximately 100 Watts in a 50 ohm system. Beyond this power level, the characteristic becomes non-linear. The calculated tunnel voltages corresponding to operation in the nonlinear region are, however, considered

to be unrealistically high. This lead to suspicions that the contact model used in this study is not applicable to aluminum surfaces, and no passive intermodulation calculations were made.

7) No power minima are exhibited by passive intermodulation signals generated as a result of tunneling at metal/oxide/metal structures.

In order to assess the possibility of the identification of passive intermodulation generators in functioning RF systems by the analysis of intermodulation power response signatures, a theoretical investigation of intermodulation signal generation by I-V nonlinearities with different shapes was performed. The following conclusions were drawn as a result of the investigation.

8) Intermodulation power response curves for "current expander type" nonlinearities in which current rises rapidly as a function of applied voltage show distinct intermodulation power minima, regardless of symmetry. These minima are not exhibited by power response curves for intermodulation signals generated by symmetrical or non-symmetrical "current limiter type" nonlinearities in which current rises to a limiting value, then remains nearly constant as a function of voltage. The tunneling nonlinearity for copper/copper interfaces, which is of the expander type is a noted exception as no passive intermodulation minima can be computed. This may be a result of the relatively smooth nonlinearities exhibited by tunneling at copper/copper-oxide interfaces as compared with the abrupt non-

linearity of the arbitrary I-V characteristics studied in Chapter IV.

9) The intermodulation power/order relationship for intermodulation signals generated by "expander-type" nonlinearities is non-monotonic. In contrast, the corresponding relationship for "limiter-type" nonlinearities is monotonic.

10) The slopes of the most linear regions of the intermodulation power/drive power relationships for "expander" and "limiter" type nonlinearities differ. In the case of the limiter type characteristic, slopes are very close to NdB/dB for the Nth order intermodulation product. Intermodulation signals generated by expander type nonlinearities often exhibit power response slopes which are significantly less than NdB/dB at Nth order.

Conclusions 8, 9 and 10 confirm that there is a relationship between intermodulation power signatures and the form of the intermodulation generating nonlinearity. By observing intermodulation power/drive power or intermodulation power/order relationships, it can be determined if the generating nonlinearity is of the limiter type or the expander type (such as that for Schottky junctions, space charge limited current flow or thermionic emission). Further research on this topic could perhaps result in the ability to distinguish between several mechanisms with limiter or expander characteristics by observing more subtle signature differences than those noted in this study. If passive intermodulation generators can be accurately identified by their

signatures, it is also possible that their position in RF circuits can be determined. For instance, if signatures show that intermodulation generation is a result of tunneling at a metal/oxide/metal interface, RF connection points can be checked for cleanliness. Alternatively, if signatures show that intermodulation generation is due to ferromagnetic nonlinearities [1], the search for the intermodulation source could concentrate on bulk properties of the materials from which components of the system under study are constructed. Hence the study of intermodulation response signatures for generator identification is viable, and could also provide information regarding the location of intermodulation generators in functioning RF systems.

5.3 Recommendations for Further Investigation

During the course of the study covered by this report, several topics which require further investigation have been identified. These topics are enumerated and discussed in the following paragraphs.

1) Additional information is required concerning the electrical properties of oxides which form on metals which could be used for the construction of UHF hardware. This would enable the prediction of the types of electrical contacts that are probable. This in turn would enable evaluation of the passive intermodulation generating potential of a wide variety of metal/metal interfaces so that "low passive intermodulation" materials can be chosen for connector fabrication. In particular, more attention should be given to metal-metal junctions with gold, silver, and rhobidium [26].

2) To confirm results presented in this report, it would be desirable to perform experiments with copper and aluminum contacts. Since it is expected that passive intermodulation generation by the outer conductor contact in a type N connector is negligible, a convenient test jig could be made by simply manufacturing replacement inner conductor contacts from copper and aluminum and testing connectors fitted with contacts of each metal. In addition to intermodulation power magnitude comparisons, benefit could result from the observation of response signatures over a wide range of transmit powers.

3) The surface textures of different metals should be studied. As surface irregularity increases the current density at contact spots increases, leading to a higher probability of passive intermodulation generation at interfering levels if tunneling contacts are formed. There is some question [1], however concerning the possibility of oxide puncture and the elimination of nonlinear conduction phenomena at rough surfaces. Experimentation and theoretical analysis are required in this area. This work could be performed simultaneously with work associated with topic 2 and could reveal that a modification to the contact model of Chapter III is required.

4) Benefit could be derived from further research concerning intermodulation power response signatures. More detailed signature analysis and the development of a data base coupled with the use of computer comparison techniques could lead to a fast efficient method for the identification and location of passive intermodulation interference sources.

5) The response behaviour of generated intermodulation signals has yet to be explained both in mathematical and physical contexts. An explanation of such behaviour could lead to valuable information that could help to minimize passive intermodulation. For example, the conditions that lead to the observed minima for the expander type nonlinearities might be simulated at a receiver input or transmitter output to effect an interference reduction.

6) Experiments should be performed with different RF connector designs. To begin with, a connector with long cylindrical contact surfaces to reduce current density, but the usual radial dimensions to maintain a desired characteristic impedence might be considered.

References

1. Bultitude, R.J.C., Chudobiak, W.J.C., and Syrett, B.A., "A study of passive intermodulation in multifrequency UHF radio communication systems", Carleton University, Ottawa, Canada, Final report prepared for The Canadian Department of Communications, Communications Research Centre, DSS Contract #OST78-00022, Aug. 1979.

2. Higa, Walter A., "Spurious signals generated by tunneling on large reflector antennas", Proc. IEEE, vol. 63, no. 2, pp. 306-313, Feb. 1975.

3. Chapman, R.C., and Darlington, J.C., "Intermodulation generation in normally passive linear components", ASASCA Intermodulation Study, Final Report on the analytical investigation of intermodulation product generation mechanisms, Report WDL-TR5242, Philco Ford Corporation, Palo Alto, Calif., Aug. 1973.

4. Bond, C.D., Guenzer, C.S., and Corosella, C.A., "Generation of intermodulation by electron tunneling through aluminum oxide films", Report 8170, Radiation Effects Branch, Radiation Technology Division, Naval Research Laboratory, Washington, D.C., Oct. 1977.

5. Sea, R.G. and Vacroux, A.G., "On the computation of intermodulation products for a power series nonlinearity", Proc. IEEE (Letters), vol. 57, no. 3, pp. 337-338, March 1969.

6. Simmons, J.G., D.C. Conduction in Thin Films, London, M&B Monographs: Mills and Boon Ltd., 1971.

7. Sze, S.M., Physics of Semiconductor Devices, Chapters 8 and 9, New York: Wiley and Sons Ltd., 1969.

8. Dubey, P.K., "Tunnel effect in Al-Al_2O_3-Al junctions: Inclusion of short range forces", Jour. of Appl. Phys., vol. 42, no. 6, pp. 2534-2542, May 1971.

9. Watson, N.A., Microwave Semiconductor Devices and Their Circuit Applications, New York: McGraw-Hill, 1969.

10. Ioffe, A.F., Physics of Semiconductors, p. 390, Bristol, England: John Wright and Sons Ltd., 1960.

11. Lindmayer, J., Reynolds, J., and Wrigley, C., "One carrier space-charge-limited current in solids", Jour. of Appl. Phys. vol. 34, no. 4, (part 1), pp. 809-812, Apr. 1963.

12. Rose, A., "Space-charge-limited currents in solids", Physical Review, vol. 97, no. 6, pp. 1538-1544, Mar. 1955.

13. Smith, R.W., and Rose, A., "Space-charge-limited currents in single crystals of cadmium sulfide", Physical Review, vol. 97, no. 6, pp. 1531-1537, Mar. 1955.

14. Lampert, M.A., "Simplified theory of space-charge-limited currents in and insulator with traps", Physical Review, vol. 103, no. 6, pp. 1648-1656, Sept. 1956.

15. Lindmayer, J., and Slobodsky, A., "Two carrier space-charge-limited current in solids and the dielectric capacitor", Solid State Electronics, vol. 6, pp. 495-503, 1963.

16. Rosental, A., and Sapar, A., "Diffusion effects in one-carrier space-charge-limited currents with trapping", Jour. of Appl. Phys., vol. 45, no. 6, pp. 2787-2788, June 1974.

17. O'Reilly, T.J., and DeLucia, J., "Injection current flow through thin insulator films", Solid State Electronics, vol. 18, pp. 965-968, 1975.

18. Edwards, C.A., and Jones, P.L., "The effects of finite contact energy barriers and traps on space-charge-limited currents in thin insulaotrs", Solid State Electronics, vol. 21, pp. 1163-1170, 1978.

19. Srivastava, S.K., and Sinha, A.P.B., "Space-charge-limited current through chromium-cadmium sulphide-chromium diodes", Solid State Electronics, vol. 13, pp. 57-60, 1970.

20. Fisher, J.C., and Giaever, I., "Tunneling through thin insulating films", Jour. of Appl. Phys., vol. 32, no. 2, pp. 172-177, Feb. 1961.

21. Sanli, H., "Nonlinear effects in contacts and coaxial cables at microwave frequencies", M.Eng. Thesis, Department of Electrical Engineering, Sheffield University, Sheffield, England, Nov. 1975.

22. Holm, R., Electric Contacts Handbook, Berlin: Springer-Verlay, 1959.

23. Henney, K., The Radio Engineering Handbook, pp. 90-91, New York, London: McGraw-Hill, 1941.

24. Jarzebski, Oxide Semiconductors, Warsaw: Pergamon Press, 1973.

25. Bultitude, R.J.C., "The generation of passive intermodulation due to the nonlinear phenomenon of space charge limited current flow in metal-oxide-metal junctions", Carleton University/CRC memorandum, Ottawa, Canada, Feb. 22, 1979.

26. Bayrak, M., and Benson, F.A., "Intermodulation products from non-linearities in transmission lines and connectors at microwave frequencies", Proc. IEE, vol. 122, no. 4, pp. 361-367, April 1975.

27. Simmons, J.G., "Electric tunnel effect between dissimilar electrodes separated by a thin insulating film", Jour. Appl. Phys., vol. 34, no. 9, p. 2581, Sept. 1963.

28. Sea, R.G., "An algebraic formula for amplitudes of intermodulation products involving an arbitrary number of frequencies", Proc. IEEE (Letters), vol. 56, no. 8, pp. 1514-1515, Aug. 1967.

APPENDIX A

COMPUTER PROGRAMS "IMPWR" AND "TUNEL"

A.1. Program IMPWR

Program IMPWR calculates the power of specified intermodulation products resulting from a two frequency input to the intermodulation generating nonlinearity using the method derived by Sea [28]. The program is based upon an algorithm reported by Sea and Vacroux [5].

A.1.1 Program Inputs

The following are the program inputs in the sequence in which they are requested.

(1) The number of coefficients in the polynomial representation;

$$Y = a_0 + a_1X + a_2X^2 + a_3X^3 + \ldots\ldots\ldots\ldots + a_nX^n \qquad (A.1.1)$$

(2) The coefficients (a_0 to a_n) of the polynomial.

The maximum number of coefficients permissible is 100.

(3) Program Options:

(a) OPTION:

i) If OPTION = "1", the power of a single specified intermodulation product at the frequency (A2F2 - A1FA1) is calculated, where A1 and A2 are inputs to the program.

ii) If OPTION = "2", the power of all odd order intermodulation products between a specified minimum (MINORD $\geq$ 1 and odd) and a specified maximum (MAXORD) are calculated. In this case intermodulation frequencies are fixed at f_{IM} = (A2F2-A1F1), where A2 is incremented in steps of "1" from A2=(MINORD + 1)/2. The maximum value for MAXORD is dependent upon the coefficients and the power of the transmit signals.

(b) PARTSUM:

i) If PARTSUM = "1", the program outputs the partial sums associated with each coefficient in the describing polynomial. This permits determination of the relative influence of each term on the computed intermodulation signal amplitudes.

ii) IF PARTSUM = "2", the partial sums are not printed. This is the normal mode of operation.

(4) EN:

EN may have the values:

"1" if it is desired to calculate the dc component in the output from the nonlinearity. This must be used in conjunction with OPTION = 1 and A1 = A2 = 0. (See Eqn. 3.3-20-a , Ref. [1])

or "2" if it is desired to compute intermodulation product amplitudes.

(5) The fifth set of input variables requested by the program is dependent upon OPTION.

(a) If OPTION = "1" (for the power of a single intermodulation product) the program will request values for:

ORDER - the intermodulation order of interest

A1 - the f_1 multiplier

A2 - the f_2 multiplier

E1 - the amplitude of the transmit signal (V or I) at f_1.

E2 - the amplitude of the transmit signal at f_2.

(b) If OPTION = "2" (for the amplitudes of intermodulation products of consecutive odd orders between MINORD and MAXORD) the program will request values for:

MAXORD - the highest intermodulation order of interest.

MINORD - the lowest intermodulation order of interest.

E1 - the amplitude of the transmit signal at f_1.

E2 - the amplitude of the transmit signal at f_2.

It should be noted that IMPWR is an interactive program and will request each input from the operator at the appropriate time after the "RUN IMPWR" command has been entered. Instructions and parameter definitions are given each time the program requests an input.

A.1.2 Program Outputs

The program outputs the polynomial coefficients in a list immediately after the last coefficient has been read in. This allows time to check for errors before proceeding. Thereafter, the form of the output from the program is dependent upon the options chosen.

(a) If OPTION = "1", the program outputs the following data in sequence.

ORDER

A1

A2

E1

E2

IMO - the order of the computed intermodulation product (IMO should equal ORDER)

AMP - the absolute amplitude of the computed intermodulation product

PWR - the relative amplitude of the computed intermodulation product (PWR = 10 $\log_{10}$ $(AMP^2)+30$)

(b) If OPTION = "2", the program outputs the following data in sequence.

MAXORD

MINORD

E1

E2

IMO - the order of the <u>first</u> computed intermodulation product

AMP - the absolute amplitude of the <u>first</u> computed intermodulation product

PWR - the relative amplitude of the <u>first</u> compute intermodulation product (PWR = $10 \log_{10}(AMP^2)+30$)

IMO - the order of the <u>second</u> computed intermodulation product

.

.

.

etc (information repeated for each intermodulation order)

.

.

.

(c) If PARTSUM = "1" with OPTION = "1" or "2", the program will print the input data as in (a) and (b) above, then the partial sums will be printed as follows

J = the IMOth index of the coefficient A(J)

F1 = $(A(J) \times J!)/2^J$

PHI(2,I) = $\Phi(2,I)$
see program explanation (Section A.1.3)

F2 = F1 x PHI(2,I)

J - the index of the (IMO + 1) th coefficient

.

.

.

etc. (information repeated for each coefficient)

.

.

.

The program then outputs:

IMO

AMP

PWR

in the normal fashion.

When the program is finished the operator is requested to enter "1" if another run is desired. This eliminates the necessity to enter the polynomial coefficients each time the input parameters are changed.

A.1.3 Program Explanation (IMPWR)

Program IMPWR is based upon an algorithm reported by Sea and Vacroux [5].

First, the magnitude of the intermodulation product wave represented by eqn. 3.3-20 (Ref. [1]) is written for the case of two transmit signals in the form:

$$Y_{IM_N} = \varepsilon_N \prod_{i=1}^{2} A_p^{|\alpha_p|} \sum_{L=0}^{\infty} \frac{a_{N+2L}(N+2L)!}{2^{N+1}} \Phi(2,L) \quad * \qquad \text{(A.1-2)}$$

where $$\Phi(2,L) = \sum_{q_1} \cdots \sum_{q_M} \prod_{p=1}^{2} \frac{A_i^{2q_i}}{(q_p+|\alpha_p|)!q_p!} \; .$$

$$q_1 + \cdots + q_M = L$$

It can be shown [5] that

$$\Phi(1,q) = \frac{A_1^{2q}}{(q+|\alpha_1|)q!} \qquad \text{(A.1-3)}$$

and, $$\Phi(2,q) = \sum_{q_2=0} \frac{A_2^{2q_2}}{(q_2+|\alpha_2|)!q_p!} \Phi(1,q-q_2) \qquad \text{(A.1-4)}$$

Thus [5] if it is desired to compute Y_{IM_N} by eqn. A.1-2 truncated at $L = L_0$, it is necessary to compute $\Phi(2,L)$ for $L = 0,1,\ldots,L_0$. Program IMPWR computes $\Phi(2,L)$ iteratively by first computing $\Phi(1,q)$ for $q = 0,1,\ldots L_0$ using eqn. A.1-3, then computing $\Phi(2,q)$ for $q = 0,1,2\ldots L_0$ using eqn. A.1-4. Values for Y_{IM_N} are then computed by substitution in eqn. A.1-2.

---

* $\varepsilon_N = 1$ for dc calculations, or 2 for intermodulation calculations (see eqn. 3.3-20, Ref [1])

A.1.4 Program Flow Chart (IMPWR)

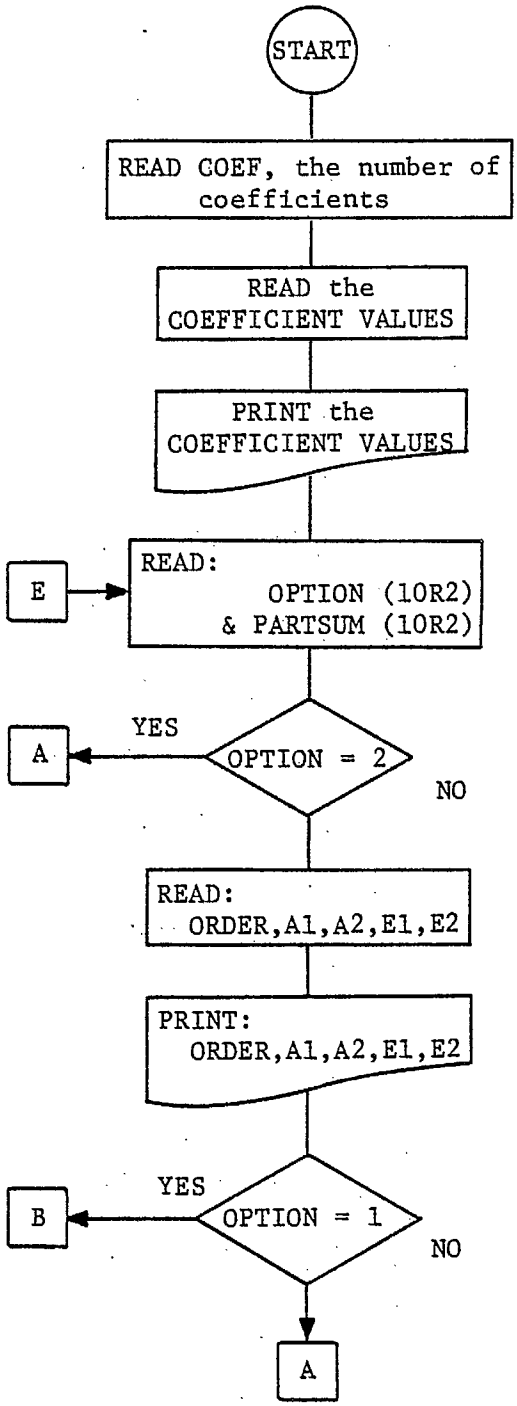

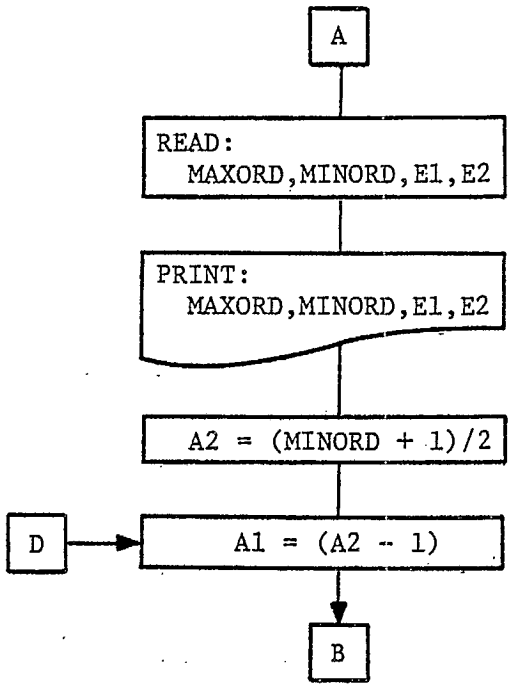
A
READ:
MAXORD,MINORD,E1,E2
PRINT:
MAXORD,MINORD,E1,E2
A2 = (MINORD + 1)/2
D
A1 = (A2 - 1)
B

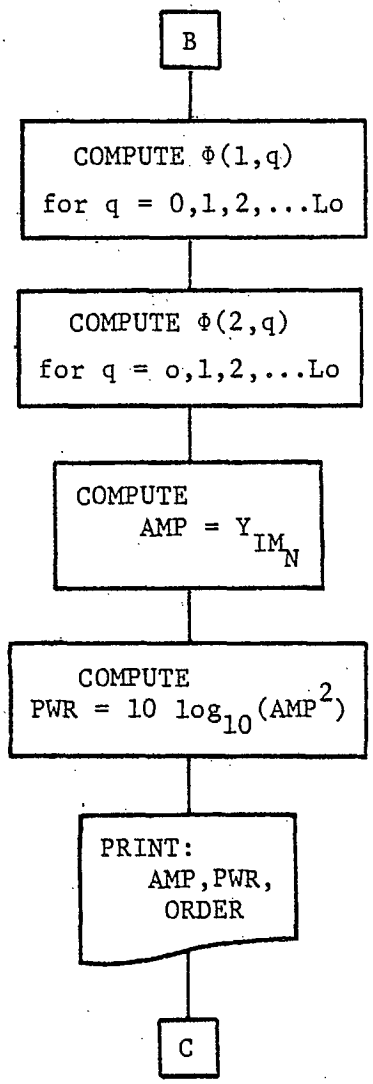
B
COMPUTE Φ(1,q)
for q = 0,1,2,...Lo
COMPUTE Φ(2,q)
for q = o,1,2,...Lo
COMPUTE
AMP = Y_{IM_N}
COMPUTE
PWR = 10 $\log_{10}$(AMP^2)
PRINT:
AMP,PWR,
ORDER
C

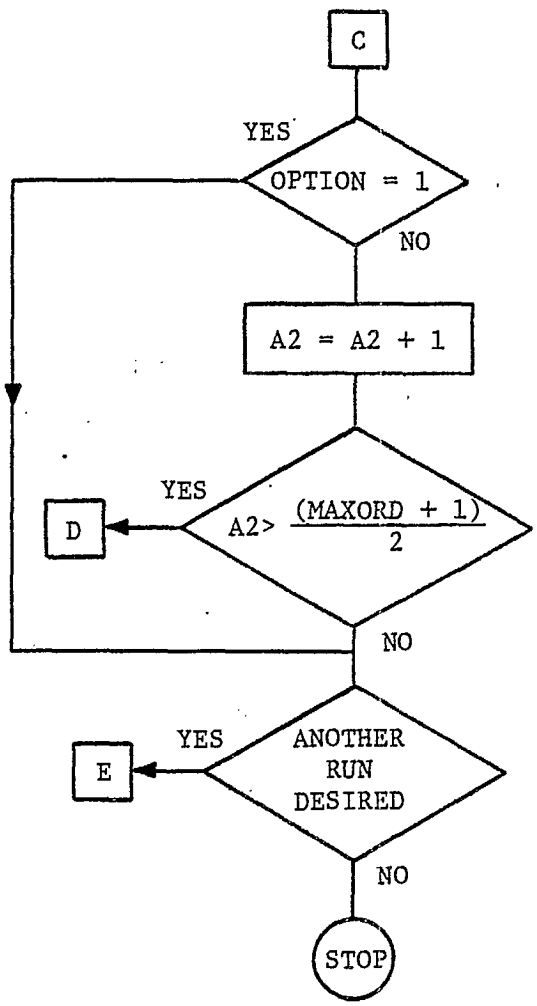
C
YES
OPTION = 1
NO
A2 = A2 + 1
YES
D
A2> (MAXORD + 1)/2
NO
YES
E
ANOTHER RUN DESIRED
NO
STOP

A.1.5 Program Statement Listing (IMPWR)

```
C     THIS PROGRAM COMPUTES IM AMPLITUDES 3RD-65TH ORDER
C     INO=MAXORD=ORDER,(A1+A2)=ORDER
C     E1 AND E2 ARE CARRIER AMPLITUDES
      INTEGER A2
      DIMENSION A(0:100)
      DO 200 I=0,100
  200 A(I)=0
      WRITE(108,202)
  202 FORMAT(//'INPUT NUMBER OF COEFFICIENTS',/)
      INPUT COEF
      WRITE(108,700)
  700 FORMAT(/,'INPUT THE COEFFICIENTS',/)
      DO 561 I=0,COEF
      INPUT A(I)
  561 CONTINUE
   10 FORMAT(6X,E.4)
      DO 11 I=0,COEF
   11 OUTPUT A(I)
C
  100 WRITE(108,80)
   80 FORMAT(/,'INPUT OPTION(10R2),PARTSUM(10R2)',
     X'EN(10R2)',/,
     X'OPTION=1 FOR AMPLITUDE OF A SINGLE ORDER',
     X/,'PARTSUM=1 OUTPUTS PARTIAL SUMS',/
     X,'EN=1 FOR DC COMPONENT  2 FOR IM PWRS',/)
      INPUT OPT,PARTSUM,EN
      IF(OPT.EQ.2) GO TO 7
      WRITE(108,1)
    1 FORMAT(/,'INPUT ORDER,A1,A2,E1,E2',/
     X,'FIM=(A2F2-A1F1)',/,
     X'E1&E2 ARE TRANSMIT SIGNAL AMPLITUDES')
      INPUT MAXORD,A1,A2,E1,E2
      OUTPUT MAXORD,A1,A2,E1,E2
      WRITE(108,701)
  701 FORMAT(//)
      IMO=MAXORD
    7 CONTINUE
      INTEGER C,D
      COMMON Q
      COMMON N,I,C,J,D,L
*
```

```
      DIMENSION PHI(2,100)
      IF(OPT.EQ.1) GO TO 13
      WRITE(108,6)
    6 FORMAT(/,'INPUT MAXORD,MINORD,E1,E2',/,
     X'MAXORD & MINORD ARE MAX AND MIN ORDERS',/,
     X'E1&E2 ARE TRANSMIT SIGNAL AMPLITUDES')
      INPUT MAXORD,MINORD ,E1,E2
      OUTPUT MAXORD,MINORD,E1,E2
      WRITE(108,703)
  703 FORMAT(//)
C
      S=(MAXORD+1)/2
      A2=(MINORD+1)/2
   20 A1=(A2-1)
      IMO=((2*A2)-1)
C
C     GENERATE PHI(M,L)
C
C
   13 L=IFIX(((COEF+2)-IMO)/2)
      DO 2 I=1,(L+1)
      PHI(1,I)=0
      PHI(2,I)=0
    2 CONTINUE
      DO 3 I=1,(L+1)
      K=2*(I-1)
      C=A1+(I-1)
    3 PHI(1,I)=(E1**K)/(FACT(I-1)*FACT(C))
      DO 4 I=1,(L+1)
      J=0
      TRM=0
    5 K=2*J
      D=A2+J
      E=(I-J)
      TRM1=PHI(1,E)
      TRM2=(E2**K)/(FACT(J)*FACT(D))
      TRM=TRM1*TRM2
      PHI(2,I)=PHI(2,I)+TRM
      J=J+1
      IF(J.GT.(I-1))GO TO 4
```

```
      GO TO 5
    4 CONTINUE
C
C     CALCULATE IMP AMPLITUDES
C
      T=(E1**A1)*(E2**A2)
      F3=0
      DO 8 I=1,(L+1)
      K=(I-1)
      J=(IMO+(2*K))
      F1=(A(J)*FACT(J))/(2**J)
      F2=F1*PHI(2,I)
      IF(PARTSUM.EQ.2) GO TO 8
      WRITE(108,45)
   45 FORMAT(//)
      OUTPUT J,F1,PHI(2,I),F2
    8 F3=F3+F2
      AMP=ABS(T*F3*EN)
      PWR=10*(LOG10((AMP)**2))+30
      WRITE(108,701)
  702 FORMAT(//)
      OUTPUT IMO,AMP,PWR
      IF(OPT.EQ.1)GO TO 25
      A2=(A2+1)
      IF(A2.GT.S)GO TO 25
      GO TO 20
   25 CONTINUE
      WRITE(108,33)
   33 FORMAT(/,'INPUT (1) IF ANOTHER RUN DESIRED',/,
     X'(2) OTHERWISE')
      INPUT AGN
      IF(AGN.EQ.1) GO TO 100
      STOP
      END
C
C     FACTORIAL GENERATION
C
      FUNCTION FACT(N)
      L=0
      FACT=1
```

```
121.000          L=N
122.000      1   IF(L)2,3,4
123.000      4   FACT=FACT*L
124.000          L=L-1
125.000          GO TO 1
126.000      2   FACT=0
127.000      3   RETURN
128.000          END
```

A.2 Program TUNEL

Program TUNEL computes the I-V characteristic for electron tunneling through an insulator sandwiched between two metal electrodes. It is assumed that tunneling takes place at a number of discrete "A" spots on the electrode surfaces which are separated by regions filled with a thicker oxide film through which a smaller capacitive current flows (Ref. Section 3.2).

A.2.1 Program Inputs

The following are the program inputs in the sequence in which they are requested.

(1) The temperature (T) in degrees Kelvin

(2) The oxide thickness (D) in Angstroms

(3) The parameter Φ_o [8], (PHIO) where;

$$\Phi_o = \Psi_m - (\Psi_i - (Eg/2))$$

and,

Ψ_m = Metal work function

Ψ_i = Insulator work function

Eg = Band gap of the insulator

all in electron volts.

(4) The high frequency permittivity (K) of the insulator.

(5) The desired value of tunnel voltage increments (IN)

(6) The minimum starting tunnel voltage (VMIN)

(7) The maximum tunnel voltage (VMAX)

(8) The area of each "A" spot (AREA) in sq. Angstroms.

(9) The capacitive reactance (XC) of the regions between "A" spots in ohms.

(10) The number of "A" spots (SPOTS) on the contact under study.

A.2.2 Program Outputs

The program outputs the I-V characteristic for the total contact area in tabular form. Also, the contact resistance corresponding to each value of tunnel voltage is printed.

A.2.3 Program Explanation

For each value of voltage (V) in the specified range program TUNEL computes tunnel current densities for each "A" spot in accordance with eqn. 2-4 of Chapter II. This current density is then added vectorially to the capacitive current for the surrounding thick insulator region to yield the total current per equivalent contact spot (see cct. model, Fig. 3.5.). This current value is then multiplied by the number of "A" spots (SPOTS) on the contact to give the total current carried by the contact at the voltage (V). The contact resistance R = V/I is then calculated and the parameters V, I, and R for the contact are printed in tabular form. The value for voltage V is then incremented by the specified amount (IN) and the process is repeated. The program stops when V = VMAX.

A.2.4 Program Statement Listing (TUNEL)

```
      REAL IN,K,L,JT,JC,JSC,JTOT1,JTOT2
    5 WRITE(108,10)
   10 FORMAT(2X,'INPUT T,D,PHIO,K,IN,VMIN,VMAX,AREA',/)
      INPUT T,D,PHIO,K,IN,VMIN,VMAX,AREA
      WRITE(106,60)
   60 FORMAT(2X,'INPUTXC,SPOTS',/)
      INPUT XC,SPOTS
      OUTPUT T,D,PHIO,K,IN,VMIN,VMAX,AREA
      WA=5.0
      ETA=0.72/(K*WA)
      WRITE(108,15)
   15 FORMAT(/,5X,'VOLTS',15X,'AMPS',14X,'R',//)
      PKT=T*2.70624E-4
      A=1.0246928
      X1=3./(K*PHIO)
      V=VMIN
   20 V=V+IN
      IF(V-PHIO)30,30,40
   30 R=(23.04/(K*D))
      S=(3*PHIO+(10.02/(K*D))-2*V)
      X2=D*(1-R/S)+X1
      GO TO 50
   40 X2=(PHIO-(14.02/(K*D)))*(D/V)
   50 L=ALOG((X2*(D-X1))/(X1*(D-X2)))
      PHII=PHIO-((V*(X1+X2))/(2*D))
     X-(2.88/(K*(X2-X1)))*(L-ETA*
     X(1/X1-1/X2+1/(D-X2)-1/(D-X1)+2*L/D))
      AX=A*(X2-X1)
      B=AX/(2*SQRT(PHII))
      BT=B*PKT
      Y=ABS(BT/SIN(BT))
      C=1.6184028E10/B**2
      AL=-AX*SQRT(PHII)
      F=(1.-EXP(-B*V))
      JT=(C*EXP(AL)*Y*F)*AREA*1.E-16
C
C     CALCULATE CAPACITIVE CURRENT
C
      JC=V/XC
C
C     ADD TUNNEL AND CAPACITIVE CURRENT
C
      JTOT1=SQRT((JT**2)+(JC**2))
      CRNT=JTOT1*SPOTS
      R1=V/CRNT
      WRITE(108,70) V,CRNT,R1
   70 FORMAT(2X,D.8,5X,D.8,5X,D.8)
      IF(V-VMAX)80,90,90
   80 GO TO 20
   90 INPUT AGN
      IF(AGN.EQ.1)GO TO 5
      STOP
      END
```

APPENDIX B

Physical Constants

B.1 Universal Constants

Boltzman's constant $K_o = 8.6171 \times 10^{-3}$ eV/^oK

Planck's constant $h = 4.1356 \times 10^{-15}$ eV.s

Electronic charge $e = 1.602 \times 10^{-19}$ coulombs

B.2 Optical permittivity K

$Al_2O_3 = 3.0$ [8]

$CU_2O = 3.454$ [3]

$\varepsilon_o = 8.854 \times 10^{-14}$ F/cm

B.3 Static permittivity ε_r

$Al_2O_3 = 8 - 12$ [10,24]

$CU_2O = 8 - 16$

B.4 Electron Mobility μ

Al_2O_3 = - -

$CU_2O = 210$ cm^2/V.sec [3]

B.5 Work functions

(a) for metals Ψ_m

Al	4.08 eV	[8]
CU	4.47 eV	[3]

(b) for oxides Ψ_i

Al_2O_3	6.24 eV	[8]
CU_2O	5.15 eV	[3]

B.6 Band Gap Energies Eg

Al_2O_3	7.0 eV	[8]
CU_2O	2.2 eV	[3]

B.7 Contact potentials ($\Phi_0 = \Psi_m - (\Psi_i - E_g/2)$)

Al/Al_2O_3	1.34 eV
CU/CU_2O	0.42 eV